

University of Windsor

Scholarship at UWindor

Electronic Theses and Dissertations

Theses, Dissertations, and Major Papers

1992

Effect of beryllium on the precipitation of S' phase and mechanical properties of aluminum(alpha)-sulfur(aluminum(2) copper magnesium).

Wei. Fang
University of Windsor

Follow this and additional works at: <https://scholar.uwindsor.ca/etd>

Recommended Citation

Fang, Wei., "Effect of beryllium on the precipitation of S' phase and mechanical properties of aluminum(alpha)-sulfur(aluminum(2) copper magnesium)." (1992). *Electronic Theses and Dissertations*. 1817.

<https://scholar.uwindsor.ca/etd/1817>

This online database contains the full-text of PhD dissertations and Masters' theses of University of Windsor students from 1954 forward. These documents are made available for personal study and research purposes only, in accordance with the Canadian Copyright Act and the Creative Commons license—CC BY-NC-ND (Attribution, Non-Commercial, No Derivative Works). Under this license, works must always be attributed to the copyright holder (original author), cannot be used for any commercial purposes, and may not be altered. Any other use would require the permission of the copyright holder. Students may inquire about withdrawing their dissertation and/or thesis from this database. For additional inquiries, please contact the repository administrator via email (scholarship@uwindsor.ca) or by telephone at 519-253-3000ext. 3208.



National Library
of Canada

Acquisitions and
Bibliographic Services Branch

395 Wellington Street
Ottawa, Ontario
K1A 0N4

Bibliothèque nationale
du Canada

Direction des acquisitions et
des services bibliographiques

395, rue Wellington
Ottawa (Ontario)
K1A 0N4

Your file / Votre référence

Our file / Notre référence

NOTICE

The quality of this microform is heavily dependent upon the quality of the original thesis submitted for microfilming. Every effort has been made to ensure the highest quality of reproduction possible.

If pages are missing, contact the university which granted the degree.

Some pages may have indistinct print especially if the original pages were typed with a poor typewriter ribbon or if the university sent us an inferior photocopy.

Reproduction in full or in part of this microform is governed by the Canadian Copyright Act, R.S.C. 1970, c. C-30, and subsequent amendments.

AVIS

La qualité de cette microforme dépend grandement de la qualité de la thèse soumise au microfilmage. Nous avons tout fait pour assurer une qualité supérieure de reproduction.

S'il manque des pages, veuillez communiquer avec l'université qui a conféré le grade.

La qualité d'impression de certaines pages peut laisser à désirer, surtout si les pages originales ont été dactylographiées à l'aide d'un ruban usé ou si l'université nous a fait parvenir une photocopie de qualité inférieure.

La reproduction, même partielle, de cette microforme est soumise à la Loi canadienne sur le droit d'auteur, SRC 1970, c. C-30, et ses amendements subséquents.

**EFFECT OF Be ON THE PRECIPITATION OF S' PHASE AND
MECHANICAL PROPERTIES OF Al(α)-S(Al₂CuMg) ALLOY**

By

Wei Fang

A Dissertation
Submitted to the
Faculty of Graduate Studies and Research
through the Engineering Materials Program,
Department of Mechanical Engineering
in Partial Fulfillment of the Requirements
for the Degree of Doctor of Philosophy at
the University of Windsor

Windsor, Ontario, Canada

1992



National Library
of Canada

Acquisitions and
Bibliographic Services Branch

395 Wellington Street
Ottawa, Ontario
K1A 0N4

Bibliothèque nationale
du Canada

Direction des acquisitions et
des services bibliographiques

395, rue Wellington
Ottawa (Ontario)
K1A 0N4

Your file / Votre référence

Our file / Notre référence

The author has granted an irrevocable non-exclusive licence allowing the National Library of Canada to reproduce, loan, distribute or sell copies of his/her thesis by any means and in any form or format, making this thesis available to interested persons.

L'auteur a accordé une licence irrévocable et non exclusive permettant à la Bibliothèque nationale du Canada de reproduire, prêter, distribuer ou vendre des copies de sa thèse de quelque manière et sous quelque forme que ce soit pour mettre des exemplaires de cette thèse à la disposition des personnes intéressées.

The author retains ownership of the copyright in his/her thesis. Neither the thesis nor substantial extracts from it may be printed or otherwise reproduced without his/her permission.

L'auteur conserve la propriété du droit d'auteur qui protège sa thèse. Ni la thèse ni des extraits substantiels de celle-ci ne doivent être imprimés ou autrement reproduits sans son autorisation.

ISBN 0-315-78898-4

Canada

To my dear wife Xueqin

© Wei Fang 1992

ABSTRACT

An investigation on the effect of Be on S' phase precipitation in pseudobinary Al(α)-S(Al₂CuMg) alloy is carried out using microhardness measurement, resistivity analysis, optical, SEM and TEM microscopy, X-ray diffraction, EDS and WDS analysis, tensile and charpy-V notch impact tests, and fractography.

It is shown that additions of 0.15% or 0.25% Be to Al-2.5Cu-1.2Mg alloy accelerated the age-hardening rate and significantly increased the peak hardness levels of the aged alloys. Kinetic data analyses show that precipitation of S' in both alloys obeys the Avrami equation. The exponential growth constant and activation energy are not significantly affected by Be addition. This indicates that the growth mechanism of S' phase is unaltered by the Be addition, and agrees with the observed lath- or rod-like morphology for the S' precipitate.

A higher value is obtained for the nuclei density parameter (k) for the Be-containing alloy, which is consistent with the higher density of S' precipitate in the alloy and suggests a Be-enhanced nucleation rate.

Be alters the defect structure from a high density of dislocation loops in the solution-treated base alloy to one of fewer dislocation helices, which is attributed to the high Be-vacancy binding energy. On aging the Be-containing alloy at 190 °C, secondary dislocation loops are formed by condensation of the vacancies released by Be atoms, which is accompanied by the simultaneous formation of S' precipitate, and indicates Be atoms are

involved in the nucleation process.

It is shown that there is a transition from S' to S phase after about 5 minutes' aging at 350 °C, which is related to a change in the precipitate growth orientation.

The X-ray diffraction data show that up to 2.5 at% Be is incorporated into the S phase, and EDS and WDS analyses indicate that both the Cu and Mg solubility in Al(α) are significantly decreased by Be. The Be incorporation in S phase, and restricted solubilities of Cu and Mg in Al(α), increase the nucleation entropy and rate, which is consistent with the S phase refinement in the Be-containing alloy.

The yield and tensile strengths, ductility, and impact toughness for the precipitation hardened alloy are increased by Be addition, which can be attributed to the refinement of S' precipitates. Fractography results show a ductile deformation mode for both alloys.

ACKNOWLEDGEMENTS

The author wished to express his gratitude to Dr. W.V. Youdelis for his supervision and guidance throughout the course of this study.

He would also like to thank Dr. D. O. Northwood for his informative direction and discussions as well as Mr. J. Robinson for his technical assistance in electron microscopy study, and to many other people in the Department of Mechanical Engineering, University of Windsor who helped to make this thesis possible.

Finally, acknowledgements are due to the Aluminum Company of Canada for supplying superpurity aluminum, and the Natural Science and Engineering Research Council of Canada for providing financial support in the form of a research grant.

TABLE OF CONTENTS

	<u>Page</u>
ABSTRACT	v
ACKNOWLEDGEMENTS	vii
LIST OF TABLES	x
LIST OF FIGURES	xi
I: INTRODUCTION	1
II: LITERATURE REVIEW	4
A. GENERAL INTRODUCTION TO PRECIPITATION HARDENING	4
1. Basic Concepts of Precipitation Hardening	4
2. Nucleation from Supersaturated Solid Solution	5
(a) Classical Nucleation Theory	6
(b) Nucleation from Supersaturated Solid Solution	8
(1) Incoherent nucleation	9
(2) Coherent nucleation	10
(c) Nucleation at Defects	11
(d) Refinement of Precipitates	13
(1) Effect of trace elements	14
(2) Effect of mechanical-thermal treatments	17
(3) Other factors	17

(e) Relation of Nucleation Entropy to Nucleation	18
3. Kinetics of Precipitation Processes	23
B. PRECIPITATION OF S PHASE (Al₂CuMg) IN Al-Cu-Mg ALLOYS	24
1. Structural aspects of Precipitating Phases	27
(a) GPB zones	27
(b) S' Intermediate phase	29
(c) S phase	30
2. Aging Behavior and Factors Affecting Precipitation of S' Phase	31
(a) Effect of Trace Elements	32
(b) Effect of Thermal-Mechanical Treatments	34
(c) Other Effects	36
III: EXPERIMENTAL	38
A. ALLOY PREPARATION	38
B. SPECIMEN PREPARATION AND ANALYTICAL PROCEDURE	39
1. Microhardness Measurement	39
2. Optical and SEM Microscopical Observations	39
3. Resistivity Analysis	40
4. TEM Microscopical Examinations	41
5. Mechanical Property Tests	41
6. S Phase Analysis	43
IV: RESULTS AND DISCUSSION	44
A. AGING BEHAVIOR AND MICROSTRUCTURES	44

1. As-Cast and Solution Treated Microstructures	44
2. Age-Hardening Behavior	44
3. Optical and SEM Microscopy	51
4. Kinetic Analysis	54
5. TEM Examinations	60
(a) Defect Structure and Formation of S' Precipitate	60
(b) S' Morphology and Density	68
(c) Preaging Deformation	71
(d) S' to S Phase Transition	78
B. S PHASE ANALYSIS	86
C. Be EFFECT ON S' PHASE NUCLEATION	91
1. Calculation of Nucleation Entropy	92
2. Nucleation Rate Comparison	96
D. MECHANICAL PROPERTIES AND FRACTOGRAPHY	98
1. Tensile Properties and Impact Toughness	98
2. Deformation Pattern and Fracture Behavior	103
V: CONCLUSIONS	107
VI: SUGGESTIONS FOR FUTURE RESEARCH	109
REFERENCES	110
PUBLICATIONS	118
VITA AUCTORIS	119

LIST OF FIGURES

<u>Figure</u>	<u>Page</u>
1. (a) Al(α)-S(Al_2CuMg) pseudo-binary diagram. (b) Al-Cu-Mg isotherm at 430°C.	26
2. Al-Be phase diagram.	28
3. (a) Experimental set up, (b) resistivity specimen dimensions.	42
4. Optical micrographs of as cast alloys. (a) base alloy, (b) 0.15Be, (c) 0.25Be.	45
5. Optical micrographs of alloys homogenized at 570°C for 60 h. (a) base alloy, (b) 0.15Be, (c) 0.25Be.	46
6. Age hardening curves for alloys aged at temperature indicated. Legend given in 6(a).	47
7. Optical micrographs of alloys aged at 300°C for 7 days. (a) base alloy, (b) 0.15Be, (c) 0.25Be.	52
8. SEM micrographs for alloys aged at 300°C for 7 days. (a) base alloy, (b) 0.15Be, (c) 0.25Be.	53
9. Specific resistivity vs time for alloys aged at 190°C and 240°C.	55
10. $\text{Log} \ln(1/(1-X))$ vs $\text{log} t$ for the 190°C aging temperature.	56
11. Fraction transformed vs time for S' phase.	58
12. Arrhenius plots for $\ln k$ and $\ln(dX/dt)_{X=0.5}$.	59
13. TEM micrographs and Kikuchi lines on corresponding diffraction patterns for as quenched alloys. (a) and (b) base alloy, (c) and (d) 0.15Be.	61
14. TEM micrographs for alloys aged for two weeks at room temperature. (a) base alloy, (b) 0.15Be.	62

15.	TEM micrographs for alloys aged at 190°C for 5 min. (a) $\langle 100 \rangle_{Al}$ and (b) $\langle 112 \rangle_{Al}$ base alloy, (c) $\langle 100 \rangle_{Al}$ and (d) $\langle 112 \rangle_{Al}$ 0.15Be.	64
16.	TEM micrographs of alloys aged at 350°C for 1 min. $\langle 100 \rangle_{Al}$ foil orientation. (a) base alloy, (b) 0.15Be.	66
17.	TEM micrographs for alloys aged at 350°C for 18 min. $\langle 100 \rangle_{Al}$ foil orientation. (a) base alloy, (b) 0.15Be.	67
18.	TEM micrographs for alloys aged at 190°C for 2 h. $\langle 100 \rangle_{Al}$ foil orientation. (a) base alloy, (b) 0.15Be.	69
19.	TEM micrographs for alloys aged at 190°C for 5.7 h. (a) $\langle 110 \rangle_{Al}$ and (b) $\langle 112 \rangle_{Al}$ base alloy, (c) $\langle 110 \rangle_{Al}$ and (d) $\langle 112 \rangle_{Al}$ 0.15Be.	70
20.	TEM micrographs for base alloy aged at 190°C for 17 h. $\langle 112 \rangle_{Al}$ foil orientation. (a) and (b) are taken from the same area with slight tilting.	72
21.	Diffraction patterns for alloys aged at 190° for 5.7 h.	73
22.	TEM micrographs for alloys aged at 190°C for 19.5 h (peak hardness). (a) $\langle 100 \rangle_{Al}$ and (b) $\langle 112 \rangle_{Al}$ base alloy, (c) $\langle 100 \rangle_{Al}$ and (d) $\langle 112 \rangle_{Al}$ 0.15Be.	74
23.	TEM micrographs. $\langle 100 \rangle_{Al}$ foil orientation. (a) base alloy (190°C for 5.7 h), (b) 0.15Be (190°C for 19.5 h).	75
24.	TEM micrographs for alloys aged at 190°C for 19.5 h. $\langle 110 \rangle_{Al}$ foil orientation. (a) base alloy, (b) 0.15Be.	76
25.	TEM micrographs for alloys aged at 190°C for 2 h. (a) $\langle 100 \rangle_{Al}$ base alloy (3% deformation), (b) $\langle 112 \rangle_{Al}$ base alloy (10% deformation) (c) $\langle 112 \rangle_{Al}$ base alloy, (d) $\langle 112 \rangle_{Al}$ 0.15Be.	77
26.	TEM micrographs and corresponding diffraction patterns for alloys aged at indicated temperatures and times. Foil orientation $\langle 100 \rangle_{Al}$.	80
27.	Angles between S precipitate growth direction and $\langle 100 \rangle_{Al}$ measured from negatives (note each angle includes a 16.5° rotation angle between crystal image and diffraction pattern).	85
28.	Optical micrographs of S phase alloys. (a) S phase, (b) S phase+2%Be.	87

29.	SEM micrographs of S phase alloys. (a) S phase, (b) S phase+2%Be.	88
30.	SEM micrograph from fracture surface of a tensile specimen for the solution treated and quenched 0.15Be alloy.	100
31.	TEM micrographs from tensile specimens aged at 190°C to peak hardness. $\sim\langle 100 \rangle_{Al}$ foils orientation. (a) base alloy, (b) 0.15Be.	104
32.	SEM micrographs from fracture surface of tensile specimens aged at 190°C to peak hardness. (a) base alloy, (b) 0.15Be.	105
33.	SEM micrographs from fracture surface of Charpy-V notch test specimens aged at 190°C to peak hardness. (a) base alloy, (b) 0.15Be.	106

LIST OF TABLES

<u>Table</u>	<u>Page</u>
1. Phases and the corresponding compositions in S phase alloy.	90
2. S phase lattice constants and microhardness.	91
3. Reaction sequence for calculating molar entropy of nucleation of Al ₂ CuMg at 463 K.	94
4. Reaction sequence for calculating molar entropy of nucleation of Al _{1.9} Be _{0.1} CuMg at 463 K.	94
5. Comparison of relative nucleation rates.	97
6. Mechanical properties of the alloys in the solution treated and quenched (A.Q.), and precipitation hardened (P.H.) conditions.	99

I. INTRODUCTION

Precipitation processes are the basis for the control of strength and mechanical properties of age-hardenable alloys by heat treatment. The influence of the precipitates on the mechanical properties of the alloys depends principally on their strength, morphology, size, spacing, as well as by the degree of misfit or coherency and relative orientation relationship of the precipitate with the matrix. Usually, control of the microstructure of precipitation hardened alloys to develop the desired mechanical properties can be exercised through appropriate solution treatment and aging procedures. In addition, microalloying, and thermal mechanical treatment (cold working plus heat treatment), are additional means for improving the mechanical properties of the alloy.

The addition of specific trace elements (microalloying) to Al-base alloys strongly affects the aging response, by changing defect concentrations (vacancies, dislocations), and/or the precipitate composition to increase its nucleation rate. A decrease in vacancy concentration can drastically lower the diffusion rate, and consequently the growth rate of the precipitate. The incorporation of trace elements into the precipitate phase could change the interfacial, strain and volume free energy of formation. The latter, which can be related to the mixing or configurational entropy change for the system, is of particular interest, since the nucleation rate is greatly affected by small entropy changes accompanying the transformation. The purpose of mechanical-thermal treatment is to develop more uniformly

distributed defects to act as nucleation sites for the precipitate, which can then preferentially nucleate heterogeneously.

In the development of the high strength, low density Al-Li base alloys, a shortcoming that still remains to be overcome is their relatively low ductility and fracture toughness, which severely restricts their application in the aerospace industry. In these alloys, the major strength increment derives from the precipitation of the coherent phase, δ' (Al_3Li). But, since this phase is readily sheared by dislocations, which can cause strain localization during deformation, the fracture toughness and ductility of Al-Li alloys are relatively poor. The mechanical properties of these alloys can be significantly improved by precipitation of S' phase (Al_2CuMg) at dislocations, which disperses slip more uniformly for increased ductility [1-6]. However, the precipitation of S' in Al alloys is sluggish [2,4-6], and a pre-aging deformation (stretch) is required to develop the necessary dislocation density for heterogeneous nucleation of S' phase. The stretch operation is often not feasible, e.g. when the final product requires a resolution treatment, and the enhancement of S' nucleation by other means must be explored.

Microalloying can be an effective means for stimulating the nucleation of precipitating phases in Al alloys, e.g. small additions of silicon [7,8] or silver [9,10] stimulates S' precipitation in Al-Cu-Mg alloys. For Al-Li-Cu-Mg alloys, however, the addition of Si results in the formation of the insoluble compound, AlLiSi (or $\text{Al}_2\text{Li}_3\text{Si}_2$), which is reported to be deleterious for the alloy's properties [11-13]. Ag additions to Al-Cu-Mg alloys mainly stimulates the precipitation of metastable T phase, ($\text{Al}_6(\text{Cu,Ag})\text{Mg}_4$), rather than S', which is also shearable by dislocations [14,15].

The addition of small amounts of Be has been shown to significantly improve the age hardening response of Al-Cu [16,17] and Al-Mg-Si [18,19] alloys through an enhanced nucleation rate. The success of Be microalloying in the above alloys suggests that Be may have a beneficial effect on precipitation of S' phase in Al-Cu-Mg or Al-Cu-Mg-Li alloys. Also, it has been reported that no new phases form when Be is added to Al-Li alloys, and that Be has no deleterious effect on the principal strengthening phase, δ' (Al₃Li) [20-22].

In this investigation the effect of Be on the precipitation of S' phase in the pseudobinary Al(α)-S (Al₂CuMg) alloy is studied, using the specific alloy composition* Al-2.5Cu-1.2Mg. The kinetic information is obtained using microhardness and electrical resistivity techniques. Structural and composition changes are determined using X-ray diffraction (XRD), energy dispersive spectrometry (EDS), wave length dispersive spectrometry (WDS), and selected area diffraction (SAD). Precipitate morphology, structure, and orientation relationships are determined using optical, scanning electron microscopy (SEM) and transmission electron microscopy (TEM) techniques. Mechanical properties examined are tensile strength and toughness (charpy). The results obtained are discussed in relation to the effect of Be on the nucleation process and morphology of the S' precipitate in the alloy.

*All compositions are in wt%, or as otherwise noted.

II. LITERATURE REVIEW

A. GENERAL INTRODUCTION TO PRECIPITATION HARDENING

1. Basic Concepts of Precipitation Hardening

In age-hardenable alloys the strength increment derives from the dispersed particles formed by precipitation from supersaturated solid solution. The basic prerequisites for an alloy to be precipitation-hardened are: (i) a limiting solubility that rapidly decreases with temperature, allowing substantial supersaturation when quenching the alloy from a homogenized single-phase region; (ii) precipitation of an (initially) coherent or partly coherent precipitate.

The formation of a precipitate in a supersaturated solution derives from a net reduction in free energy, and thus the essential driving force for a precipitation process is the difference in the free energies of the initial and final configurations of the alloy phases. The basic stages involved in a precipitation process are: i) the formation of stable nuclei of the new phase (nucleation stage), ii) the growth of the new phase nuclei (growth stage), and iii) the coarsening of the precipitate without change in its volume fraction (Ostwald ripening stage). It also often occurs that the equilibrium phase may not precipitate directly i.e., the precipitation process may involve the formation of one or more metastable transition phases, for example: Guinier and Preston (GP) zones, θ'' , and θ' as precursors

of θ phase (Al_2Cu) in the Al-Cu system; and GPB zones and S' as precursors of S phase (Al_2CuMg) in the Al-Cu-Mg system. Metastable phases are partially or fully coherent with the matrix, and form when the atomic fit between the precipitate and matrix is good and results in a lower interfacial energy. There is always a particular orientation-relationship between the precipitating and parent phases that minimizes the interfacial energy. The precipitation sequence, and the corresponding mechanism for each stage of transition depends on the particular alloy system and on aging temperature. The effect of precipitation on strength and mechanical properties of alloys depends on the nature of the precipitates, i.e. their morphology, density, distribution, size and orientation relationships with matrix.

2. Nucleation from Supersaturated Solid Solution

Nucleation is the process by which the smallest stable particle of a new phase is formed within a parent phase. During this process the energy change consists of: i) a decrease in the volume free energy due to the formation of a more stable phase, ii) an increase in the interfacial energy due to the creation of interphase boundary, iii) elastic strain energy arising from any change in volume accompanying the structural change, and iv) lattice strain energy associated with the lattice distortion or misfit produced by partial or complete coherency between the two lattices.

The classical nucleation theory was originally developed by Volmer and co-workers [23,24] and Becker and Döring [25] for condensation from vapors. Turnbull and Fisher [26] extended Volmer's theory to solid state phase transformations, and Servi and

Turnbull's [27] investigation of precipitation in Cu-Co alloys provided the classic test of homogeneous nucleation theory in metallic solids. The subject of solid-state nucleation has been comprehensively reviewed by several authors, e.g. Kelly and Nicholson [28] in 1963, Christian [29,30] in 1965 and 1975, Nicholson [31] in 1970, Russell in 1970 [32], Aaronson, Lee and Russell [33] in 1976, and Russell [34] in 1980.

(a) Classical Nucleation Theory-Strain Free System

For a stable nucleus to form the interfacial energy barrier must be overcome by the decrease in the volume free energy of transformation. In the absence of strain energy, the free energy change (ΔG) for the formation of a spherical embryo of radius r is given by [26]

$$\Delta G = \frac{4}{3}\pi r^3 \Delta G_v + 4\pi r^2 \gamma \quad (1)$$

where ΔG_v and γ are the volume free energy change and the interfacial energy respectively. Minimizing Eq. (1) with respect to "r" gives for the free energy of formation of a critical-sized embryo

$$\Delta G^* = \frac{16\pi\gamma^3}{3\Delta G_v^2} \quad (2)$$

The resulting homogeneous nucleation rate, which is proportional to the density of critical-sized embryos and the diffusion rate across the embryo's boundary, is then expressed as

$$\dot{N}_{\text{homo}} = K \exp\left[-\frac{16\pi\gamma^3}{3\Delta G_v^2 kT}\right] \quad (3)$$

where the parameter K includes the embryo surface concentration of atoms, and the jump frequency for the atom across the interface, which has exponential dependence on the activation energy for the jump process.

The volume free energy of transformation ΔG_v is related to the volume entropy change (ΔS_v) and the degree of undercooling ΔT by

$$\Delta G_v = -\Delta S_v \Delta T \quad (4)$$

so that the nucleation rate becomes

$$\dot{N}_{\text{homo}} = K \exp\left[-\frac{16\pi\gamma^3}{3(\Delta S_v)^2 (\Delta T)^2 kT}\right] \quad (5)$$

Eq. (5) shows that the nucleation rate is exponentially dependent on the square of the undercooling and entropy change for the transformation (referred to as nucleation entropy), so that small increases in entropy or undercooling can have very large effects on the nucleation rate.

(b) Nucleation Involving Strain Energy

The above treatment of nucleation is applicable only to phase transformations for which the strain energy due to volume change is negligible, e.g. in liquid-solid transformations. In solid state transformations, however, strain energy usually results from the associated volume changes, which must be included in the free energy of nuclei formation, i.e.

$$\Delta G = V(\Delta G_v + W) + A\gamma \quad (6)$$

where V is the volume of the new phase, A the interface area and W the strain energy per unit volume of precipitate.

The strain energy arises from two sources [35]: (i) the strain caused by whatever misfit exists between the two coherent phases before the precipitate has grown to a sufficient size to induce a dislocation to take up the distortion (e.g. GP zones), and (ii) the strain due to the different specific volumes of the matrix and precipitate. Local strains around a precipitate will produce large energy increases if the strain is taken up elastically, since elastic moduli of metals are large. For example, Doherty [35] shows that in aluminum (Young's modulus ~ 70 GPa), a 1% shear strain results in an elastic energy of 3.5 MJ/m^3 ($\sim 35 \text{ J/g-atom}$), and a 5% deformation gives an energy 25 times larger. This energy can be reduced plastically by the introduction of dislocations into the interface at the expense, however, of raising the interfacial free energy. A dilational type of elastic strain can be relaxed plastically, by dislocation motion, or by diffusional motion of point defects. Strain energy release mechanisms operate easier at higher temperatures, especially where motion of point defects are involved.

Lee et al. [36,37] have reviewed the results of current theoretical and experimental

studies on the influence of elastic and plastic strains on precipitation in general, and nucleation in particular. For the elastic situation, the detailed theoretical analysis shows that the elastic energy is minimized when the precipitate is formed with a thin disc- or plate-like shape, as originally proposed by Nabarro [38].

The type of strain energy is closely related to the morphology of the precipitate, and models to analyze strain energy effects have been developed separately on this basis. The models are generally divided into two groups according to the type of precipitate/matrix interface, incoherent or coherent.

(1) Incoherent nucleation

An incoherent interface is one across which there is no crystallographic continuity. In such a case, the strain associated with the formation of an embryo in a crystalline lattice is hydrostatic [39], and this problem has been considered by Nabarro [38], who proposed a general equation that includes the effect of the shape of the nucleus formed in the elastically isotropic matrix. For oblate and prolate spheroidal particles (with semi axes r and c), the strain energy per unit volume is expressed as

$$W = \frac{2}{3} \mu_m \left(\frac{\Delta V}{V} \right)^2 f\left(\frac{c}{r}\right) \quad (7)$$

where μ_m is the shear modulus of the matrix, $\Delta V/V$ is the fractional volume change in the matrix accompanying the transformation, $f(c/r)$ is a function of particle shape, which is

unity for a sphere ($c/r=1$), 0.75 for a rod ($c/r \gg 1$), and $3\pi c/4r$ for a thin plate ($c/r \ll 1$). Thus the strain energy is minimum when the precipitate is of a plate-like shape and approaches zero as c/r decreases to zero. For an oblate spheroid ($c/r \ll 1$, $V=4/3\pi r^2 c$, $A=2\pi r^2$, $f(c/r)=3\pi c/4r$), the free energy of formation of a critical-sized embryo (nucleus) becomes [40]

$$\Delta G^* = \frac{8\pi^3 \mu_m^2 \gamma^3}{3\Delta G_v^4} \left(\frac{\Delta V}{V} \right)^4 \quad (8)$$

(2) Coherent nucleation

For a coherent interface, the crystallographic planes of matrix and precipitate, i.e. the atomic configurations and spacings, are identical or very nearly identical. A theoretical analysis of the elastic strain energy associated with an ellipsoidal coherent precipitate in an isotropic matrix was first presented by Eshelby [41,42]. Lee *et al.* [43,44] extended Eshelby's treatment to the general anisotropic case, and showed that the free energy is minimized when the particle is an oblate ellipsoid, for which

$$\Delta G = \frac{4}{3} \pi r^3 \beta [\Delta G_v + W] + \pi r^2 \gamma [2 + g(\beta)] \quad (9)$$

where $\beta=c/r$ is the ratio of the ellipsoid's semi-minor to semi-major axes. The function $g(\beta)$ is given by

$$g(\beta) = \begin{cases} \frac{2\beta^2}{\sqrt{1-\beta^2}} \tanh^{-1}(\sqrt{1-\beta^2}) & \text{when } \beta < 1 \\ 2 & \text{when } \beta = 1 \\ \frac{2\beta}{\sqrt{1-\beta^{-2}}} \sin^{-1}(\sqrt{1-\beta^{-2}}) & \text{when } \beta > 1 \end{cases} \quad (10)$$

In order to find the ΔG^* , ΔG is minimized with the respect to both r (for r^*) and β (for β^*) to give

$$\Delta G^* = \frac{\pi\gamma^3 [2 + g(\beta^*)]^3}{12 (\beta^*)^2 (\Delta G_v + W)^2} \quad (11)$$

The strain is a function of the aspect ratio, and for the anisotropic case varies markedly with the orientation relationship between matrix and precipitate. The analysis of ΔG^* indicates that the minimum value of ΔG^* is obtained at $\beta=1$, i.e., the spherical nucleus, until $(W/|\Delta G_v|) > 0.82$. So the critical free energy of formation of a spherical embryo is obtained by substituting $\beta=1$ and $g(\beta)=2$ into Eq. (9), to give

$$\Delta G^* = \frac{16\pi\gamma^3}{3 (\Delta G_v + W)^2} \quad (12)$$

(c) Nucleation at Defects (Heterogeneous)

It is well known that defects, such as grain boundaries, dislocations, stacking faults, etc., are effective catalysts for nucleation of precipitates under certain circumstances [45-

48]. The energy of formation of the nucleus in the heterogeneous nucleation situation is reduced due to a reduction in interfacial and/or strain energies. For nucleation on grain boundaries, part of the boundary area is eliminated for a net reduction of interfacial energy. When there is an appreciable volume strain energy associated with nucleation, transition phases will nucleate preferentially at dislocations if there is a net reduction in the volume strain energy [49,50]. Nucleation at dislocations can be incoherent [48,51] or coherent [52-54], and in both cases, the associated volume strain energy may be reduced. Actually, most intermediate precipitates appear to nucleate either on dislocations or on pre-existing GP zones [55,56]. Nucleation involving dislocations may occur in four relatively different ways [34]:

- (1) Formation of an incoherent particle on the dislocation line, so as to release the strain energy of the latter and to make additional contributions to the free energy available to aid the nucleation process.
- (2) Formation of a coherent particle near a dislocation, where the transformation strain is already provided, to minimize the volume strain energy of the nucleus.
- (3) Formation of a semicoherent particle in contact with the dislocation, with the direction of worst misfit aligned parallel to the Burgers vector. This arrangement allows a maximum release of strain energy and uses part of the dislocation core energy for creating the incoherent interface.
- (4) Nucleation on the stacking fault between two partial dislocations. In addition to being a high energy region, the stacking fault represents a thin layer of material of a different crystal structure.

In the heterogeneous nucleation case where substrates reduce only the interfacial energy for the formation of a nucleus, the substrate effect on the free energy is taken into account by the contact angle function $f(\theta)$ at the nucleus/substrate interface, where

$$\Delta G_{hoc}^* = \frac{16\pi\gamma^3}{3\Delta G_v^2} f(\theta) = \Delta G^* f(\theta) \quad (13)$$

and

$$f(\theta) = \frac{(2 + \cos\theta)(1 - \cos\theta)^2}{4} \quad (14)$$

(d) Refinement of Precipitates

Refinement of structure is often the principal means for improving the mechanical properties of precipitation-hardenable alloys, and the nucleation rate is the controlling factor in precipitate refinement. The mechanisms for enhancing the nucleation rate can be related to the general equation for the heterogeneous nucleation rate

$$\dot{N}_{hoc} = Ke^{-\frac{\Delta G^*}{kT}} f(\theta) \quad (15)$$

where, as in the case for homogeneous nucleation, the parameter K includes the embryo surface concentration of solute atoms and the jump frequency for the atom, which has exponential dependence on the activation energy for atom transfer across the interface. It

is evident that nucleation rate can be increased by either decreasing the activation energy for the atom transfer process, which is related to the point defect concentrations at the precipitate/matrix interface, or reducing the free energy of formation for a stable nucleus, ΔG^* . For heterogeneous nucleation, the change in the number and distribution of available defects, which act as nucleation sites, is an important factor for influencing the nucleation rate.

The highest rate of nucleation corresponds to the smallest possible ΔG^* . It is evident that any change in one or more of the parameters determining ΔG^* , i.e. interfacial energy, strain energy, and volume free energy will strongly affect the nucleation rate because of its exponential dependency on ΔG^* . Two methods used to refine structure in alloys through the nucleation process are microalloying and thermal-mechanical processing.

(1) Effect of trace elements

The mechanisms by which trace additions of microalloying elements may affect nucleation, as outlined by Polmear [57,58], are:

(i) Trace elements may interact with vacancies, leading to a change in the vacancy availability, distribution, or condensation. Any change in one or more of these characteristics will significantly affect the rate of lattice diffusion of substitutional elements and the kinetics of the precipitation. The reported marked effects of small amounts of cadmium, indium and tin in reducing the rate of GP zone formation in Al-Cu alloys may be attributed to this type of solute-vacancy interaction [59-70]. Trace element additions may also affect the nature of precipitate free zones (PFZs). Polmear [71] has shown that

a small addition of Ag to the Al-Zn-Mg system markedly refines the precipitation of the η' phase ($\text{Al}_2\text{Mg}_3\text{Zn}_3$), and significantly reduces the width of the PFZs. This is attributed to the interaction between silver atoms and vacancies, with the latter being retained within the matrix by the Ag atoms, rather than migrating to the grain-boundary sink.

Trace elements may also prevent vacancy condensation for vacancy loop formation, which would otherwise serve as nucleation sites for heterogeneous nucleation. It has been shown that the addition of Li to Al-Cu-Mg alloy markedly reduces the number of dislocation loops due to the high Li-vacancy binding energy [2-6], and renders the precipitation of S' phase sluggish.

(ii) Trace elements can modify the interfacial energy (γ) between a precipitate and the matrix, and thereby affect the precipitate morphology and nucleation rate (c.f. Eq. (3)). The most well known and applied example of this effect is the modification of the Si particles in Al-Si alloys by trace additions of Na or Sr. Stewart and Martin [72] have shown that the plate-like Si particles in Al-Si alloy can also be modified to an equiaxed shape by Cu addition, which they attributed to the decreased growth rate of the Si particles when Cu is added.

(iii) Trace elements can change the free energy relationships in an alloy system, so that precipitation of a different phase is favored. Vietz and Polmear [73] have shown that the addition of approximately 0.1at% Ag to an Al-Cu-Mg alloy induces homogeneous nucleation of the ternary compound ($\text{Al}_6(\text{Cu,Ag})\text{Mg}_4$) instead of the usual GP zone and S'

formation. This type of effect could not arise through an interaction between Ag atoms and vacancies alone, and requires an interaction between Ag atoms and Mg atoms also. In a computer calculation of the Al-Ti-Be system, Youdelis and Fang [74] have shown that the addition of as little as 0.1at%Be to an Al-0.2at%Ti alloy greatly restricts the mutual solubility of Be and Ti in Al. The thermodynamic calculations show that the early precipitation of $TiBe_{12}$ is favored, which may then act as preferred nucleation sites for other active precipitates in precipitation hardening alloys, e.g. the Be-enhanced precipitation of $TiAl_3$ and induced age hardening in Al-0.2Ti alloy [75]. The decreased solubility of Ti in Al would also increase the nucleation entropy and nucleation rate for $TiAl_3$, which may also be a contributing factor for the observed refinement of the $TiAl_3$ particles when Be is added.

(iv) Trace elements may segregate to grain boundaries and inhibit discontinuous precipitation. Martin [76] reports that when Cu-Be alloys are aged, after the initial formation of coherent zones of CuBe, the precipitation process proceeds by a discontinuous mechanism, in which cellular grain-boundary precipitates grow at the expense of the zones with associated grain-boundary migration. This combined precipitation and recrystallization process, which leads to the formation of a relatively coarse dispersion of an intermetallic phase, is associated with a dramatic fall in hardness. However, for commercial beryllium bronzes, which contain 0.2% of Ni or Co in addition to 1.9%Be, Ni and Co evidently segregate preferentially to the grain boundaries and inhibit the discontinuous precipitation process, allowing a higher peak hardness to be obtained.

(v) Trace elements may be incorporated into the precipitating phase to modify the thermodynamic properties such as surface energy, strain energy and volume free energy of the precipitating phase [16,17].

(2) Effect of thermal-mechanical treatment

A prior aging plastic deformation increases the defect population within the alloy matrix, and provides sites for heterogeneous nucleation. This would increase the density of precipitate particles in grain interiors, and decrease the tendency for forming PFZs at grain boundaries. When a supersaturated and plastically deformed alloy is aged at higher temperatures, the effectiveness of the defects depends on the rate of recovery of the dislocation substructure. If the alloy recrystallizes before precipitation commences, the deformation stage will be of little or no value. The order of occurrence of precipitation and recrystallization in solution treated and cold-worked alloy has been considered in detail by Köster [77].

(3) Other factors

Solute concentration, solution treatment temperature, quenching rate and thermal history (duplex aging) are also factors that influence precipitation processes of age-hardenable alloys. An increase in solute content will increase the driving force for precipitation. Generally, higher solution treatment temperatures and quenching rates lead to higher supersaturation in the matrix for solutes and point defects (vacancies), which affects the

diffusion rate of solute atoms, and the extent of vacancy condensation to form heterogeneous nucleation sites. All of these factors greatly influence the subsequent precipitation processes. Duplex aging, in which an alloy is aged below and then above the solvus temperature for GP zone formation, is also utilized to improve the microstructure and mechanical properties of age-hardened alloys. At lower aging temperatures, the supersaturation (driving force) for nucleation is higher, but the low atomic mobility results in a lower overall transformation rate. However, the structure developed at lower aging temperatures may contain a higher density of nuclei or pre-precipitation zones. When an alloy is first aged at low temperature, and then aged at higher temperatures, a higher density and more uniform distribution of precipitates may be developed, based on the structure obtained at lower aging temperature.

(e) Relation of Nucleation Entropy to Nucleation Rate

The entropy change during nucleation was first considered by Youdelis [78,79], to account for the variation of undercooling with composition of binary alloys during solidification [78], and the enhanced grain refinement of Al-Ti alloys obtained when microalloyed with Si [79] and Be [80]. It was shown that the refinement could be related to the increase in the magnitude of nucleation entropy (ΔS_v), and thereby the nucleation rate (c.f. Eq. (5)).

Youdelis [78] derived expressions for the nucleation entropy for the binary alloy phases having regular solution behavior. The molar entropy of nucleation is separated into the entropy change due to freezing of the pure components (ΔS_F), and the change in the

configurational or mixing entropy for the solid/liquid system resulting from the precipitation of the solid phase (ΔS_M), i.e.

$$\Delta S = \Delta S_F + \Delta S_M \quad (16)$$

where

$$\Delta S_F = N_1^s (S_1^s - S_1^l) + N_2^s (S_2^s - S_2^l) \quad (17)$$

and

$$\Delta S_M = -R \left[N_1^s \ln \left(\frac{N_1^l}{N_1^s} \right) + N_2^s \ln \left(\frac{N_2^l}{N_2^s} \right) \right] \quad (18)$$

In the above equations, the N's refer to the mole fractions, the S's to the molar entropies, the subscripts 1, 2, to the components, the superscripts s, l, to the solid and liquid phases respectively.

The extension of Eq. (15) and (16) to the multicomponent system is straightforward and is obtained by including terms for all components in the system to give [79]

$$\Delta S_F = \sum_{r=1}^n N_r^s (S_r^s - S_r^l) \quad (19)$$

and

$$\Delta S_M = -R \sum_{r=1}^n N_r^s \ln \left(\frac{N_r^l}{N_r^s} \right) \quad (20)$$

where N_r^s and N_r^l refer to the mole fractions of the r th component in the solid and liquid phases respectively, and S_r^s and S_r^l are the molar entropies of the r th component in the pure solid and liquid states respectively at the nucleation temperature.

The application of Eq. (17) and (18) to simple binary eutectic systems shows that ΔS_M is always negative, and $|\Delta S_M|$ increases with increasing separation of solidus and liquidus lines, and for a eutectic alloy is maximum at the eutectic composition. It follows that the nucleation rate (and thus grain refinement) should increase with solute concentration for a binary eutectic system. Moreover, that the tendency for nucleation and precipitate refinement should be particularly strong in alloys precipitating intermetallic compounds, since the concentration effect on the alloy's dilute components and the resulting ΔS_M is large.

The behavior of ΔS_F and ΔS_M for the multicomponent system is similar to that for the binary system, i.e., both ΔS_F and ΔS_M are always negative, and $|\Delta S_M|$ increases with difference in composition between solid and liquid phases. For the multicomponent system $|\Delta S_M|$ will also increase with the number of components present in the system. This is so particularly for the precipitation of intermediate compounds or phases of limited solubility range, when only the principal component (solvent, 1) is concentrated in the liquid phases ($N_1^l > N_1^s$), and the remaining minor components (solutes 2, 3, ..., n) are concentrated in the solid phase ($N_r^l \ll N_r^s$, $r=2,3,\dots,n$), so that only the first term in Eq. (20) is positive (decreasing $|\Delta S_M|$), while the remaining terms are negative. In general, since a redistribution of all components necessarily occurs during the nucleation of the primary phase or intermediate compound in the liquid alloys, it follows that the nucleation entropy

and corresponding nucleation rate (other factors being equal) increase with the number of components comprising the alloy system.

Compound formation usually involves a high concentration of one or more components present in dilute concentrations in the alloy, e.g. Ti in TiAl_3 in dilute Al-Ti alloys, so nucleation entropy is particularly significant in precipitation of intermediate compounds. Youdelis [79] has developed a method for determining the nucleation entropy of intermediate compounds, or phases of limited solubility, which do not have regular solution behavior. For a pure metal, $\Delta S_v (= \Delta H_v/T)$ is readily calculated. In a two (or more) phase alloy system, ΔS_v is more difficult to obtain for the precipitation of a phase due to redistribution of solute between the phases, and the general nonideality of the system. The problem is solved in two stages: first, regular solution behavior is assumed for both phases, for which the nucleation entropy is readily formulated. Then the regular solution constraint is removed by a suitable combination of reactions that includes the compound formation reaction and (known) formation entropy.

The role of nucleation entropy in determining the nucleation rate and the degree of structure refinement has been confirmed in several investigations [16-19,79-85]. The enhanced grain refinement of Al-Ti alloys by third element addition of Si or Be has been attributed to the concentration of Si or Be in the peritectic compound TiAl_3 [79-83], which increases the nucleation entropy and nucleation rate of the compound, and which subsequently undergoes the peritectic reaction to form the Al grains [86].

The nucleation entropy theory has also been successfully applied to account for the refinement of carbides in Co-base (HS21) superalloy by small additions of Ta and Nb

[84]. It is shown that when Ta or Nb is added to the superalloy, the primary $M_{23}C_6$ -type carbide, with an approximate stoichiometric formula $(Cr_{0.77}Co_{0.15}Mo_{0.08})_{23}C_6$, is replaced by the MC-type carbides, TaC or NbC, which have significantly higher nucleation entropies and rates than the $M_{23}C_6$ carbides.

In a similar study of Ni-base superalloy (713C), the addition of Ta or Nb did not alter the basic MC type structure of the primary carbides in the alloy $(Nb_{0.77}Ti_{0.23})C$ [85], and the small replacement of Ti in the carbide by Ta or Nb that resulted did not significantly change the nucleation entropy or nucleation rate. The experimental results showed no refinement of the primary carbides in the Ni-base alloy by the Ta or Nb addition, in agreement with the nucleation entropy theory.

Youdelis and co-workers have shown that small additions of Be markedly enhance the refinement and precipitation of θ' (Al_2Cu) in Al-Cu [16,17] and β' (Mg_2Si) in Al-Si-Mg alloys [18,19]. An analysis of the kinetic data showed the refinement of the precipitate particles, and increased precipitation rate, is the result of a Be-enhanced nucleation rate. It was proposed that the increased nucleation rate of θ' in the Al-Cu alloy may be attributed to the concentration of Be in the $CuAl_2$ precipitate [87], which increases the nucleation entropy and the corresponding nucleation rate for the precipitate [88]. A recent study [89] of the effect of Be on the quasi-binary Al-Mg₂Si alloy system shows that some Be is incorporated into Mg_2Si (~2 at%), and also significantly decreases the solubility of Si in Al(α) solid solution. Both factors contribute to an increase in the nucleation entropy and nucleation rate, to which the refinement of Mg_2Si may be attributed.

3. Kinetics of Precipitation Processes

The kinetics of precipitation and growth involving diffusion is generally described using the Avrami or Johnson-Mehl equation [90,91]

$$X = 1 - \exp(-kt^n) \quad (21)$$

where X is the fraction of supersaturated solute precipitated at time t from the solution with a constant number of growth centers, n is the growth constant determined by the growth mechanism and precipitate morphology, and k is a parameter related to nuclei density (N_0) given by [92]

$$k = a [N_0 r_f^3 D]^{\frac{3}{2}} \quad (22)$$

where r_f the final mean radius of the particle, D the solute diffusion coefficient, and a constant.

The rate of a precipitation reaction for soft impingement, i.e., when precipitate growth is diffusion controlled, and the diffusion fields around adjacent particles overlap, can be described using Eq. (21). Resistivity [17,18] and differential scanning calorimetric [DSC] techniques [93] are methods frequently used to study the kinetics, and to obtain activation energies and other kinetic parameters.

Specific resistivity data obtained from precipitation processes can be converted to fraction transformed (X) using the relationship [17,18]

$$X = \frac{\rho_0 - \rho_t}{\rho_0 - \rho_\infty} \quad (23)$$

where ρ_t , ρ_0 and ρ_∞ are the resistivities at time t , and initial and final (transformation completed) times, respectively.

The slope and coordinate intercepts in a $\log \ln[1/(1-X)]$ vs. $\log t$ plot will give the n and k parameters in Eq. (21) respectively. The activation energy for the precipitation process is obtained from an Arrhenius plot of the fraction transformed, i.e. from the plot of $\ln(dX/dt)_{X=0.5}$ vs. $1/T$, where T is absolute temperature.

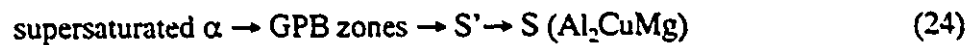
Precipitation is a complex process involving several stages (nucleation, interfacial reactions, diffusional growth), and the kinetic analysis using the Avrami equation will usually not identify the exact mechanisms or rate controlling stages. However, where the transformation follows the Avrami equation, the kinetic parameters obtained are useful in postulating precipitation models that may be amenable to confirmation by other experimental techniques.

B. PRECIPITATION OF S PHASE (Al₂CuMg) IN Al-Cu-Mg ALLOYS

Aluminum alloys containing copper and magnesium in Cu:Mg weight ratios ranging from 2.2:1 to 7:1 form the basis of several commercially important age-hardening alloys (e.g. AA2024 and RR58 (D.T.D.5070A)). The strengthening of these alloys is associated with the presence of coherent (GPB) zones and finely dispersed, partially-coherent

precipitates: S' (Al₂CuMg) for the pseudobinary alloys (2.2:1), and both S' and θ' (Al₂Cu) for the alloys with higher Cu:Mg weight ratios [94,95].

The pseudo-binary system Al(α)-Al₂CuMg(S) (c.f. Fig. 1(a)) forms part of the ternary Al-Cu-Mg system (c.f. Fig. 1(b)), and its alloys are capable of developing high strength and retaining their strength at relatively high temperatures [94,73]. Early studies on the ageing behavior of this system were carried out by Hardy *et al.* [94] and Silcock [95]. The precipitation sequence in the dilute alloys systems is described as



It is interesting to note that Rhodes and Garrmang [97] propose a different sequence for precipitation in Al(α)-S alloys of eutectic composition (Al-33.1Cu-6.25Mg), with the S' forming first followed by GPB zones and finally the equilibrium S phase.

The nucleation and refinement of the S' phase is enhanced by plastic deformation (which increases the dislocation density), which increases the peak hardness values of the aging curves [9]. It has been shown that small additions of Ag [10] or Si [8] also increase the nucleation rate and refinement of the S' precipitate, with attendant increases in the peak hardnesses for the aging curves.

Youdelis and co-workers [16-19] have shown small additions of Be to be highly effective in accelerated precipitation in Al alloys through the nucleation mechanism. The Be-enhanced nucleation and refinement of θ' in Al-3.0Cu alloy [16,17], and β' in the natural aging Al-0.75Mg-0.5Si alloy [18,19], with corresponding improvements in alloy's

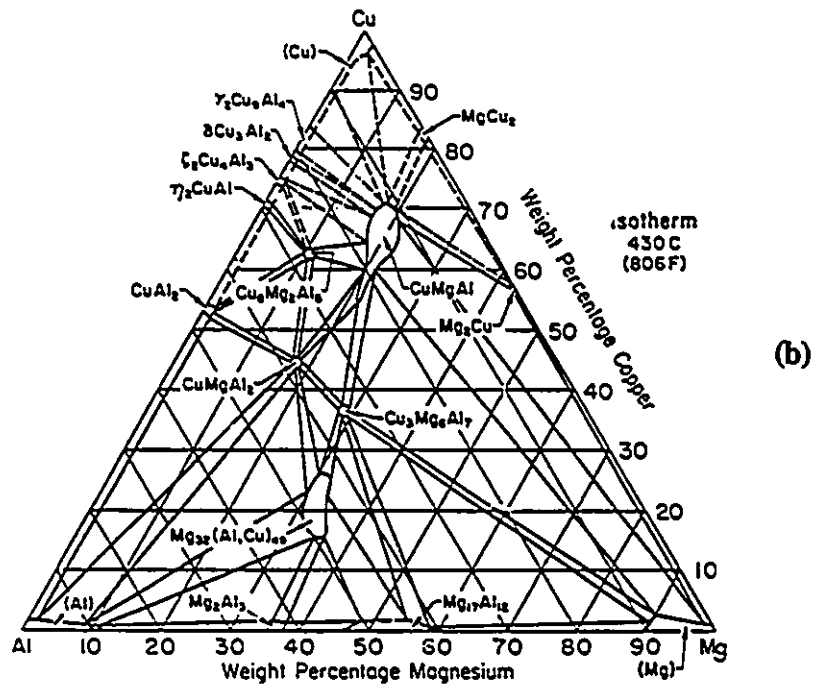
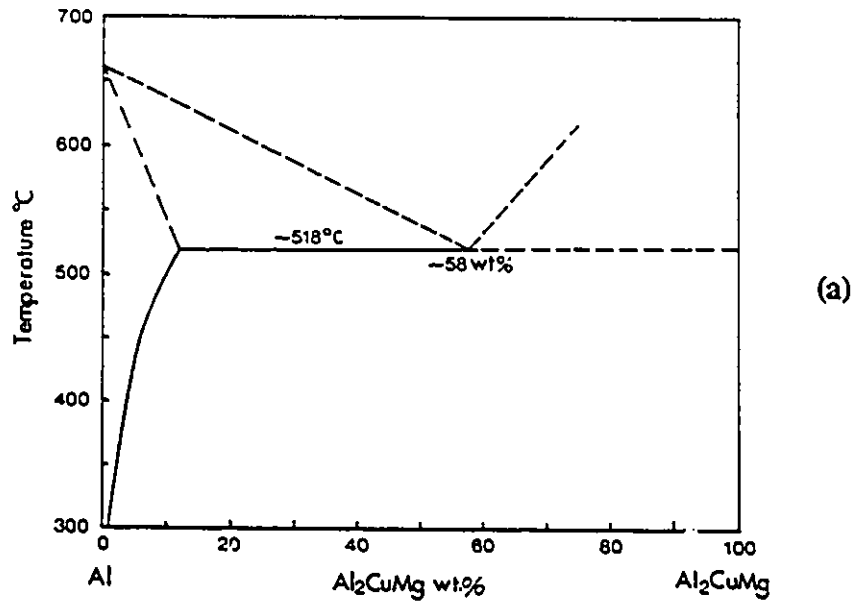


Fig.1. (a) Al(α)-S(Al_2CuMg) pseudo-binary (estimated from data published in ref. 96), (b) Al-Cu-Mg isotherm at 430°C [96],

age-hardening responses, suggests that Be may also have a beneficial effect on precipitation in Al-Cu-Mg alloys. The Al-Be system (c.f. Fig. 2) is a simple eutectic with limited solubility of Be in Al solid solution. The solubility of Be in Al(α) (maximum 0.1% at eutectic temperature 644 °C) decreases rapidly with decreasing temperature is the result of a large positive activity coefficient for Be in Al [74], which is conducive to combination with other alloying elements for precipitation as Be compounds.

1. Structural Aspects of the Precipitating Phases

(a) GPB zones

Two types of zones can be formed in Al-Cu-Mg alloys depending on the alloy compositions. For pseudo-binary Al-S alloys, Lambot [99] and Bagaryatsky [100,101] obtained diffuse X-ray scattering in alloys aged at room temperature, which was attributed to rod-like zones along $\langle 100 \rangle$ matrix direction. This was also confirmed by Silcock [95] using single crystal X-ray methods, who termed the structures GPB (rather than GP) zones because their connection with S phase was questionable. This designation is arbitrary, however, since the same argument could be used concerning the relationship of GP zones to θ phase in Al-Cu alloys. For alloys of high Cu:Mg ratio ($\sim 3:1$), Silcock [95] reports a different type of GP zone formation, that is very similar to the GP zones found in Al-Cu alloys, although the formation kinetics are somewhat altered by the presence of the Mg atoms. The nature of GPB in the pseudo-binary alloys is still ambiguous. It appears in alloys having equal amounts of Cu and Mg, but is more stable in the Cu-rich alloys [95].

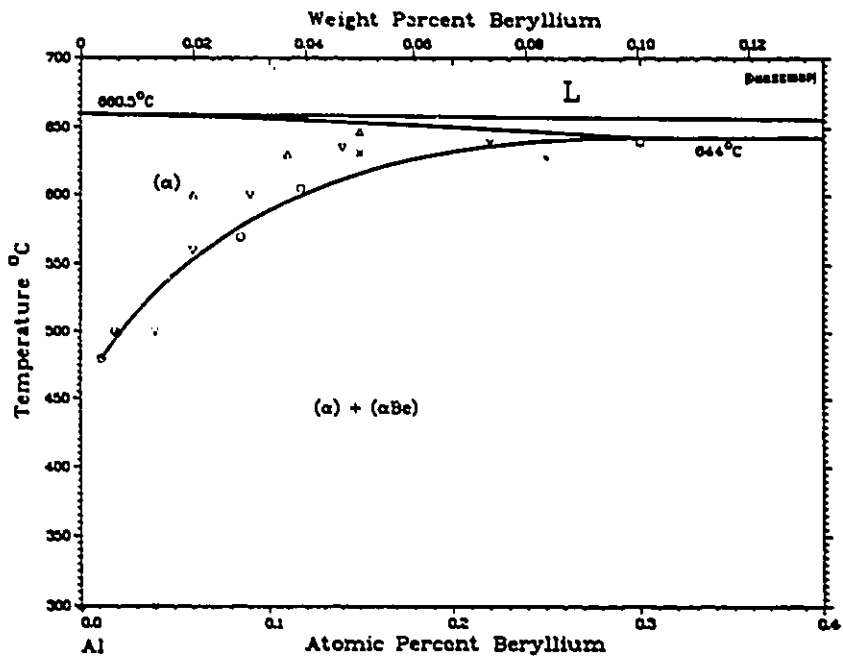


Fig. 2. Al-Be phase diagram [98].

Bagaryatsky [101] proposed GPB zones are clusters of atoms composed of 1 Cu, 1 Mg and several Al atoms. Gerold and Haberkorn [102] consider the structure to be small spherical zones (about 16 Å diameter) containing ordered Cu and Mg planes parallel to a $(100)_{Al}$ plane, with a CuAlI type tetragonal lattice. Based on detailed X-ray diffraction pattern studies, Silcock [95] suggested that GPB zones are rich in copper, probably approximating the intermetallic compound $Mg_2Al_5Cu_3$ in composition, and that the zone structure can be roughly indexed as a face centered tetragonal cell with $a=b=5.5$ Å and $c=4.04$ Å. The dimensions of the resultant cylindrical-shaped zone are 40-80 Å length by 10-20 Å diameter. A more recent report by Alekseyev and co-workers [103] suggests the zone structure is the same as that for the equilibrium S phase.

(b) S' Intermediate Phase

The intermediate S' phase is the partially coherent precursor of the S phase, and was shown by Bagaryatsky [100,101] and Silcock [95] to have an orientation relationship with the aluminum matrix of $[100]_{S'} \parallel [100]_{Al}$; $[010]_{S'} \parallel [021]_{Al}$; $[001]_{S'} \parallel [012]_{Al}$. Wilson and Partridge [104], using electron diffraction, determined S' to be orthorhombic, with $a=4.04$ Å, $b=9.25$ Å and $c=7.18$ Å. They reported that the S' precipitate in Al-2.5Cu-1.2Mg alloy was heterogeneously nucleated on loops and dislocations, and grew as laths on $\{210\}_{Al}$ in $\langle 100 \rangle_{Al}$ directions. Precipitation sheets were formed at dislocations by growth and contact of the $\{210\}_{Al}$ laths with a common $\langle 100 \rangle_{Al}$ direction, resulting in the formation of corrugated-like precipitate sheets on $\{110\}_{Al}$. Gupta *et al.* [105] reported another habit form for S' precipitates, viz., rod-like precipitates that align in the $\langle 100 \rangle_{Al}$ directions with

a tendency to cluster on $\{110\}_N$ planes. Gregson and coworkers [4,106] reported homogeneous nucleation of S' could be induced in Al-Li alloys by varying the Cu and Mg content. The morphology for S' was either rod-like or lath-like. Gupta *et al.* [105] showed that the precipitate morphology depends on the net solute concentration of Cu+Mg, and for relatively dilute alloys only rods can be formed. Radmilovic *et al.* [107] reported both rod-like and lath-like precipitates formed at the same subgrain boundary, and attributed this to the change in the subgrain boundary orientation. The exact relationship between GPB and S' still remains to be determined. Flower and Gregson [6] suggested that Cu and Mg rich clusters in Al matrix may act as nucleation sites to cause continuous nucleation for S', and this was confirmed by Badmilovic *et al.* [107] using high resolution electron microscopy images. According to Bagaryatsdy [100,101], GPB zones do not act as nuclei for the S' phase. However, Weatherly [108] provided strong evidence to show that the nucleation of S' is associated with GPB zones.

(c) S phase

The structure of S phase was determined by Perlitz and Westgren [109] in 1943. It has an orthorhombic crystal structure (Cmcm space group) and an orientation relationship to the matrix similar to the S' phase, with only slightly different lattice parameters, $a=4.00 \text{ \AA}$, $b=9.23 \text{ \AA}$, $c=7.14 \text{ \AA}$. The similarity of the S and S' phases is the reason for much of the disagreement in identification of the phases. Weatherly and Nicholson [110] studied the loss of coherency of lath-shaped precipitates in Al-2.7Cu-1.36Mg aged at 325 °C for 24 hours. They found that the laths lost coherency by first attracting dislocations to the

lath/matrix interface, followed by the formation of an array of loops with Burgers vectors of the type $a/2[101]$ spaced along the length of the lath. The average spacing of the loops was 260 Å, which was compared to the calculated value of 170 Å for total relief of the misfit. Gupta *et al.* [105] suggested that the confusion in the identification of precipitates in Al-Cu-Mg alloys may be due to the difficulty in unambiguously interpreting the diffraction patterns, since the electron diffraction patterns from these alloys are quite complex due to the 12 possible orientations of S' or S with the Al matrix. Regarding this complexity, Gupta *et al.* [105] examined the Al-1.53Cu-0.79Mg alloy aged at 190 °C by selected area diffraction (SAD), and showed that the S' phase is only the slightly strained version of the equilibrium S phase. Based on the electron microscopy results reported by Weatherly [108], Wilson [7] suggested that the difference between S' and S phase is probably the result of orientation, and not due to a difference in crystal structure.

2. Aging Behavior and Factors Affecting Precipitation of S' Phase

The aging process of S' phase is quite complicated and the related mechanisms are not well understood. The first age hardening studies on S' phase alloys were those of Hardy [94] and Silcock [95]. Hardy showed that significant age hardening can be obtained at various aging temperatures for alloys containing Cu:Mg ratios of 2.2:1 and 7:1. Silcock used single crystal X-ray methods to relate the structural changes to the hardness for two Al-Cu-Mg alloys with Cu:Mg ratios of 7:1 and 2.2:1. For the pseudo-binary alloys with Cu:Mg ratio of 2.2:1, Silcock reported that GPB zones are able to cause considerable

hardening of the matrix without sensitivity to the details of zone size or degree of ordering. Maximum response to hardening is attained with the presence of partially coherent S' precipitates and coherent GPB zones, but a decrease in hardness results on further aging.

Jena *et al.* [93] have studied the kinetics and obtained the relative kinetic parameters for the precipitation in an Al-1.53Cu-0.79Mg alloy using the DSC method. Their results showed that the formation of GPB occurs in the temperature interval 25 to 170 °C, with an activation energy of 55.6 kJ/mole, which is close to the value of 64.0 kJ/mole reported by Horiuchi and Minonishi [111] using resistivity measurements for the Al-4.2Cu-1.4Mg alloy. The precipitation of S' occurred between 253 and 367 °C, and required an activation energy of 129.9 kJ/mole.

(a) Effect of Trace Elements

The effect of small additions of Ag to pseudo binary Al-Cu-Mg alloys is typical of the effects of several trace elements in Al alloys. Polmear and co-workers [14,73] attributed the change in age hardening response of Al-Cu-Mg alloys resulting from small additions of Ag to two factors: a change in the quenched-in defect structure, and a modification of the structure of the precipitate itself. Polmear *et al.* [73] proposed that for small additions of Ag, many dislocation loops were replaced by fewer dislocation helices, due to the decreased mobility of the vacancies resulting from the high Ag atom/vacancy binding. The Ag atom/vacancy binding effect was quantitatively investigated and reported by Sen and West [112]. The modification in the defect structure slows down the coarsening rate of S laths in the Ag containing alloys. The major effect of the silver addition is to stimulate

precipitation of another, finely dispersed T phase $[Al_6(Cu,Ag)Mg_4]$, rather than S' or S. Tensile properties at room temperatures are increased, however T phase is metastable, and prolonged aging at even moderate temperatures (e.g. 200 °C) leads to its replacement by S. Moreover, dislocations shear through the T phase particles and concentrate in localized bands, so that the fatigue properties of the Ag containing alloys are overall inferior to the equivalent ternary Al-Cu-Mg alloys [113]. Sen and West [9] reported that T phase formation during aging at 190 °C in Ag-containing alloy could be prevented by a preaging deformation.

Wilson and co-workers [7,8] studied the effect of small additions of Si on aging response and the microstructure and mechanical properties of an Al-2.5Cu-1.2Mg alloy. They found that small addition of Si modified the as-quenched defect structure, reducing the number and size of vacancy loops and dislocation helices. The rate of formation of GPB zones and the growth rate of S' also decreased, to give a more uniform distribution and higher density of S' precipitates. Wilson suggested that Si increases the effective binding energy between the solute atoms, vacancies, and GPB zones, thus enhancing the stability of the zones and raising the temperature at which the S' precipitate could form by transformation from GPB zones. Tensile tests for alloys aged at 190 °C showed a strength increase about 25% for alloys containing 0.25%Si.

The addition of 1%Fe or 1%Ni to Al-2.5Cu-1.2Mg alloy was also studied by Wilson and Forsyth [114]. The additions of Fe or Ni lessened the alloy's ability to age harden by combining with some of copper to form insoluble phases, thus decreasing the amount of copper available for forming the active age-hardening precipitates.

More recently, Özbilen and Flower [115] studied the effect of Zr on S' precipitation in an Al-1.17Cu-0.67Mg alloy. It is shown that 0.13%Zr addition reduces the number of vacancy loops and causes precipitation of fewer and larger S' laths. Özbilen and Flower proposed that the high Zr-vacancy binding energy (0.24 ± 0.02 eV) prevented vacancy condensation into loops, thus providing less available nucleation sites for heterogeneous nucleation of S'.

The effect of Si microadditions on the kinetics of precipitation in an Al-1.52Cu-0.74Mg alloy was examined by Chaturvedi *et al.* [116]. A 0.23%Si addition changed the kinetics of GPB formation, and lowered the activation energy to 45.1 kJ/mole compared to 55.6 kJ/mole for the silicon-free alloy [93]. The morphology and distribution of S' was not altered by the Si addition. The Si effects were attributed to the strong interaction of Si atoms with other solutes and vacancies [116].

Gupta and co-workers [117,118] reported that the Al-1.52Cu-0.75Mg alloy can retain about 0.3% Si in solid solution and S' phase precipitates in this saturated alloy. A higher content of Si will produce insoluble particles, which can change the matrix composition considerably, and cause significant change in the precipitation kinetics as well as the formation of other phases.

(b) Effect of Mechanical-Thermal Treatment

A small amount of plastic deformation has long been recognized as an effective means to enhance the precipitation of S' in the Al-Cu-Mg alloys [73,114,119-121]. An investigation of this effect by Sen and West [9] showed that the nucleation and refinement

of the S' phase can be enhanced by a preaging plastic deformation, to give an increase in peak hardness and more uniform and finer distribution of the S' precipitates. This is attributed to the increased dislocation density resulting from the preaging stretch, which provides the preferred sites for heterogeneous nucleation. The plastic deformation was also shown to prevent the formation of T phase in Al-Cu-Mg-Ag alloy [9]. Broek and Bowles [122] reported a reduced crack propagation rate and improved fracture properties for an Al-Cu-Mg alloy that was plastically deformed prior to aging, and attributed this to the presence of smaller and finer S precipitates. Tavassoli [123] observed that the precipitation of β' in an Al-Mg-Si alloy was not greatly influenced by a preaging stretch, whereas the formation of θ' in Al-Cu and S' in Al-Cu-Mg alloys is significantly affected by the plastic deformation.

The effect of a preaging deformation on the aging response and mechanical behavior of Al-Cu-Mg alloys containing Li (e.g. 8090) has been extensively investigated recently. Martin and co-workers [124,125] reported that the volume fraction of S' phase increases with increasing degree of preaging stretch (<7%), and that the distribution of S' particles is strongly influenced by the thermomechanical treatment. The improved fatigue properties in 8090 and 8091 Al-Li alloys are attributed to the increased S' precipitation and refinement resulting from the preaging deformation. Ahmad and Ericsson [126] also showed that a stretch before aging increased the nucleation rate and density of S' and T₁ (Al₂CuLi) precipitates in an Al-Li-Cu-Mg alloy, which significantly improved tensile properties.

(c) Other Effects

Factors such as solute content, solution treatment temperature, quenching rate and thermal history are also found to influence the precipitation of S' phase.

Silcock [95] reported that in contrast to Al-Cu alloys, a slower quenching rate gives a higher peak hardness than a faster quenching rate, when single crystals of Al-Cu-Mg alloys are aged. The higher peak hardness is associated with retention of a greater quantity of GPB in the presence of S'. Sen and West [9] found that reducing the initial quenching rate reduces the subsequent hardening and coarsens the S-lath size on aging Al-3.3Cu-1.6Mg alloy, but additions of Ag dissipates the effect. The homogeneous precipitation of S' in Al-Li-Cu-Mg alloys is considered by Gregson *et al.* [4] to depend on the attainment of a critical combination of free vacancies and supersaturation of Cu and Mg, both of which are controlled by the solution temperature. Gupta *et al.* [105] reported that the morphology of S' is dependent on the net solute concentration of Cu+Mg, and in relatively dilute alloys, only rod-like S' is found. Duplex aging, in which an alloy is aged below and then above the GP solvus temperature, also influence the precipitation of S' phase. Sen and West [9] found that three day preaging treatment at 130 °C increased the peak hardness in both Al-Cu-Mg and Al-Cu-Mg-Ag alloys aged at 190 °C. Flower *et al.* [127] and Martin and co-workers [124,125] obtained microstructures with higher volume fractions and more uniformly dispersed S' precipitates, when Al-Li-Cu-Mg alloys were subjected to duplex aging treatments. In a more recent study of the effect of microstructure on tensile and fatigue properties of superplastically formed Al-Li-Cu-Mg-Zr 8090 alloy, Shakesheff *et al.* [128] observed that a natural aging prior to artificial aging can result in a high

concentration of free vacancies, which promotes a homogeneous dispersion of S' on aging at elevated temperature, and gives higher strength.

III. EXPERIMENTAL

A. ALLOY PREPARATION

Superpure Al and Mg (99.99%), electrical conductivity grade Cu (99.99%), and Al-5.23Be master alloy were used in the preparation of an Al-2.5Cu-1.2Mg base alloy and the base alloys containing 0.15%Be and 0.25%Be. The alloys were prepared in graphite crucibles by induction melting in air. The melts were maintained above the liquidus temperature (~ 750 °C) for about 10 minutes and periodically stirred to ensure complete homogenization, then poured into graphite molds 20 mm dia.x70 mm length at room temperature. All subsequent experimental work was carried out on the central part of the ingots to ensure similar initial microstructures and compositions.

For mechanical property tests the alloys were cast in larger-sized graphite molds 33 mm dia.x 110 mm length at room temperature.

Pure S phase alloy and S phase alloy containing 2% Be were also prepared and cast similar to the base alloy, except for a pouring temperature of 850 °C. The S phase and Be-containing S phase alloy were used for XRD, EDS and WDS analyses to determine the effect of Be on the composition and crystallographic structure of S phase.

All the as-cast alloys were annealed for 60 hours at 575 °C for homogenization. The process of cold working as a supplemental homogenization was omitted, since the goal in this investigation is to determine if S' nucleation can be stimulated by Be microalloying

alone.

B. SPECIMEN PREPARATION AND ANALYTICAL PROCEDURES

1. Microhardness Measurement

Microhardness measurements were used to monitor the age-hardening process. Sections about 5 mm thick, cut from the central regions of the ingots, were used for the studies. The solution treatment for these specimens consisted of a 60 h anneal at 575 °C, followed by a quench in iced-brine. The samples were then aged at five different temperatures: room temperature (22 °C), 130, 190, 240, 300 °C. An electric furnace with the temperature controlled to ± 1 °C was used for the solution and aging treatments. Microhardness measurements (HV0.05) were made by constantly interrupting the aging treatments. Before taking the measurements, the aged specimens were polished using a conventional polishing technique, and at least five readings were randomly taken for each hardness determination to obtain a mean with a typical uncertainty of about $\pm 5\%$.

2. Optical and SEM Microscopical Observations

Specimens for optical and SEM microscopy (~5 mm thick) were prepared in the conventional manner, starting with 0.05 μm alumina and finishing with colloidal silica suspension (Buehler) as the polishing media. The etchant used was Keller's etchant and dilute hydrofluoric acid solution (0.5 ml HF (48%) + 99.5 ml H₂O). A progressive etch

was carried out, and for SEM examinations, longer etching times were used to obtain sufficient topographic contrast. The scanning electron microscope used was a Nanolab 7 model, with a resolution of 70 nm and maximum useful magnification of 10,000.

3. TEM Microscopical Observations

Thin foils for TEM studies were prepared from the homogenized alloys (60 h at 575°C). Thin sections (~1mm) were cut from the cylindrical samples using a low speed diamond saw. The cut sections were solution treated at 575 °C for an additional two hours to ensure the maximum supersaturation of Be, and then quenched in iced-brine. Aging treatment were carried out at 190 °C and 350 °C, with TEM determinations of the microstructures obtained at various stages of the aging process. The 190 °C study provided microstructural evidence of dislocation loop and early stage of S' formation, and the 350 °C age was to study the S' to S phase transition. The sections were mechanically ground on silicon carbide papers down to a thickness less than 0.1 mm. Three mm dia. disks were made from the ground sections using a punch tool, and the final thinning was performed using a Fishione twin-jet electropolisher. The electrolyte used was methanol-30% HNO_3 maintained at -10 to -30 °C using a dry ice-ethanol bath. The thin foils were examined under the JEOL 100 CX transmission electron microscope operated at 100 kV, with a resolution of 2 Å. Bright field image, dark field image, and selected area diffraction modes were employed. Both double tilting and rotation-tilt specimen holders were used for the electron diffraction and direction determination.

4. Resistivity Analysis

Resistivity measurements were used to determine the amount transformed, from which the kinetic parameters of the Avrami equation relating to precipitation of S' and S phases, were obtained. For the resistivity measurements, ~2mm thick sections were cut from the solution treated and quenched samples, and cold rolled to strips approximately 0.1 mm thick, from which resistivity specimens (72x4x0.1 mm) were prepared. To remove the cold work the strip samples were solution treated again at 575 °C for two hours. Strip specimens were aged at 4 temperatures over the range 190-270 °C, with the aging interrupted periodically for the resistivity measurements. A standard potentiometric method was used to measure resistivity changes, in which the ends of the strip sample were split and connected to the current and potential leads, and the potential drops were compared against a well annealed, superpure aluminum strip used for the reference. The measurements were carried out in distilled and deionized water maintained at 26±0.01 °C. The potentiometric facility consisted of a Leeds-Northrup potentiometer (resolution of 10⁻⁷V) and a power supply, which enabled regulation of the current to ±0.02%. Resistivity changes of 10⁻¹¹ Ωm could be detected, and the overall accuracy for the readings obtained was ±0.03%. The experimental set-up and specimen dimensions for resistivity measurement are shown in Fig. 3.

5. Mechanical Property Tests

Specimens for Charpy-V impact and tensile tests were prepared from alloys homogenized at 540 °C for 72 hours. The longer annealing time was used to further

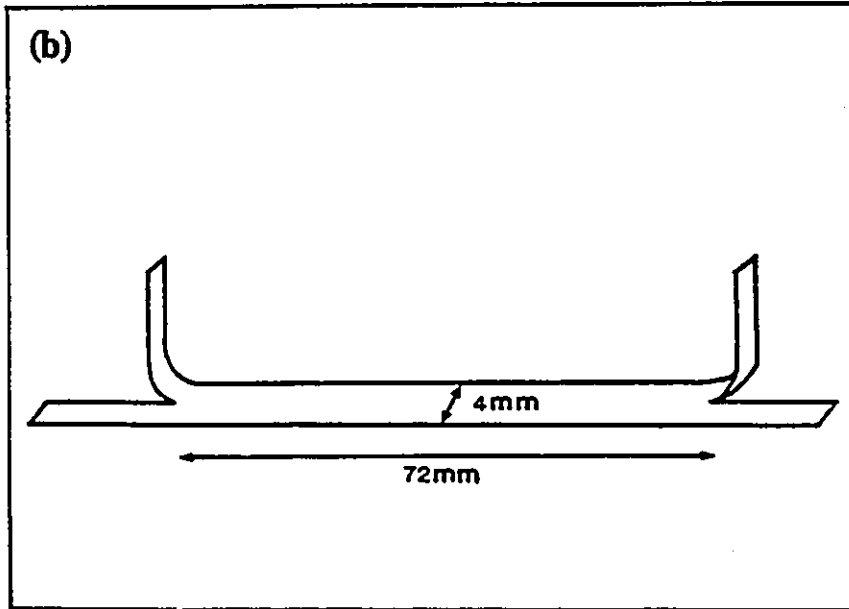
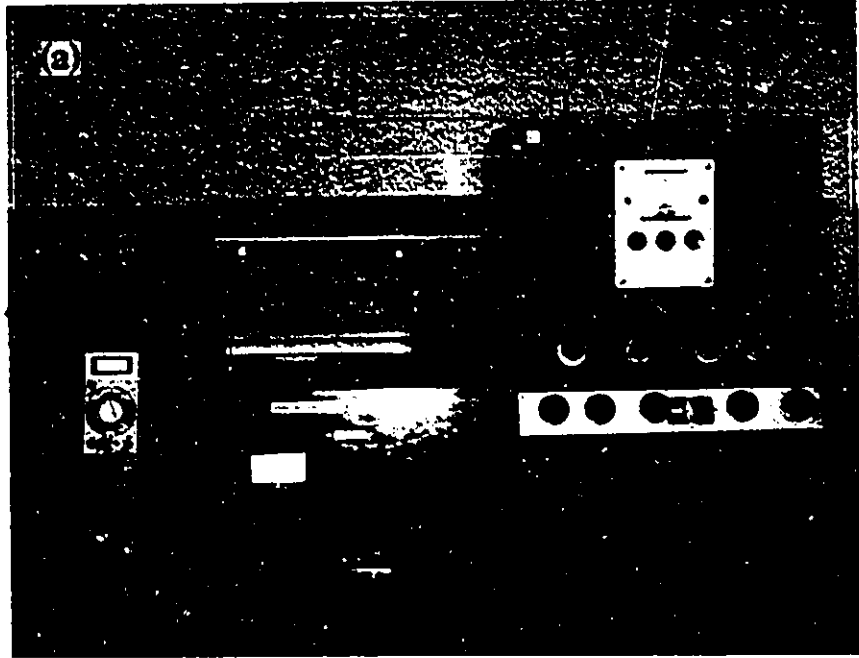


Fig. 3. (a) Experimental set up, (b) resistivity specimen dimensions.

improving the homogenization. Standard Charpy-V notch specimens were made from parts cut longitudinally from the central region of the ingots. The tensile test specimens, with a gage section dimension 25x9x4 mm, were prepared from longitudinal sections cut from the ingots. The stress relief and solution treatment for the test specimens consisted of an additional three hours annealing at 575 °C, followed by a water quench. Tensile tests were performed on an Instron machine at an initial strain rate of $3.3 \times 10^{-4} \text{ s}^{-1}$. Fracture surfaces were observed by SEM, and the deformed microstructure immediately below the fracture surface was examined by TEM.

6. S Phase Analysis

The S phase, and S phase alloy containing 2%Be were analyzed by Energy Conversion Device Inc. of Troy Michigan. The ingots were wrapped in Al foil for protection and homogenized at 550 °C for 72 hours. The lower homogenization temperature was used to minimize surface loss of Mg, which has a relatively high vapor pressure. Specimens ~5mm thick were cut from the homogenized ingots for XRD, EDS, and WDS analyses to determine the solubility of Be in S phase, and the corresponding lattice changes. For XRD study, powder specimens were prepared by grinding. Silicon powder was added to the powder specimens as an internal calibration reference. The XRD patterns were analyzed using the "Appleman" program to search for the best-fitted lattice constants of the "known" phase. EDS was used to determine the concentrations of all elements except O and Be, for which WDS was used. Pure elements were used as standards, except for O, for which the standard was SiO₂.

IV. RESULTS AND DISCUSSION

A. AGING BEHAVIOR AND MICROSTRUCTURES

1. As-Cast and Solution Treated Microstructures

The microstructure for the as-cast alloys are shown in Fig. 4. Interdendritic regions of Al-S eutectic in the base alloy, and both Al-S and Al-Be eutectic regions in the Be-containing alloys are evident. The microstructure of the homogenized alloys are shown in Fig. 5. Complete dissolution of the S phase was achieved in the base alloy (Fig. 5(a)), whereas in the Be-containing alloys (Fig. 5(b) and (c)) an insoluble phase remained, which was determined to be excess Be. The amount of Be precipitate increases with increasing Be content (compare (b) and (c) in Fig. 5).

2. Age-Hardening Behavior

The age hardening curves for specimens aged at room temperature, 130, 190, 240 and 300 °C are shown in Fig 6(a) to (e) respectively. The room temperature results for the base alloy show good agreement with these reported by Wilson *et al.* [8]. To determine if the independent precipitation of Be from the supersaturated alloy contributed to the age-hardening process, an Al-0.2Be alloy was subjected to an aging treatment for two solution treatment temperatures, 540 and 630 °C, the latter to obtain maximum supersaturation. The room temperature aging curve for the Al-0.2%Be alloy (solution

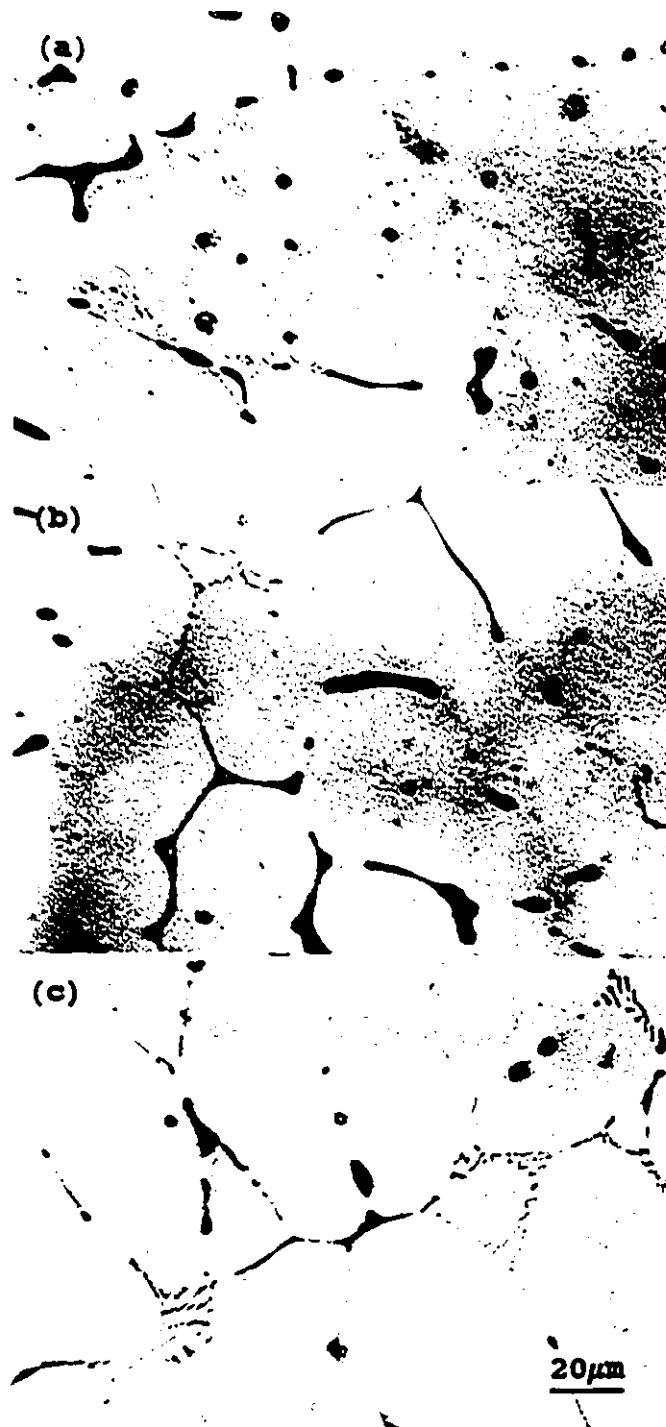


Fig. 4. Optical micrographs of as cast alloys.
(a) base alloy, (b) 0.15Be, (c) 0.25Be.



Fig.5. Optical micrographs of alloys homogenized at 570°C for 60 h.
(a) base alloy, (b) 0.15Be, (c) 0.25Be

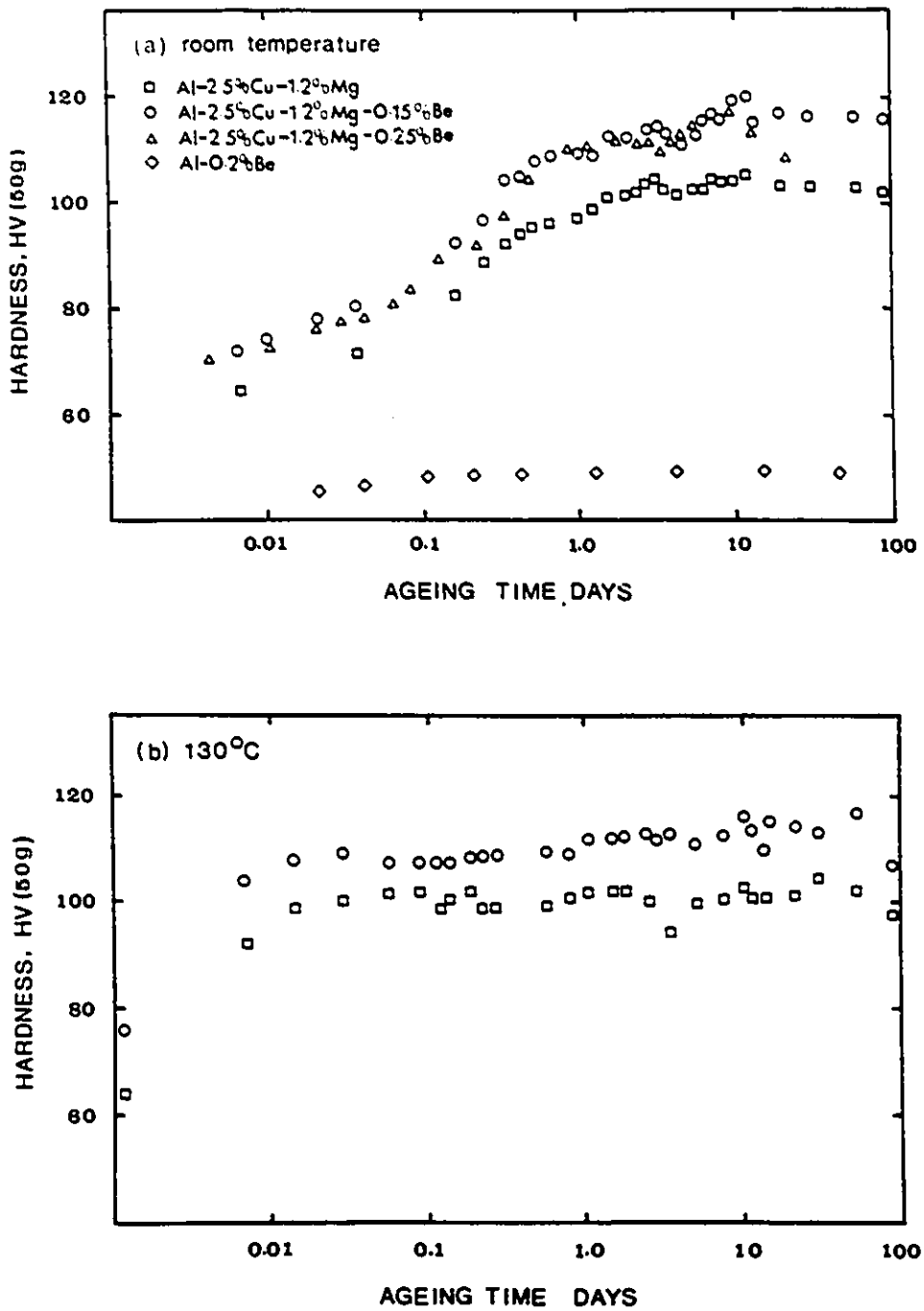


Fig. 6. Age hardening curves for alloys aged at temperature indicated. Legend given in 6(a).

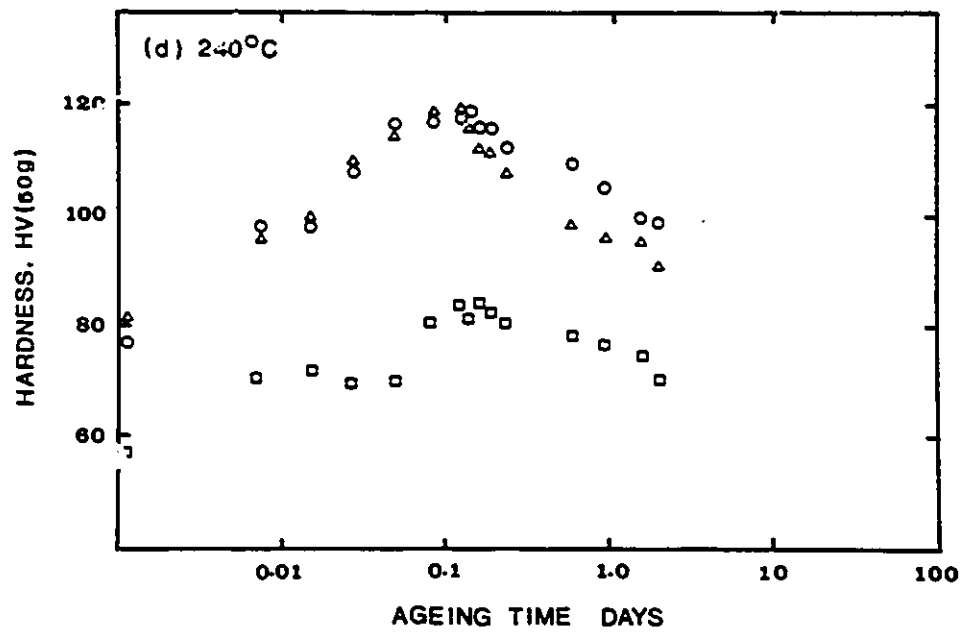
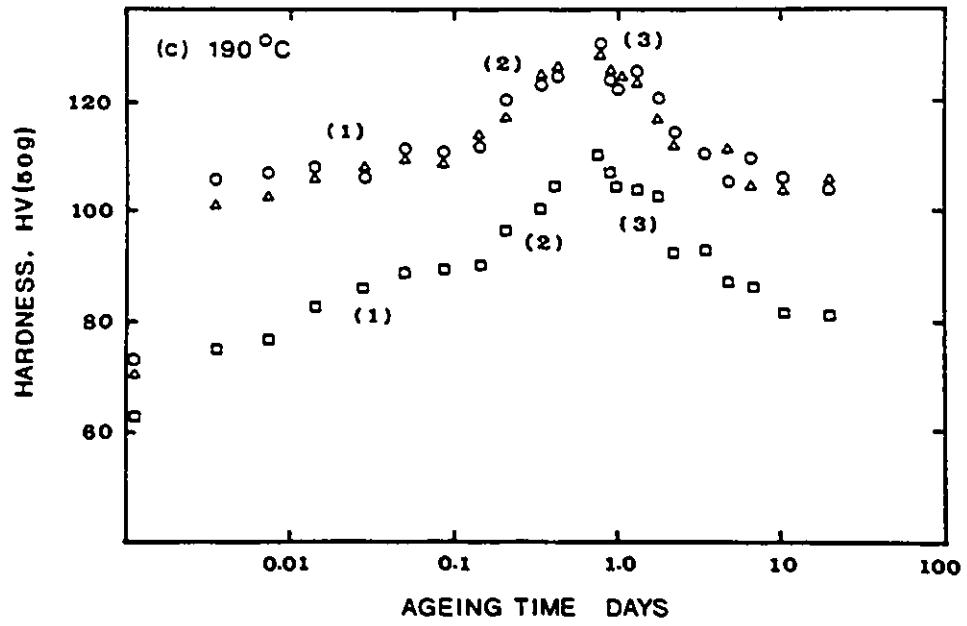


Fig. 6.

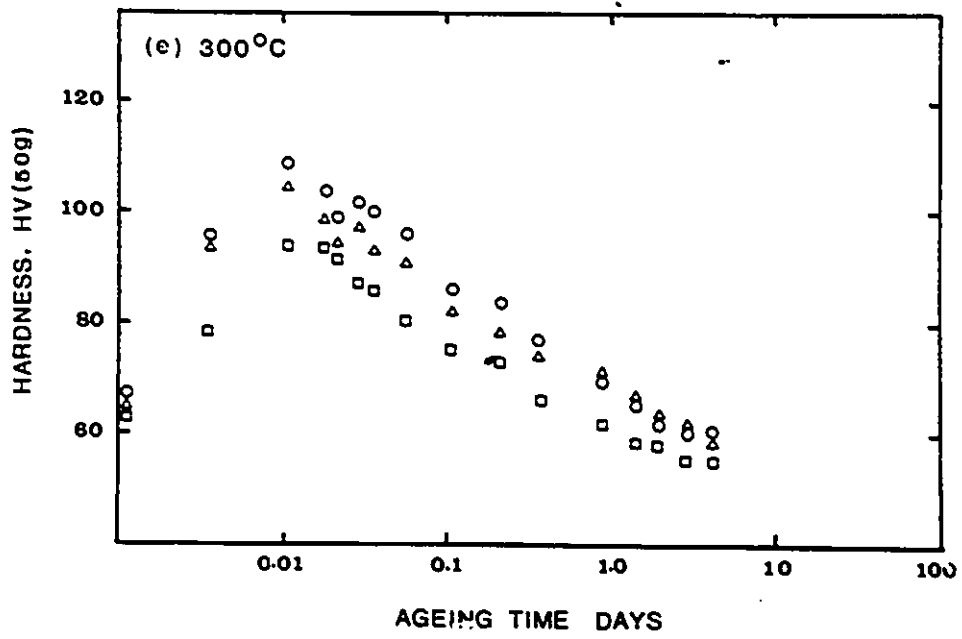


Fig. 6.

treated at 630 °C) is given in Fig. 6(a). It is evident Be itself does not contribute to age hardening of Al alloy, and this was also confirmed for the higher aging temperatures (where a decrease in hardness results due to precipitation of the excess Be from solution). However, Be has a marked improvement on the age hardening of the Al-Cu-Mg alloy, increasing the maximum hardness levels by 35 HV units at the 190 °C aging temperature. A small increase in the aging rate is also noted in the Be containing alloy. The transformation process is greatly accelerated by aging at 240 °C, with a peak hardness of ~HV 120 reached after only 2 hours aging time for the Be containing alloy. On the other hand the peak hardness for the base alloy aged at 240 °C was only ~HV 85. Increasing the Be content to 0.25% does not significantly change the age-hardening response of the alloy from that obtained with 0.15%Be, which already exceeds the solubility limit in the alloy (the maximum solubility of Be in Al at the eutectic temperature 644 °C is 0.10% (c.f. Fig. 2). Thus in the subsequent studies (kinetic, mechanical, TEM) only the alloy containing 0.15%Be is investigated.

The age-hardening curves for all aging temperatures showed several stages for the precipitation process, the number depending on the aging temperature. Three stages are readily distinguished for both base alloy and the Be-containing alloys for the 190 °C aging treatment. The dependency of the number of stages on aging temperature is well known. Hardy [94] reported that for the Al-Cu-Mg alloys with the Cu:Mg weight ratio of 7:1, three stages were evident in the curves at lower aging temperatures, decreasing to two and then one stage as the aging temperature was increased above 220 °C. The stages are generally associated with cluster and coherent zone formation, followed by their transformation (or

dissolution and reformation) to partly coherent and finally to non-coherent (stable) precipitate forms. Assuming the generally accepted sequential representations of the transformation stages for precipitation in age-hardening alloys (c.f. Eq. (24)), the following stages might be associated with the 190 °C aging curve (identified in Fig. 6(c)): stage (1), GPB zone formation associated with the gradually rising curve to -HV 110 (0.1 day); stage (2), S' formation as the curve rises to -HV 130 (<1 day); stage (3), resolution of GPB zones to produce the initial fall in the curve to -HV 120, nucleation of additional S' phase to produce the second (lower) peak at -HV 125 (~1 day), and finally overaging of S' to give the non-coherent S phase as the aging curves continue to fall. The above discussion is consistent with the results obtained by Silcock [95].

It is noted that the initial (as-quenched) hardness values show a certain amount of variation, which is dependent on several factors, including cooling rate (quench severity), alloy composition, as well as the elapsed time and temperature in preparing the alloy samples for the hardness measurements. However, the consistently higher initial hardness of the Be-containing alloy is in agreement with that reported by Youdelis *et. al.* [75], which showed that Be had a strong solid solution hardening effect in Al.

3. Optical and SEM Microscopy

The optical and SEM micrographs obtained for specimens aged at 300 °C for 7 days are shown in Fig. 7 and Fig. 8 respectively. The specimens were overaged to obtain optically resolvable precipitates. The precipitates are equilibrium S phase with a rod-like morphology, which also appears round-like depending on orientation. The rod or lath-like

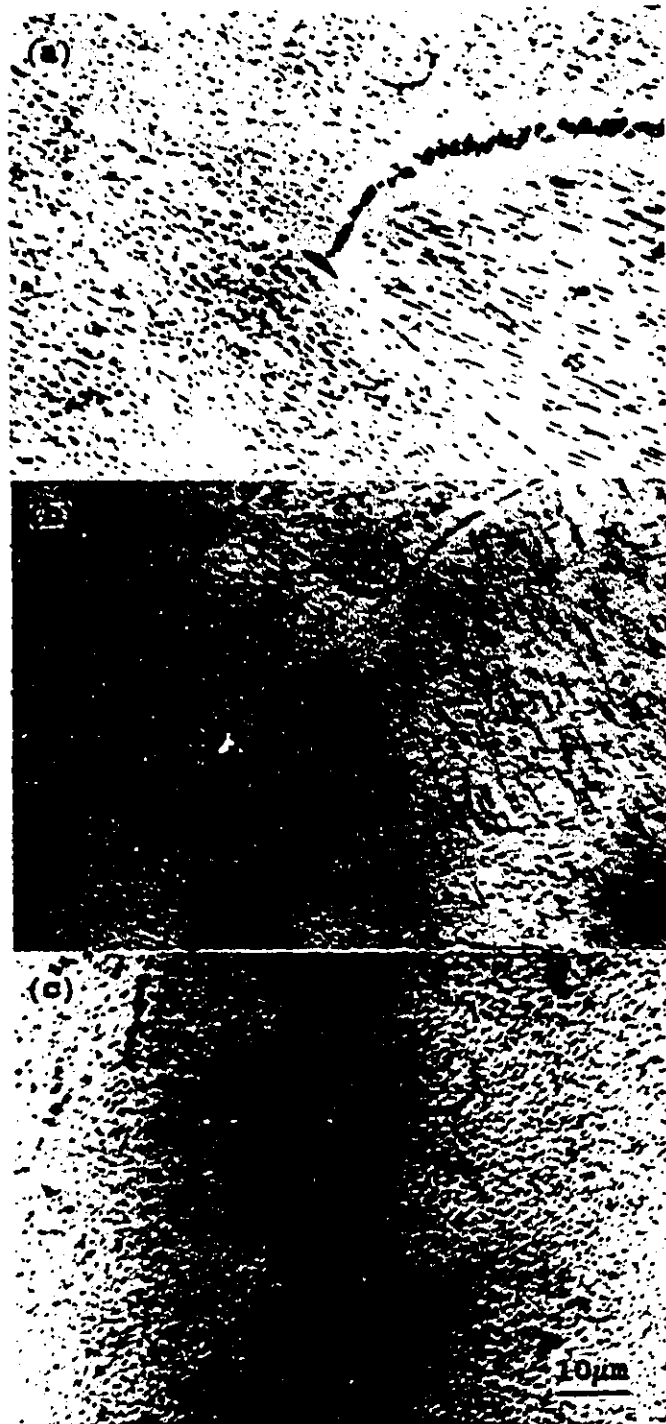


Fig. 7. Optical micrographs of alloys aged at 300°C for 7 days.
(a) base alloy, (b) 0.15Be, (c) 0.25Be.

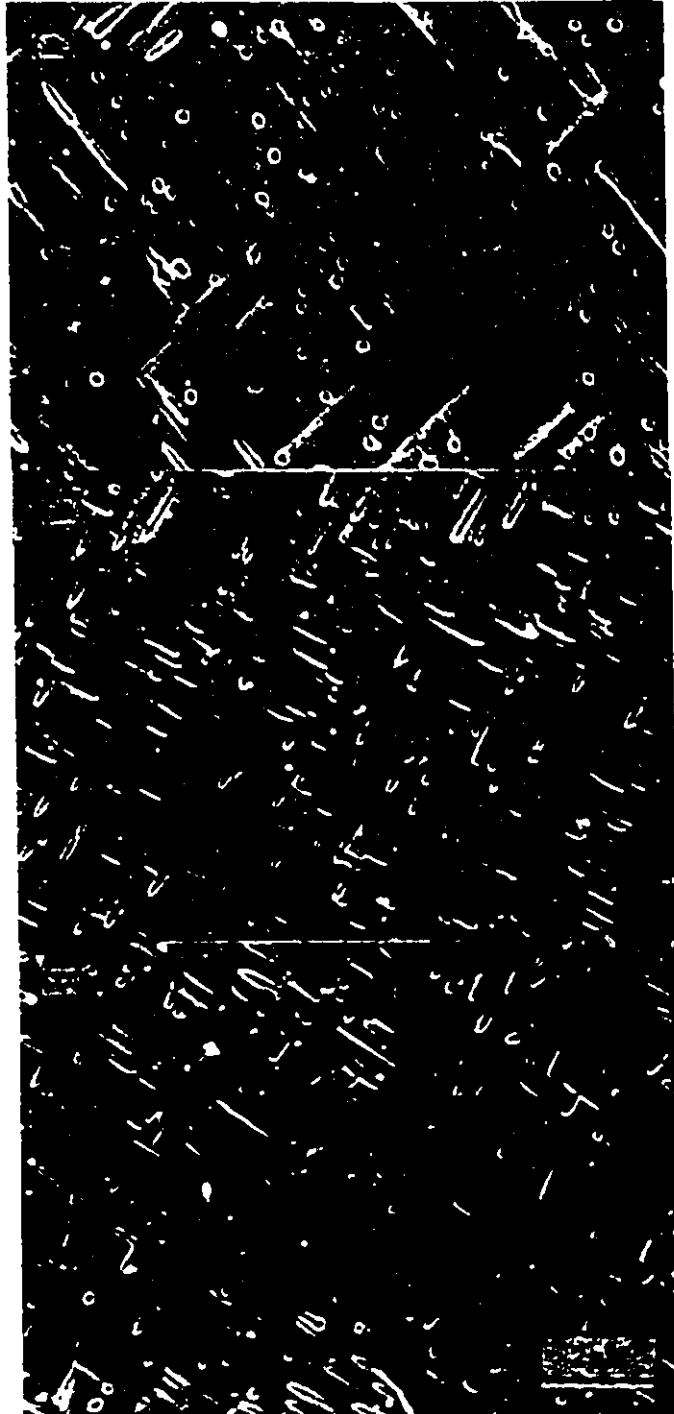


Fig. 8. SEM micrographs for alloys aged at 300°C for 7 days.
(a) base alloy, (b) 0.15Be, (c) 0.25Be.

morphology is more evident in the SEM micrographs. Both the optical and SEM micrographs clearly show a much higher density of precipitate particles in the Be-containing alloy, estimated to be 3 to 4 times that in the base alloy. The higher S precipitate density suggests a Be-enhanced nucleation rate for its precursor phases, i.e., the S' phase and the GPB zones. The assumption in this investigation that GPB zones are precursors of S' precipitates, and S' precursor of S phase, is in agreement with Weatherly [108], who reports transformation of the GPB zones to S' precipitates in Al-2.7Cu-1.5Mg-0.2Si alloy, and that S' phase is only slightly strained version of the equilibrium S phase [105].

4. Kinetic Analysis

The specific resistivity vs. time plots for the alloys aged at 190 °C and 240 °C are shown in Fig. 9, and are typical of the results obtained at the other aging temperatures. The resistivity curves at several temperatures investigated provide all the results required for determining the Avrami equation (c.f. Eq. (21)-(23)), and the pertinent kinetic parameters characterizing the transformation process. The overall shape of the curves for the base alloy are not altered by addition of Be, and the three distinguishable stages observed in the age-hardening curves are also evident in the resistivity curves. Fig. 10 gives the $\log \ln[1/(1-X)]$ vs. $\log t$ plot for the 190 °C aging treatment, from which the growth parameter n is obtained from the slope. Three straight line segments are evident, which in order of increasing time represent GPB zone formation, S', and S precipitation respectively [95]. For S' precipitation (central straight-line segment), $n=1.56 \pm 0.11$ for the

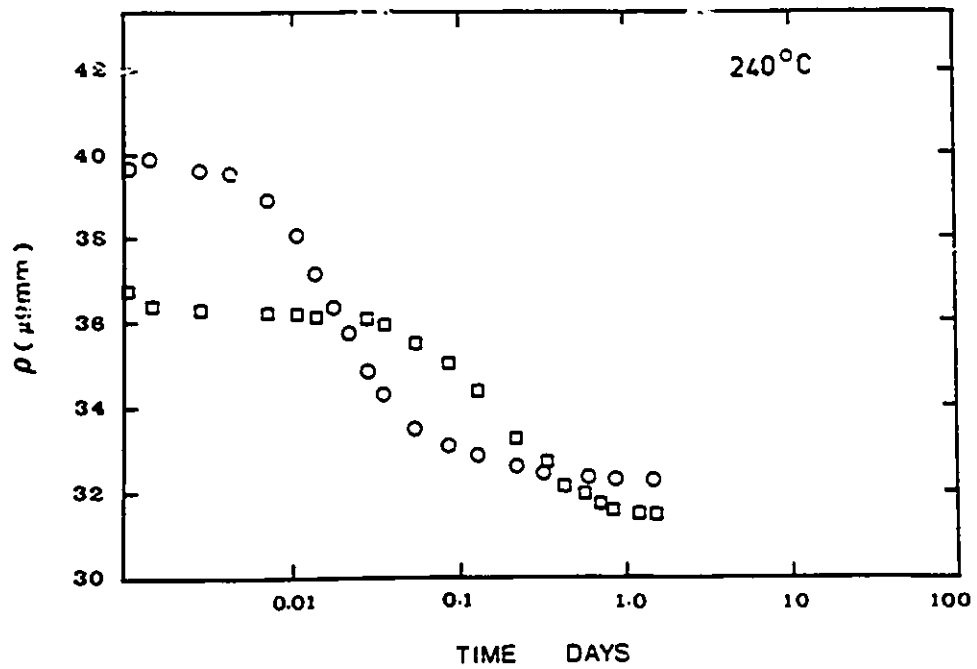
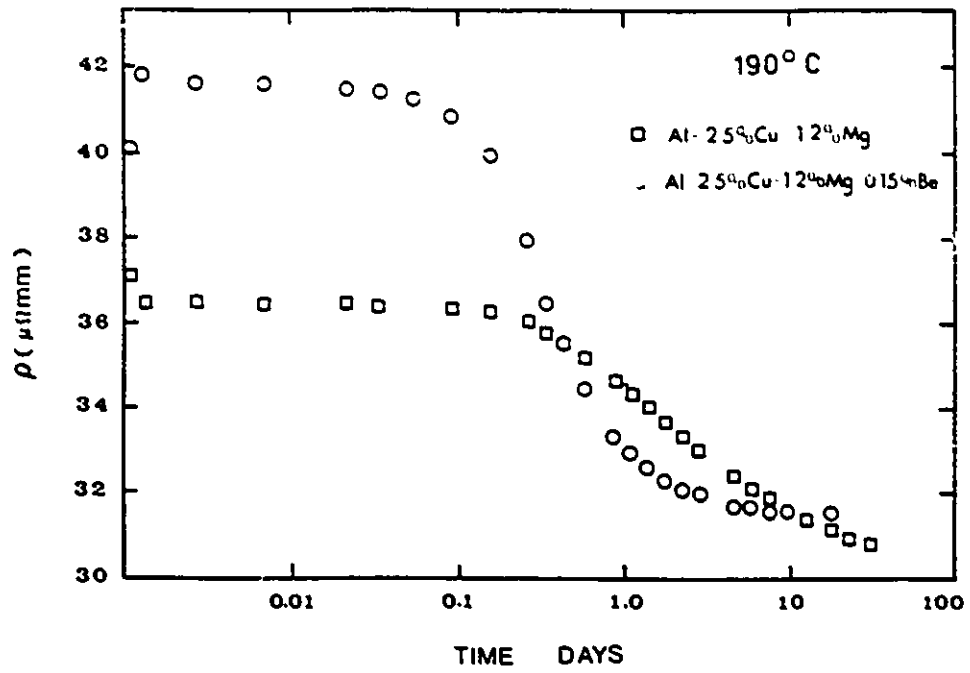


Fig. 9. Specific resistivity vs time for alloys aged at 190°C and 240°C.

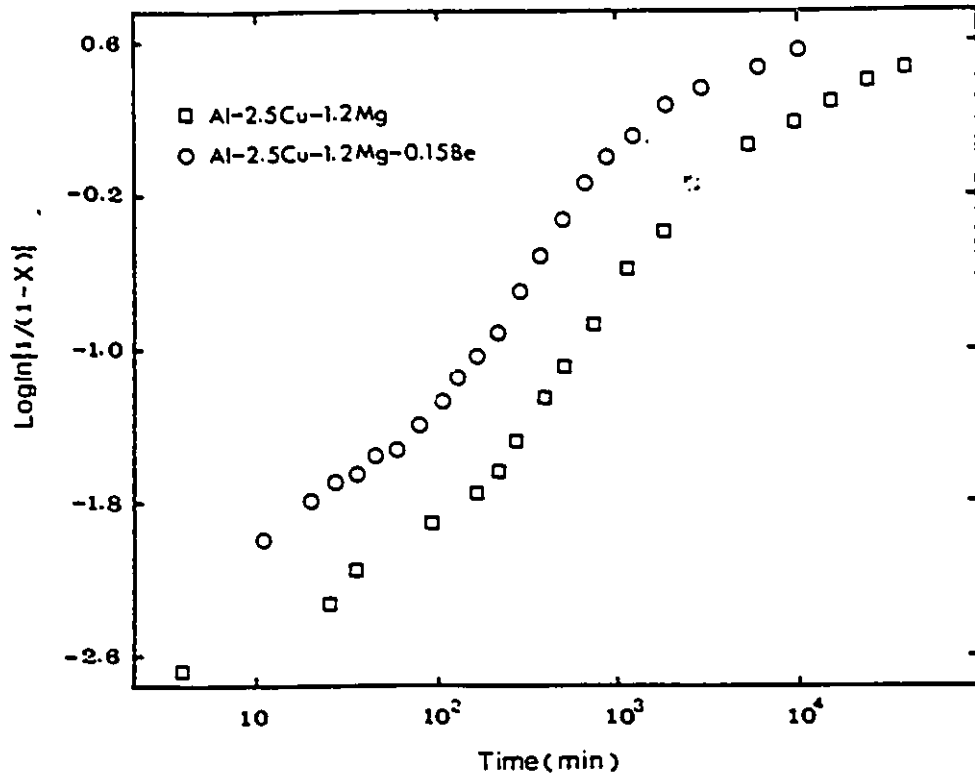


Fig. 10. $\text{Log}n/(1-X)$ vs $\text{log}t$ for the 190°C aging temperature.

Be-containing alloy which is essentially the same for the base alloy, and implies that the growth mechanism for S' phase is not significantly affected by the Be addition. Fig. 11 shows the fraction of S' precipitation completed for the 190 °C aging treatment, calculated using Eq. (23). Figs. 10 and 11 show that the addition of 0.15%Be to the Al-2.5Cu-1.2Mg alloy forces the GPB zone to S' transition to earlier times, and increases the rate of precipitation of S' phase, and these effects were observed for all aging temperatures investigated.

The nuclei density parameter (k) for the transformation is obtained from the ordinate intercepts of the central straight line segments in Fig. 10, and the activation energy for S' precipitation from the Arrhenius plots of the fraction transformed (Fig. 12). It is evident that the k parameter for the Be-containing alloy is consistently higher compared to that for the Be free alloy, which suggests that Be addition accelerated the nucleation rate for S' precipitation. The activation energies for the transformations, obtained from the slopes of the Arrhenius plots, are $Q=109.6 \pm 12.4$ and 115.3 ± 13.4 kJ/mole for the base and Be-containing alloy respectively, indicating Be has no significant effect on the growth of S' precipitate. The activation energy obtained in this investigation is in good agreement with 129.9 kJ/mole reported by Jena et. al. [93] using a DSC technique for an Al-1.53Cu-0.79Mg alloy, and is in the range for the activation energies reported for diffusion of Cu in Al [129]. It should be noted that the Arrhenius plot for the k parameter (Fig. 12) also gives similar values for the activation energies ($Q=102$ kJ/mole), which, according to Eq. (22), is the activation energy for diffusion of the major solute (Cu) in aluminum (Eq. (22) represents diffusional growth in 3 dimensions to give $D^{3/2}$ dependency, whereas for the

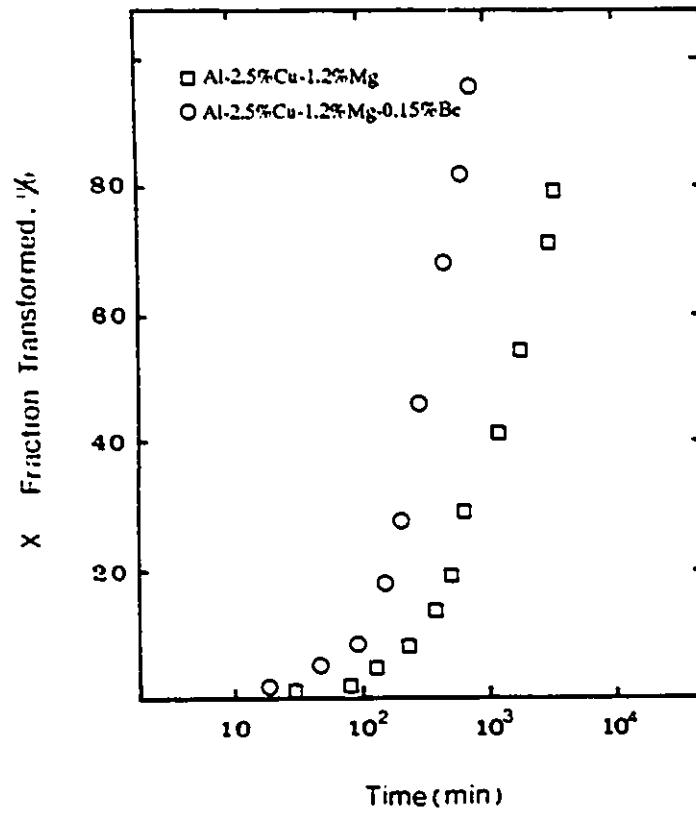


Fig. 11. Fraction transformed vs time for S' phase.

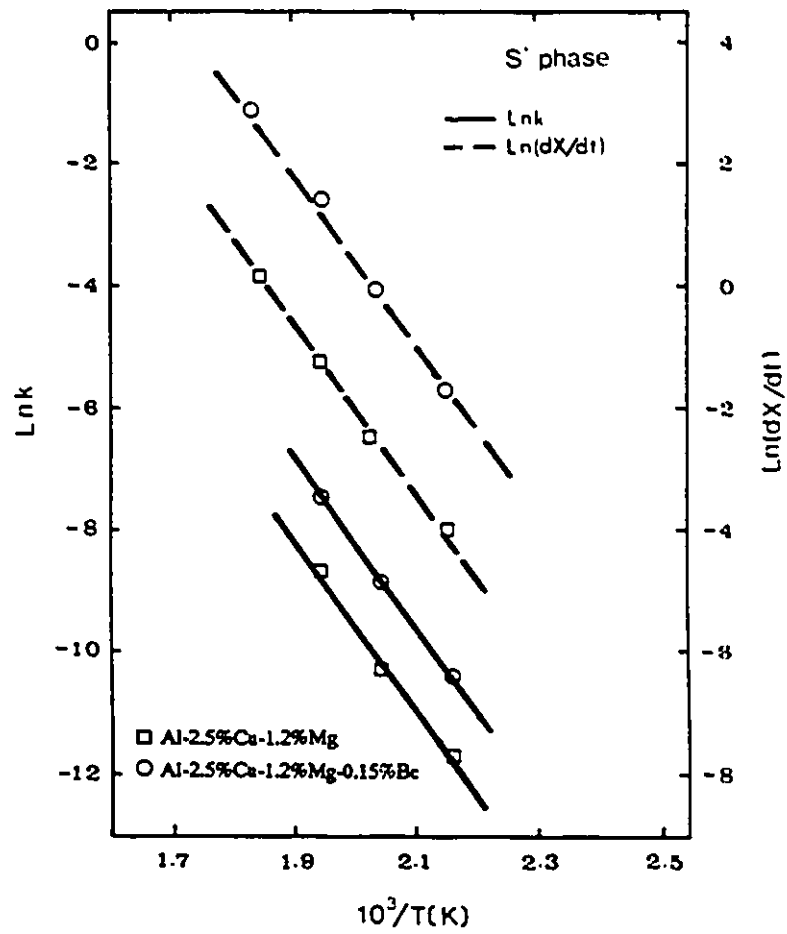


Fig. 12. Arrhenius plots for $\ln k$ and $\ln(dX/dt)_{X=0.5}$.

present case growth is largely 2 dimensional, i.e. laths or plates, giving a D^1 dependency).

Precipitation is a complex process involving various processes, e.g. vacancy release and dislocation loop formation, which occurs simultaneously during S' precipitation. Resistivity measurement is a measure of all the processes occurring during precipitation of S' , and reflects the kinetics of the overall transformation process.

5. TEM Analysis

The age hardening results, kinetic analysis, and optical and SEM observations show clearly that the addition of 0.15%Be or 0.25%Be to the base alloy significantly increases the age hardening rate and peak hardness for Al-2.5%Cu-1.2%Mg alloy. Also, the S' precipitate is refined, which may be attributed to the Be-enhanced nucleation of S' precipitates. The TEM analysis of the alloy microstructure at various stages of precipitation is an attempt to identify the specific role of Be in the transformation process.

(a) Defect Structure and Formation of S' Precipitate

Figs. 13 and 14 show the dislocation distribution in the as-quenched alloys and alloys aged at room temperature for two weeks respectively. For the base alloy, the as-quenched structure is characterized by a high density of dislocation loops, which are assumed to form by vacancy condensation (Fig. 13(a)). The configuration and distribution of the defects in the as-quenched base alloy is similar to the TEM results reported by other investigators [8,112]. However, for the as-quenched alloy containing 0.15Be (Fig. 13(b)), the number of dislocation loops is significantly less. Another feature to be noted in the as-quenched,



Fig. 13. TEM micrographs and Kikuchi lines on corresponding diffraction patterns for as quenched alloys. (a) and (b) base alloy, (c) and (d) 0.15Be.

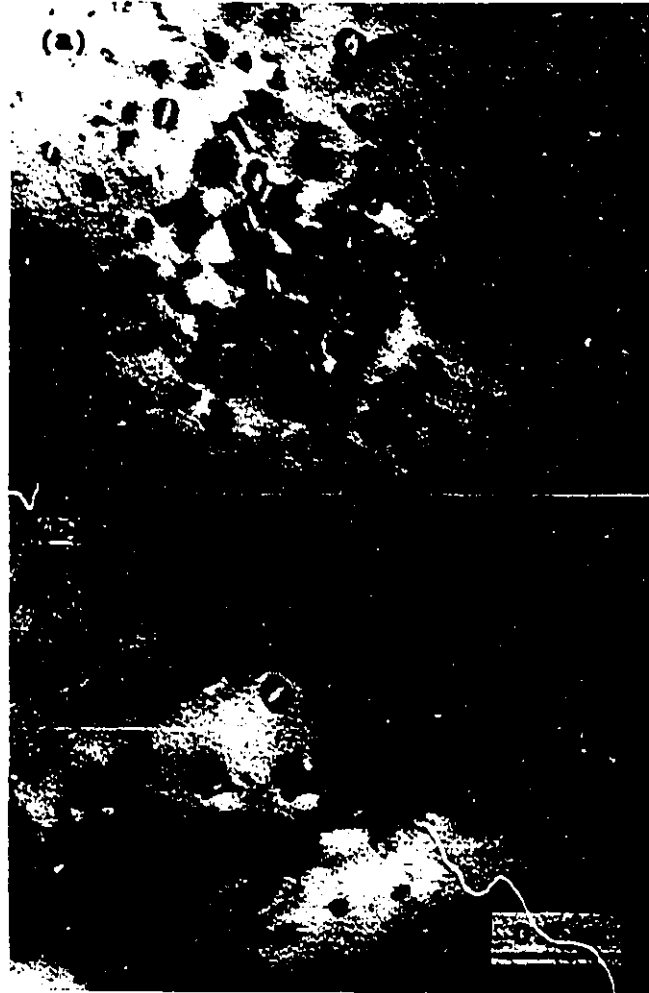


Fig. 14. TEM micrographs for alloys aged for two weeks at room temperature. (a) base alloy, (b) 0.15Be.

Be-containing alloy, is the formation of dislocation helices, in contrast to the single dislocation loop distribution in the base alloy. These micrographs were taken at multiple beam conditions, which do not provide quantitative solutions of the number of the loops, but qualitatively demonstrate the overall changes resulting from the Be addition. Fig. 14 shows that the dislocation loops and helices have enlarged with time (two weeks) in alloys aged at room temperature. The fewer dislocation loops in the Be-containing alloy can be attributed to the high Be-vacancy binding energy in Al alloys, which prevents the vacancies from condensing to dislocation loops [130-133]. The latest reported value for the Be-vacancy binding energy is 0.26 eV [134]. A similar effect on dislocation distribution has been reported when small additions of Si ($E_{\text{Si-v}}=0.5$ eV) [7,8], Zr ($E_{\text{Zr-v}}=0.24$ eV) [115], or Li ($E_{\text{Li-v}}=0.25$ eV) [135,136] are added to Al-Cu-Mg alloys. In Zr or Li-containing Al-Cu-Mg alloys, the high binding energy between Zr or Li atoms and quenched-in vacancies markedly reduced the quantity of nucleation sites, resulting in a sluggish and coarse precipitation of S' phase. For the Si-containing alloy, it is reported that the initial stage of age hardening at 190 °C is delayed by the presence of Si. In the present investigation, the aging and resistivity results show that the precipitation process is accelerated by the Be addition, even at the very start of the aging, indicating the involvement of Be atoms themselves in the precipitating phase and this will be discussed in detail later.

Fig. 15 shows TEM micrographs for the alloys aged at 190°C for 5 minutes for two orientations of the Al lattice. The dislocation loops have increased in size from the as-quenched state for the base alloy (Fig. 13(a)), however, for the Be-containing alloy there is an increase in the number of dislocation loops, and the formation of some S' precipitates

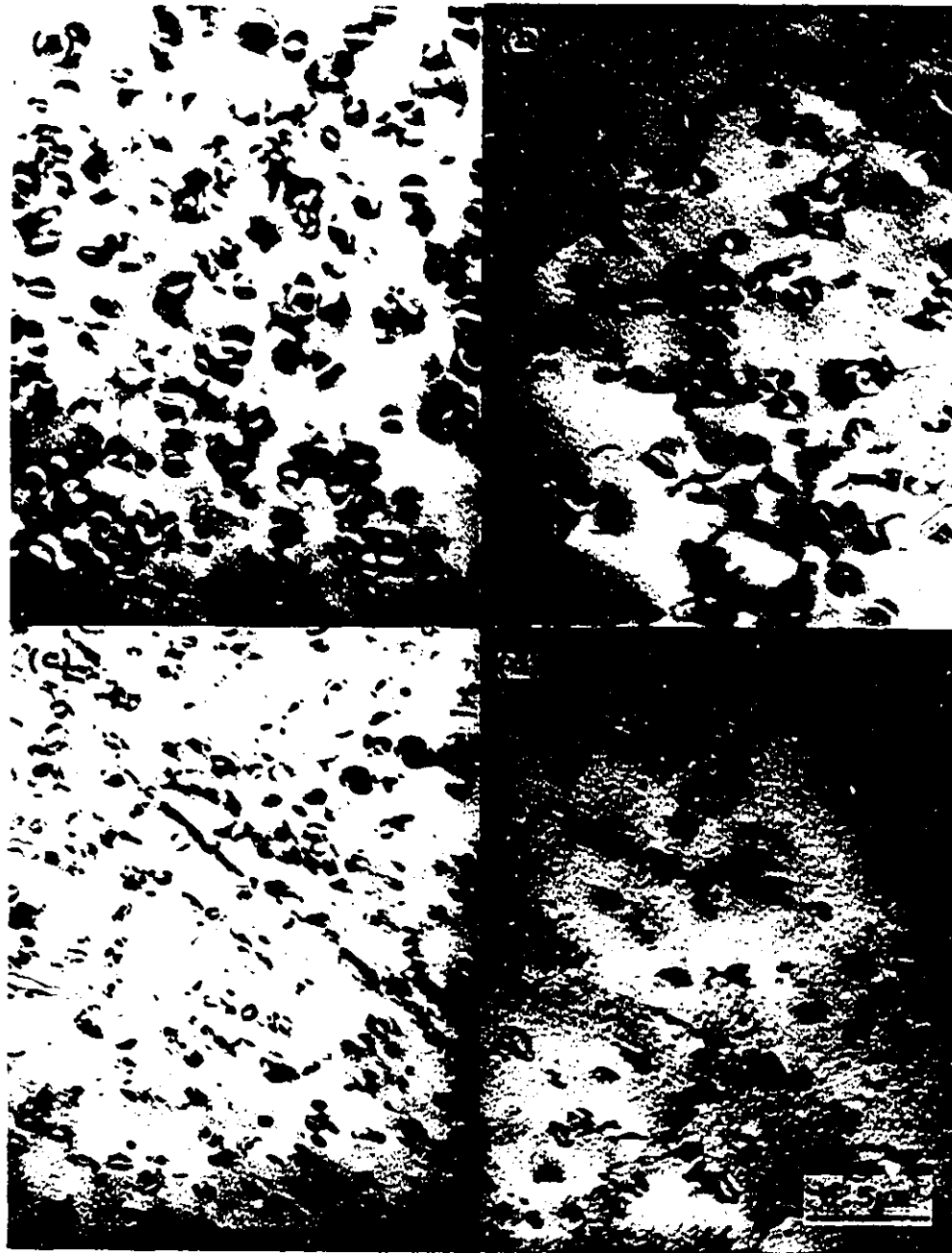


Fig. 15. TEM micrographs for alloys aged at 190°C for 5 min. (a) $\langle 100 \rangle_{Al}$ and (b) $\langle 112 \rangle_{Al}$ base alloy, (c) $\langle 110 \rangle_{Al}$ and (d) $\langle 112 \rangle_{Al}$ 0.15Be.

as indicated by the segmenting of the dislocation loops. The acceleration in S' and dislocation loop formation during the initial stage of aging for the Be-containing alloy suggests Be atoms are involved in the precipitating phase itself and its precursors, i.e., GPB zones. The above microstructures suggest that the vacancies, initially bound by Be, are released and condense forming secondary dislocation loops, which can then act as additional nucleation sites for the precipitation of S' precipitates.

The vacancy release is more evident when observed at higher aging temperatures. Fig. 16 shows the TEM micrographs for alloys aged at 350 °C for only 1 minute. For the base alloy (Fig.16(a)), most of the dislocation loops have been replaced by S' phase. For the Be-containing alloy, however, many newly formed dislocation loops and larger S' precipitates formed at primary dislocation loops are evident (Fig. 16(b)). Fig. 17. shows the microstructure for the alloys aged at 350 °C for 18 minutes. It is evident that all the dislocation loops in the Be-containing alloy have now been replaced by finely distributed S' or S precipitates.

The vacancy release mechanism as described here is similar to that observed in Li-containing Al-Cu-Mg alloys. Gregson et. al. [4] reported that the high density of as-quenched dislocation loops is completely altered by the presence of Li atoms due to high Li-vacancy binding energy. On aging, during which δ' (Al_3Li) precipitates formed during quenching grow, a large number of free vacancies are released and condense forming dislocation loops to act as nucleation sites for S' phase, with the Li atoms being consumed in the formation of δ' . For the Be-containing alloy of the present investigation, it is proposed that the Be atoms on release from the vacancies enter into the S' phase itself,



Fig. 16. TEM micrographs of alloys aged at 350°C for 1 min, $\langle 100 \rangle_{Al}$ foil orientation. (a) base alloy, (b) 0.15Be.

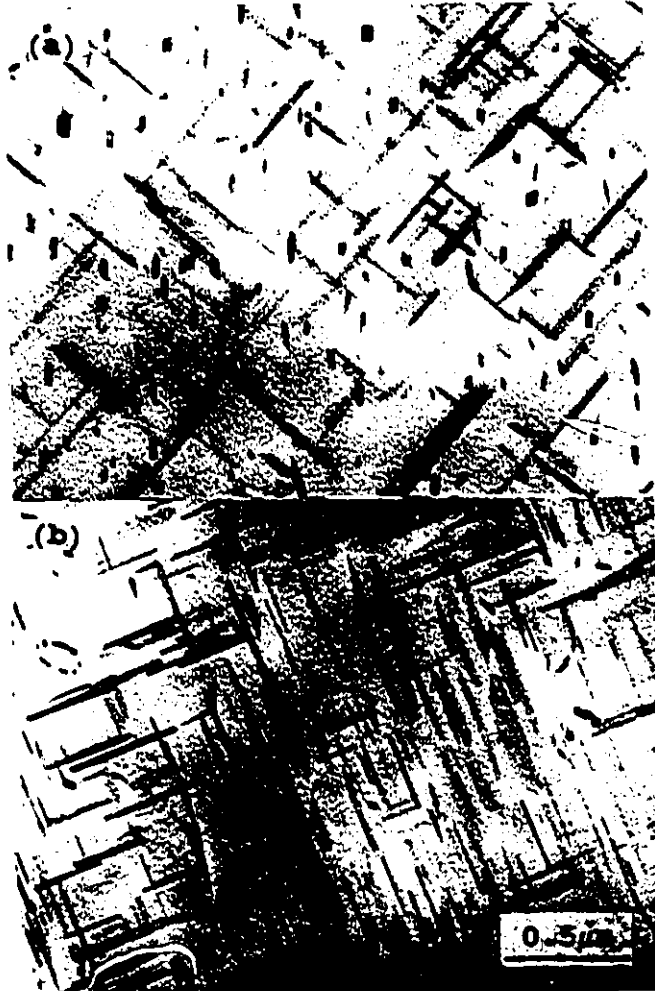


Fig. 17. TEM micrographs for alloys aged at 350°C for 18 min.
 $\langle 100 \rangle_{Al}$ foil orientation, (a) base alloy, (b) 0.15Be.

which will be discussed in more detail below.

(b) S' Morphology and Density

Fig. 18 shows the TEM micrographs for the alloys aged at 190 °C for 2 hours. The base alloy shows enlarged and segmented dislocation loops, which is characteristic of the formation of S' precipitates. The Be-containing alloy shows that the high density of dislocation loops have been mostly replaced by S' precipitates, which is further evidence of the dissociation of the Be-vacancy pairs, with the probable incorporation of Be into the S' phase that forms.

Wilson and Partridge [104] reported that S' precipitates were nucleated at loops and dislocations, and grew as laths on $\{210\}_{Al}$ in a $\langle 100 \rangle_{Al}$ direction. Composite sheets of S' precipitates reportedly formed on dislocations by growth and contact of several $\{210\}_{Al}$ laths with a common $\langle 100 \rangle_{Al}$ direction, resulting in the formation of corrugated-like precipitate sheets on $\{110\}_{Al}$. Composite precipitate sheets are also observed in both alloys as shown by micrographs of Fig. 19(a) and 19 (c). Rod-like precipitates are also present and show a preference to form at grain or subgrain boundaries in the base alloy (Fig.19(b)). It was earlier noted that Gupta *et al.* [105] reported that the S' precipitate morphology, (rods or lath), depends on the net Cu+Mg solute concentration, and only rods will form in dilute alloys. Radmilovic *et al.* [107] observed both rod-like and the lath-like precipitates forming at the same subgrain boundary, which they attributed to a change in the orientation of the subgrain boundary. The results of this investigation indicate that both lath-like and rod-like morphologies can be formed in the same grain, and that the precipitate morphology



Fig. 18. TEM micrographs for alloys aged at 190° C for 2 h.
— $\langle 100 \rangle_{Al}$ foil orientation. (a) base alloy, (b) 0.15Be.

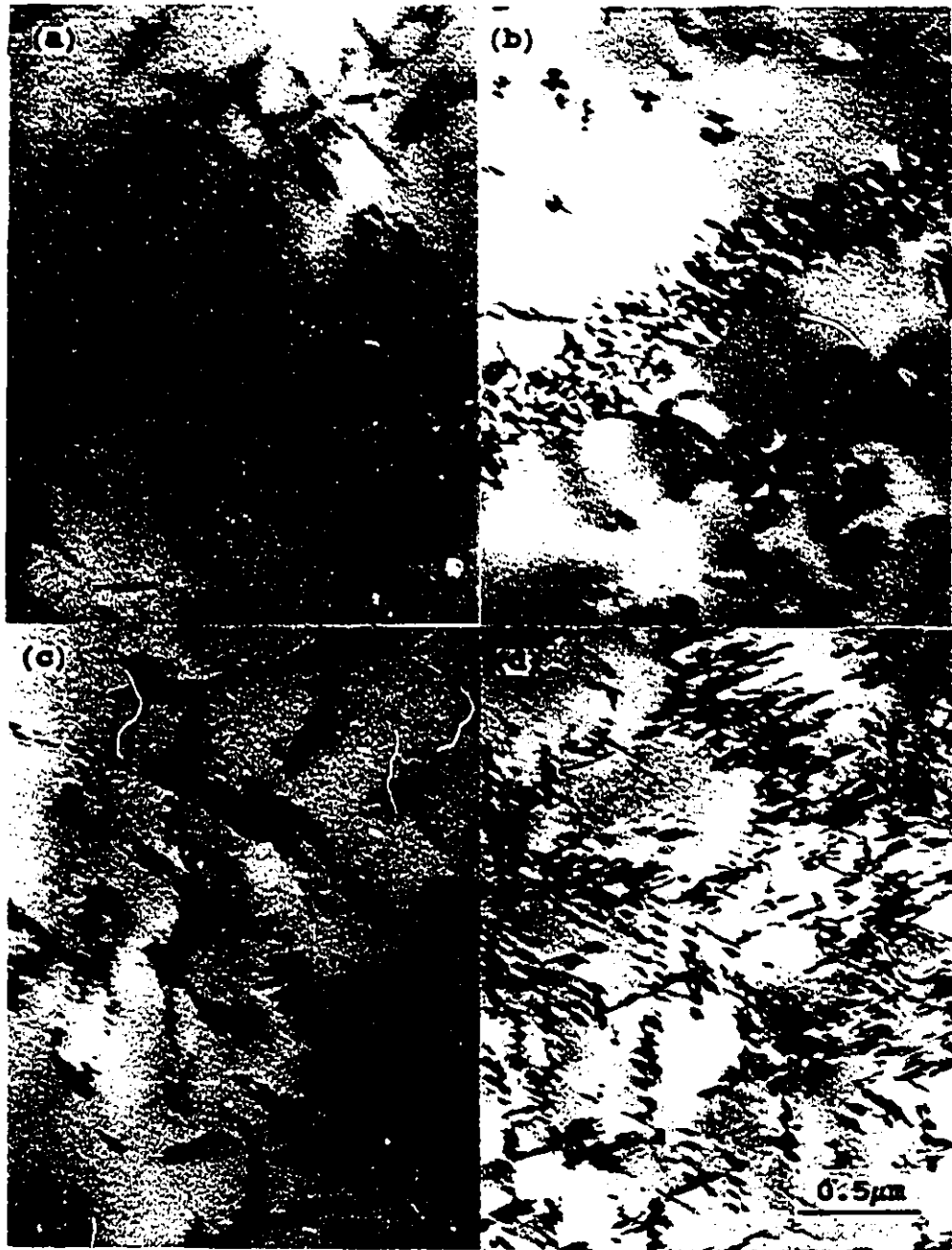


Fig. 19. TEM micrographs for alloys aged at 190° C for 5.7 h. (a) $\langle 110 \rangle_{Al}$ and (b) $\langle 112 \rangle_{Al}$ base alloy, (c) $\langle 110 \rangle_{Al}$ and (d) $\langle 112 \rangle_{Al}$ 0.15Be

seems to depend on the nature of the defect on which it forms. Rod-like precipitates form where several dislocation loops are aligned in one direction, and this is clearly shown in the two micrographs of Fig. 20, taken from the same area with slightly tilted direction. When dislocation loops form a circle, precipitate sheets tends to form (c.f. Fig. 19(a)).

Figs. 19(c) and (d) show the TEM micrographs for the Be-containing alloy, aged at 190 °C for 5.7 hours. It is evident that the basic lath or rod morphology of S' precipitate is not altered by the Be addition. Fig. 21 shows the $(100)_{\text{Al}}$ electron diffraction patterns of the S' phase for both the base and Be-containing alloys aged at 190 °C for 6 hours. The patterns are similar, indicating Be does not alter the crystal structure of the S' phase.

The TEM micrographs in Fig. 22, for the alloys aged at 190 °C for 19.5 h (peak hardness), show that the density of S' precipitate particles in Be-containing alloy (Fig. 22(c) and (d)) is higher compared to the base alloy (Fig. 22(a) and (b)), which is consistent with the SEM results discussed earlier. Also, there appears to be no preference for S' phase precipitation in the Be-containing alloy at grain or subgrain boundaries, as is the case for the base alloy (Fig. 23), and that the amount of the corrugated sheet or composite precipitate is larger in the Be-containing alloy (Fig. 24).

(c) Preaging Deformation

To determine the effects of pre-ageing deformation on the precipitation process, two base alloy specimens, one with 3% and another with 10% pre-aging deformation, were aged at 190 °C for 2 hours and examined by TEM. The 3% pre-aging deformation specimen shows a higher density of dislocations but very few S' precipitates (Fig. 25(a)), and the

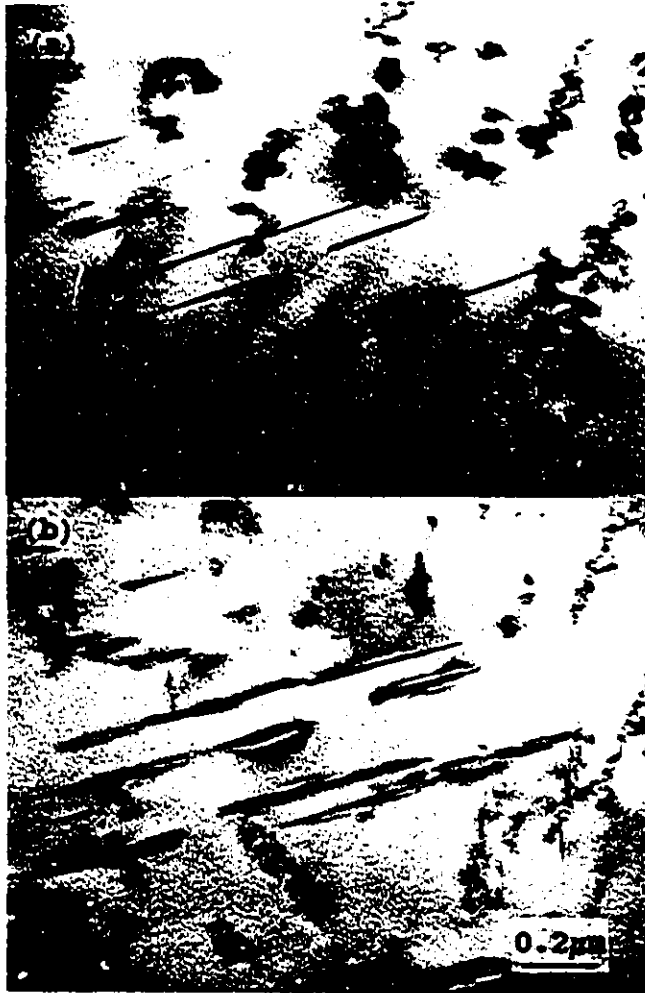


Fig. 20. TEM micrographs for base alloy aged at 190°C for 17 h. $\sim\langle 112 \rangle_{Al}$ foil orientation. (a) and (b) are taken from the same area with slight tilting.

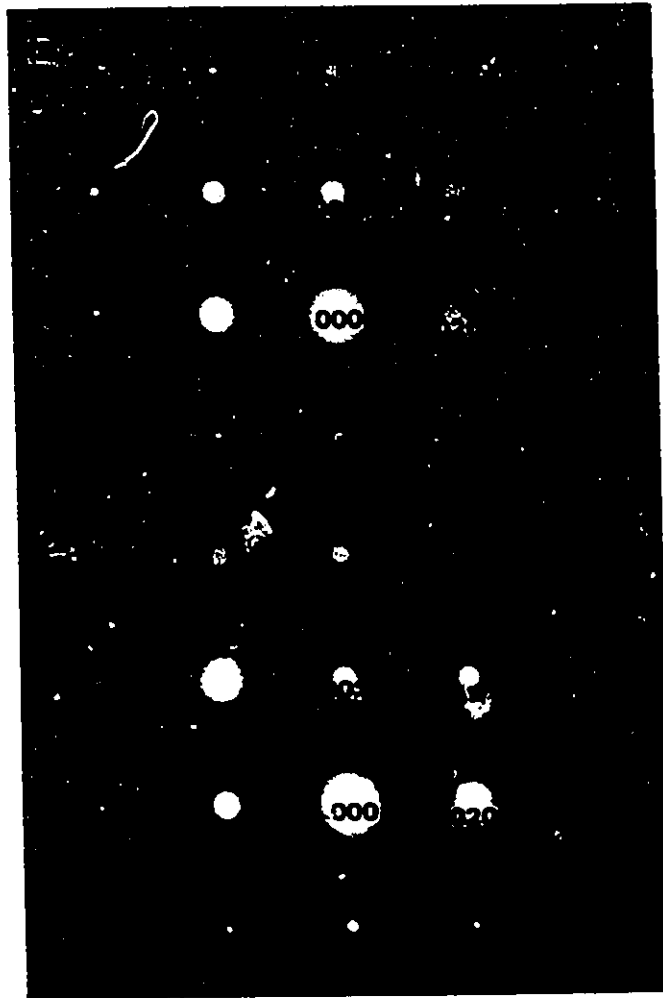


Fig. 21. Diffraction patterns for alloys aged at 190 °C for 5.7 h. $\langle 100 \rangle_{Al}$ foil orientation, spots indexed are from matrix. (a) base alloy, (b) 0.15Be.

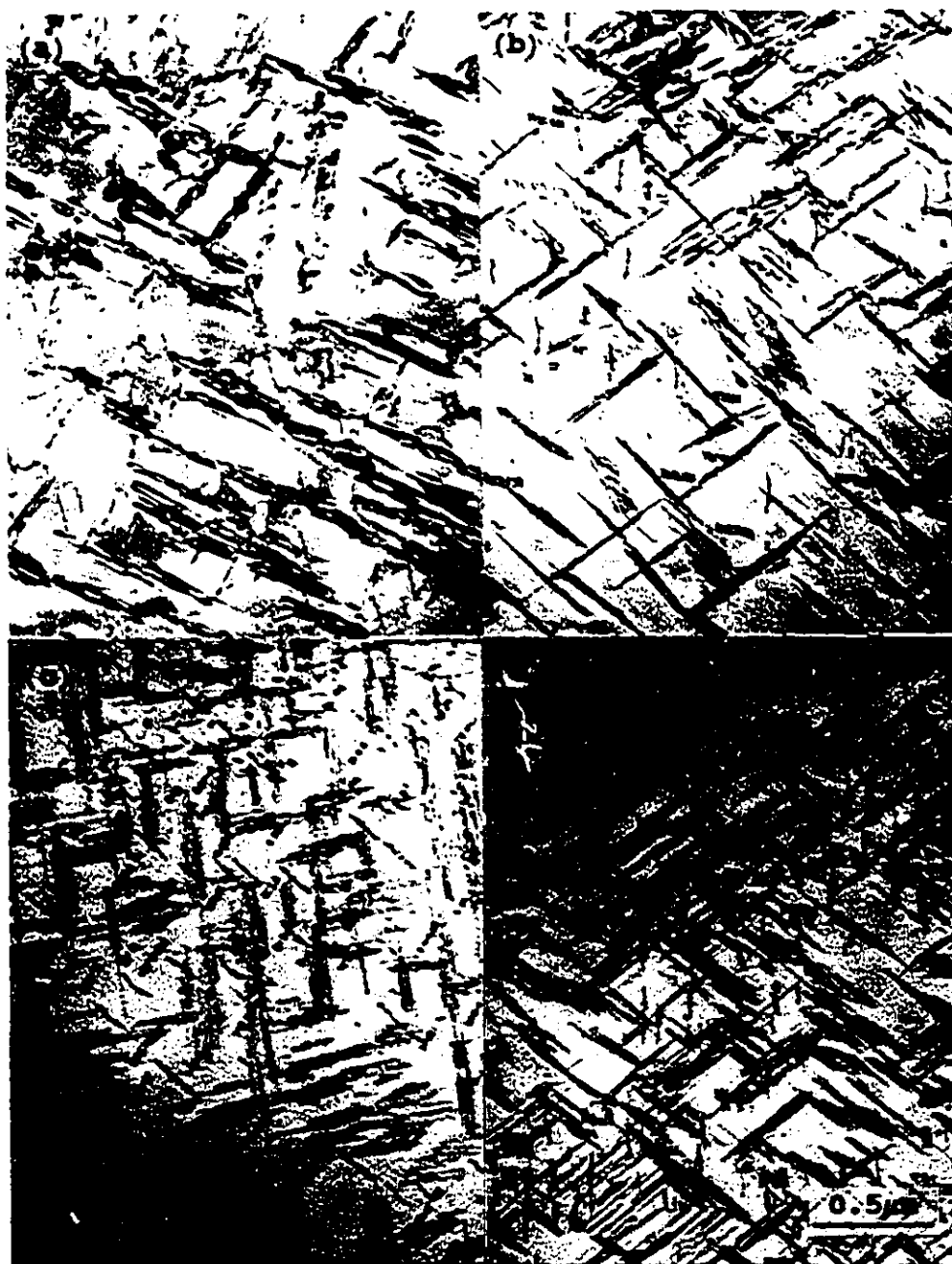


Fig. 22. TEM micrographs for alloys aged at 190°C for 19.5 h (peak hardness).
(a)-$\langle 100 \rangle_{Al}$ and (b)-$\langle 112 \rangle_{Al}$ base alloy, (c)-$\langle 100 \rangle_{Al}$ and (d)-$\langle 112 \rangle_{Al}$ 0.15Be.



Fig. 23. TEM micrographs. $\sim\langle 100 \rangle_{\text{Al}}$ foil orientation.
(a) base alloy (190°C for 5.7 h)
(b) 0.15Be (190°C for 19.5 h).



Fig. 24. TEM micrographs for alloys aged at 190°C for 19.5 h. $\langle 110 \rangle_{Al}$ foil orientation. (a) base alloy, (b) 0.15Be.



Fig. 25. TEM micrographs for alloys aged at 190°C for 2 h.
(a) $\langle 100 \rangle_{Al}$ base alloy (3% deformation),
(b) $\langle 111 \rangle_{Al}$ base alloy (10% deformation)
(c) $\langle 112 \rangle_{Al}$ base alloy, (d) $\langle 112 \rangle_{Al}$ 0.15Be.

10% deformation specimen shows more S' precipitates (Fig. 25(b)). For comparison, the micrographs for base and Be-containing alloys aged at 190 °C for 2 hours without preaging deformation are also shown in Fig. 25. It is evident that the Be-containing alloy Fig. 25(d) shows the highest density of S' precipitates, which indicates that the dislocation density is not the only factor to affect the nucleation of the S' precipitates.

(d) S' to S Phase Transition

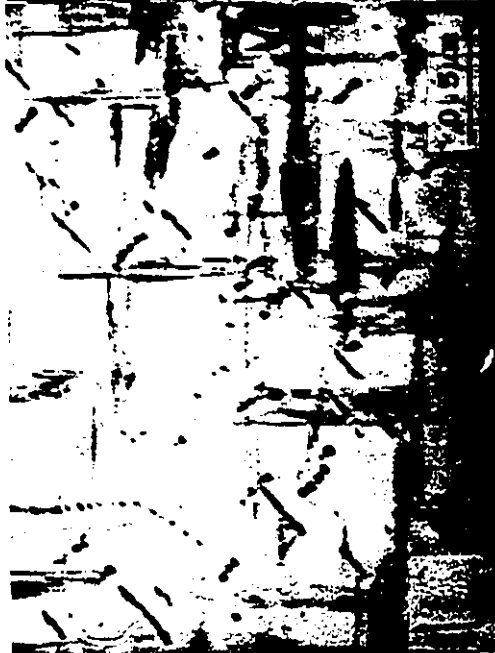
There is still disagreement on the mechanism for transition of S' to S phase, which is largely due to the conflicting evidence on the structure of the S' phase. There are 12 possible orientations of S' or S with the Al matrix, which gives a complex diffraction pattern and gives rise to the difficulty in identifying the precipitates by selected area diffraction method (SAD). Regarding this problem, Gupta *et al.* [105] recently examined the Al-1.53Cu-0.79Mg alloy aged at 190 °C by SAD and concluded that the S' phase is only the slightly strained version of the stable S phase. Based on the electron microscopy results reported by Weatherly [108], Wilson [7] suggested that the difference between the S' and S phase was probably not due to their crystal structure difference, but was a result of the orientation, and consequently the habit plane of the precipitate lath being less precisely defined at the low aging temperature. To confirm Wilson's hypothesis, a TEM examination combined with corresponding SAD patterns of the precipitates was carried out in the present investigation. A relatively high aging temperature of 350 °C was used, since according to Silcock [95], the true S phase can only be found at high aging temperatures in the region of 300 °C. To eliminate the errors resulting from the calibration of

crystalline image and diffraction pattern rotation, which occurs when using different magnifications, and also from interpreting the corresponding diffraction pattern, all the micrographs were taken at the same magnification, the same foil direction, and the same camera constant for the corresponding diffraction pattern.

Fig. 26 gives a series of micrographs and their corresponding diffraction patterns for the base alloy aged at 350 °C for various times, which are compared against the base and Be-containing alloy aged at 190 °C (including a room temperature age of 180 days). The short time intervals were chosen to trace the fast change from the metastable to the stable phase. The orientation relationship of the precipitates with the matrix for both alloys aged at 190 °C is the same, and remains constant to peak hardness. Therefore, it may be assumed that Be has no effect on the habit plane and growth direction of the S' precipitates, so that for the higher aging temperature, only base alloy is considered. Since all the micrographs were taken from $\langle 100 \rangle_{Al}$ foil, and the S' or S precipitates grow in $\langle 100 \rangle_{Al}$, an orthogonal relationship in the orientation of the precipitates is evident. The change in the growth direction of the precipitate relative to the matrix, which is obtained by measuring the angles between the laths or rods shown in the micrographs and the $\langle 100 \rangle_{Al}$ directions of the corresponding diffraction patterns, are given in Fig. 27.

For alloys aged at 190 °C followed by 180 day room temperature aging, the measurements show that the precipitates in both base alloy and Be-containing alloy have grown in directions close to $\langle 100 \rangle_{Al}$. For the base alloy aged at 350 °C for different periods, from 1 min to 120 min, the results show some changes in the orientation of the precipitate. After 1 min aging, the precipitates are formed and the length direction of the

(a) 190°C/19.5 h



(b) 190°C/19.5 h (0.15Be)



(a') 190°C/19.5 h



(b') 190°C/19.5 h (0.15Be)

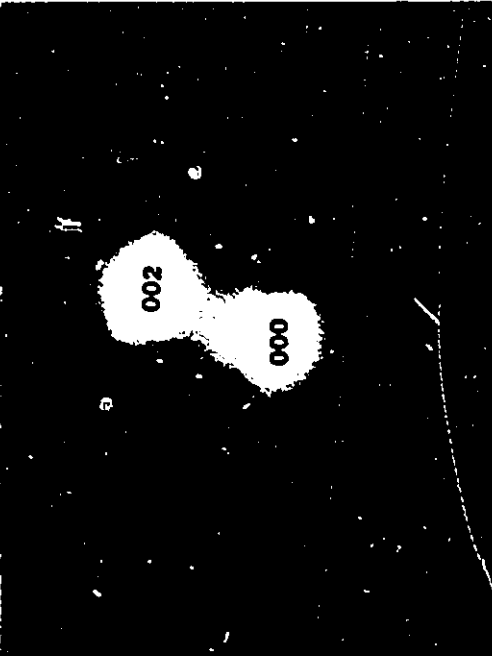


Fig. 26. TEM micrographs and corresponding diffraction patterns for alloys aged at indicated temperatures and times. Foil orientation $\sim \langle 100 \rangle_{Al}$.

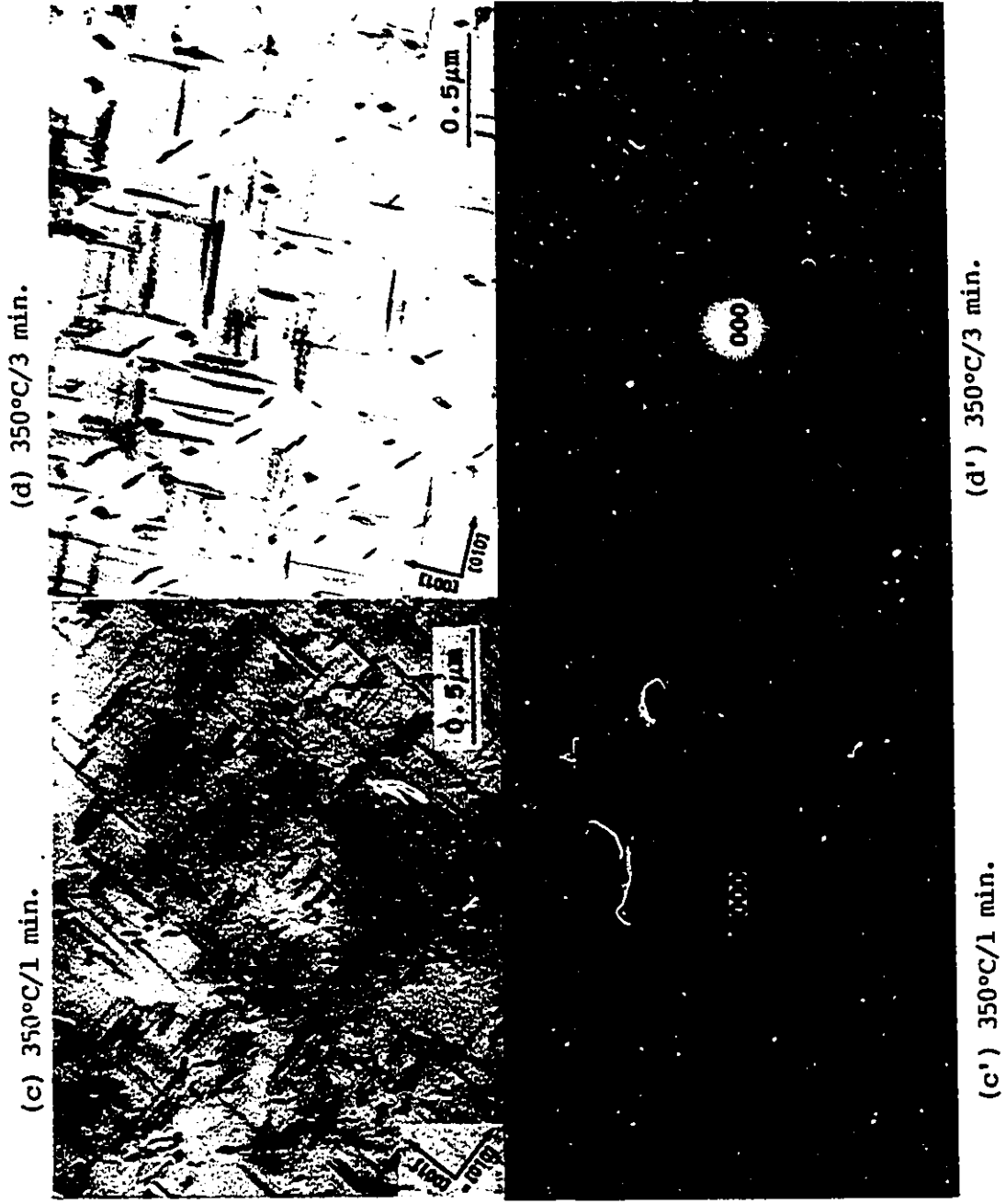
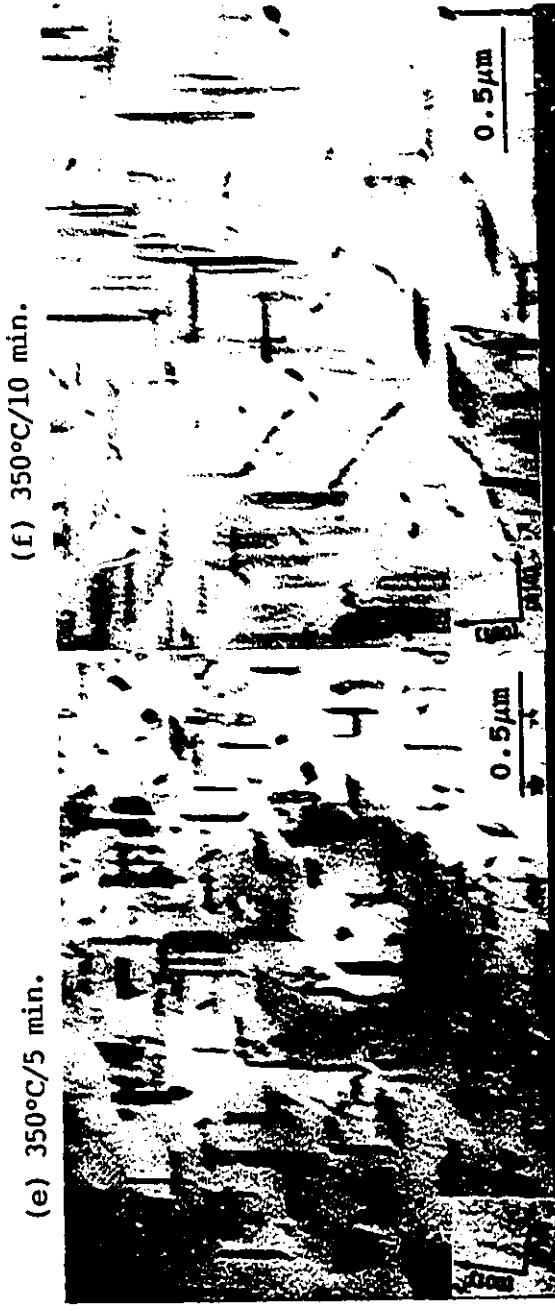
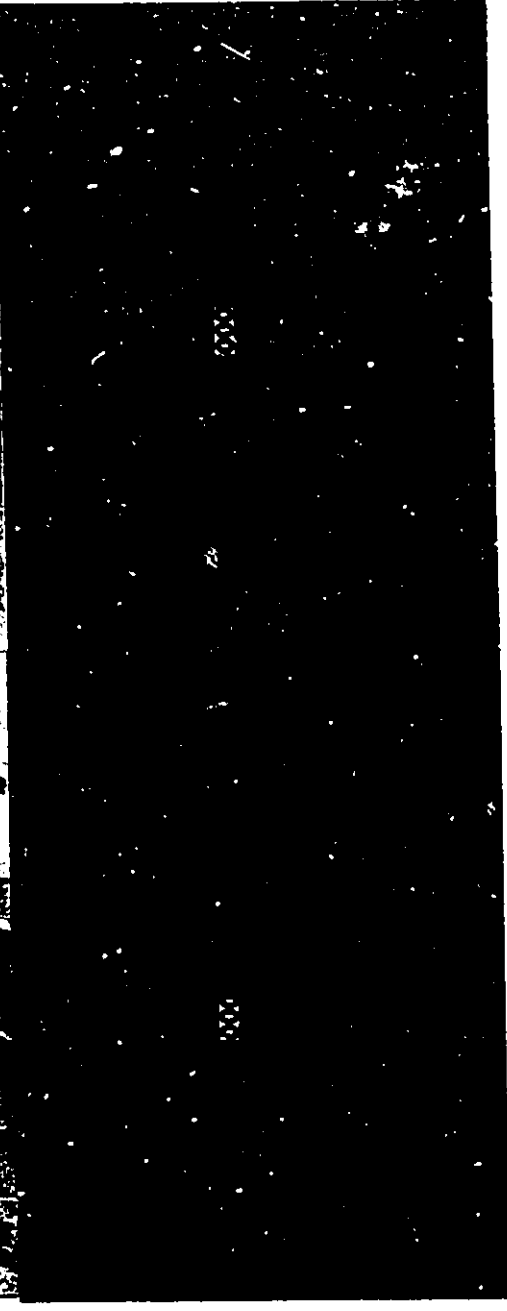


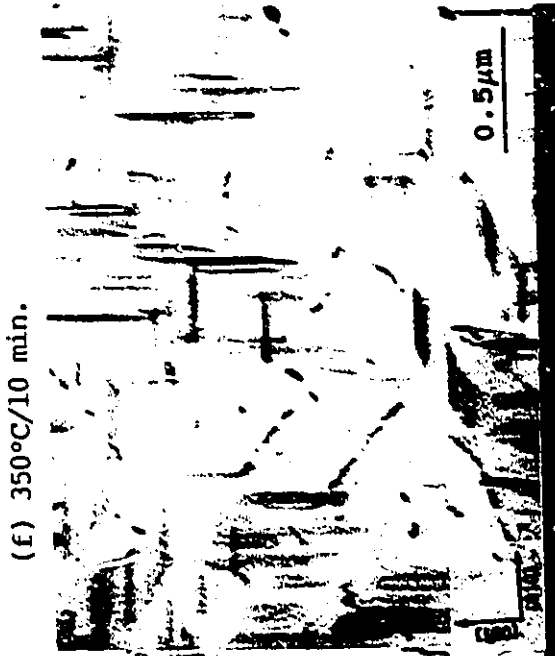
Fig. 26



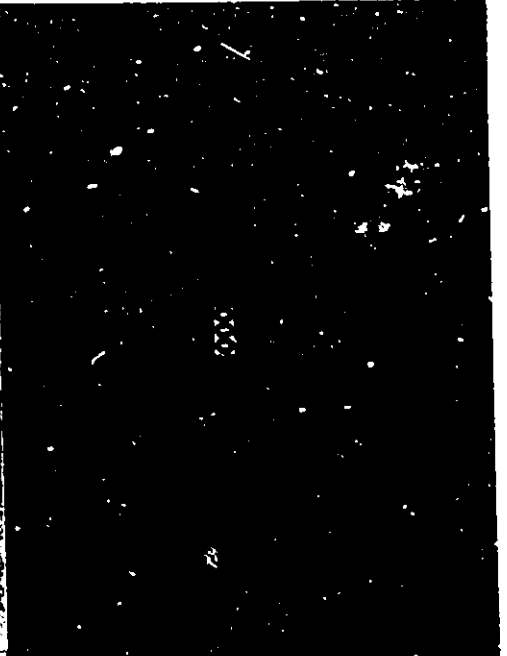
(e) 350°C/5 min.



(e') 350°C/5 min.



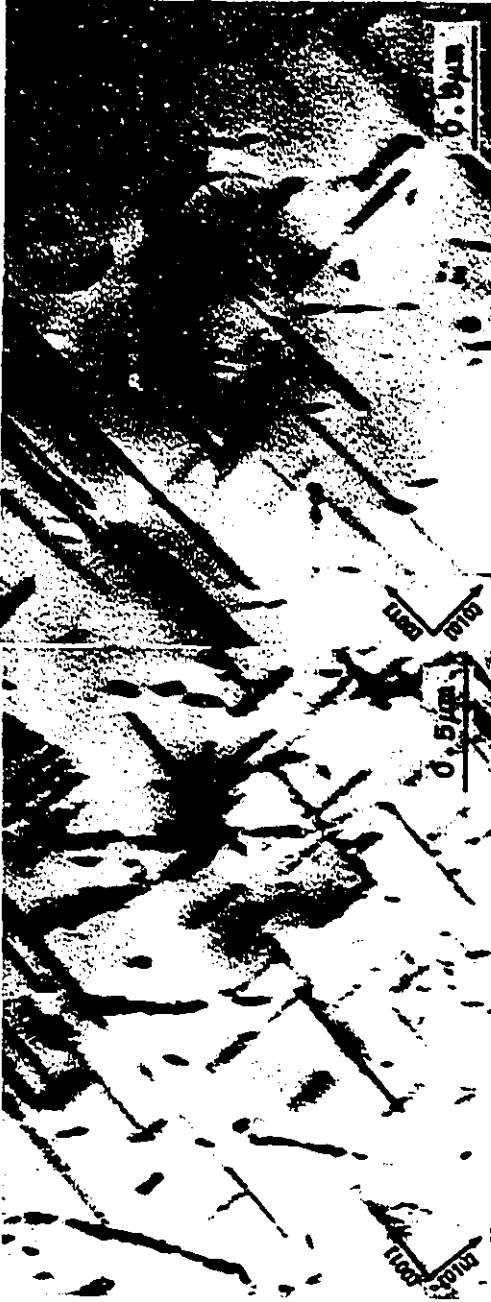
(f) 350°C/10 min.



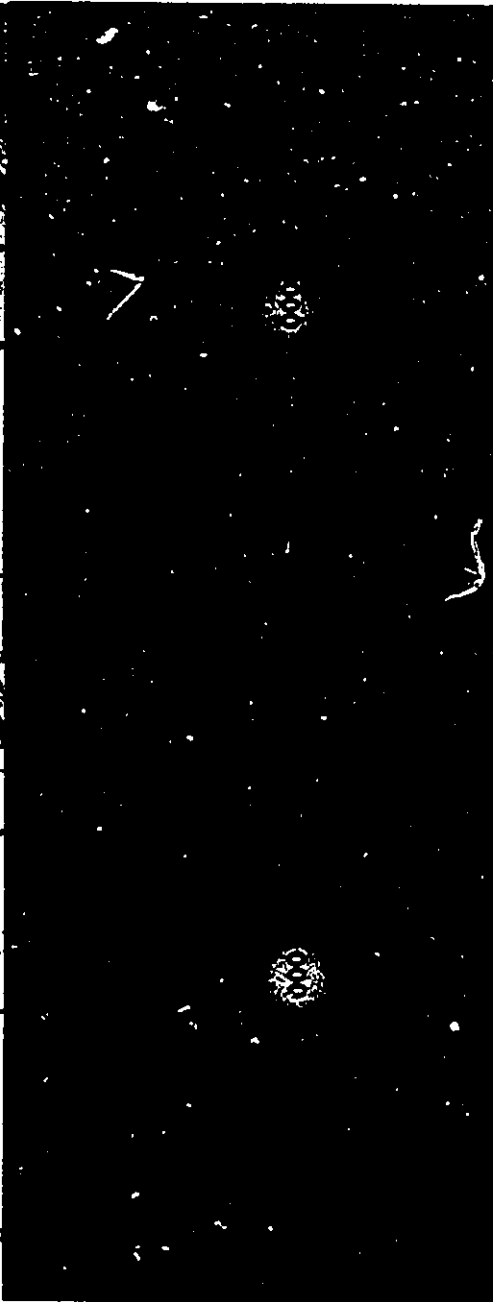
(f') 350°C/10 min.

Fig. 26

(g) 350°C/18 min.



(h) 350°C/30 min.



(g') 350°C/18 min.

(h') 350°C/30 min.

Fig. 26

(i) 350°C/60 min.



(j) 350°C/120 min.



(i') 350°C/60 min.

(j') 350°C/120 min.

Fig. 26

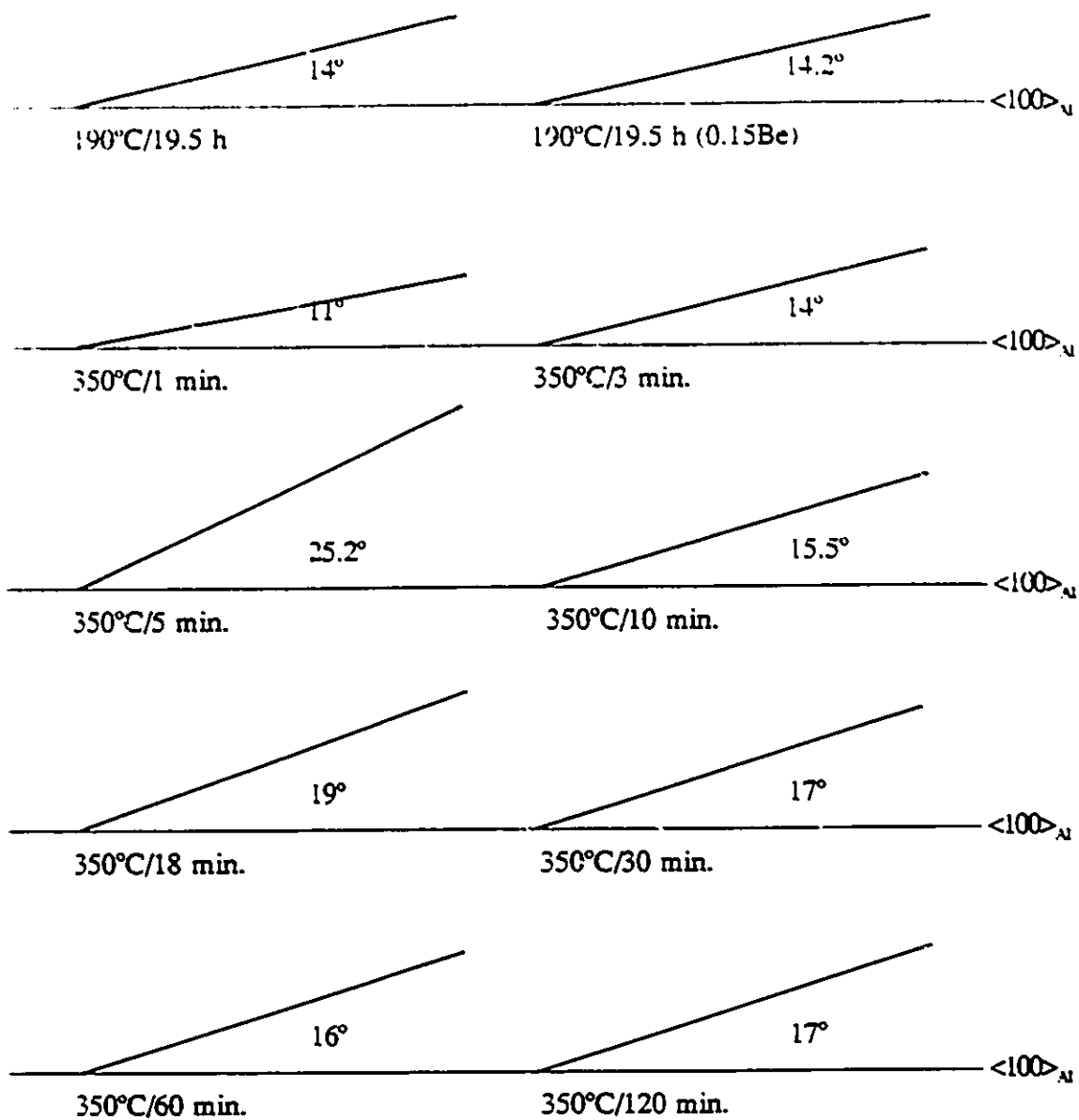


Fig. 27. Angles between S precipitate growth direction and $\langle 100 \rangle_{Al}$ measured from negatives (note each angle includes a 16.5° rotation angle between crystal image and diffraction pattern).

precipitates shifts 5.5° away from the $\langle 100 \rangle_{Al}$ direction, indicating that at early stages of precipitation, the growth direction is not exactly the $\langle 100 \rangle$ direction of Al matrix. After 3 min the precipitate length direction approaches $\langle 100 \rangle_{Al}$, which is the same orientation obtained for the alloys aged at $190^\circ C$, at which time the precipitates are assumed to be S' . When aged 5 min, however, the precipitates show a large change in both the length direction and the morphology, i.e. the mean length/width ratio of the precipitates is much smaller compared to alloys aged to other stages, which suggests that a transition from the S' to S phase occurred around this time. After 10 min aging at $350^\circ C$, the transition appears to be completed, as indicated by the relatively constant precipitate morphology and orientation, with the growth direction close to the $\langle 100 \rangle_{Al}$. The above results of the present investigation support Wilson's [7] interpretation of Weatherley's TEM micrographs [108] for S' to S transition.

B. S PHASE ANALYSIS

Alloys of Pure S phase and S phase containing 2% Be (7.4 at%Be) were prepared for analysis to determine if Be is incorporated into the S phase. Figs. 28 and 29 show the optical micrographs and the corresponding back scattered electron images respectively for the alloys following an homogenization anneal at $550^\circ C$ for 72 hours. The microstructure of the pure S phase alloy shows excess $Al(\alpha)$ phase present (identified as 3), and a small amount of oxide inclusion of a copper rich phase (identified as 1) dispersed in the S phase



Fig. 28. Optical micrographs of S phase alloys.
(a) S phase, (b) S phase + 2% Be.

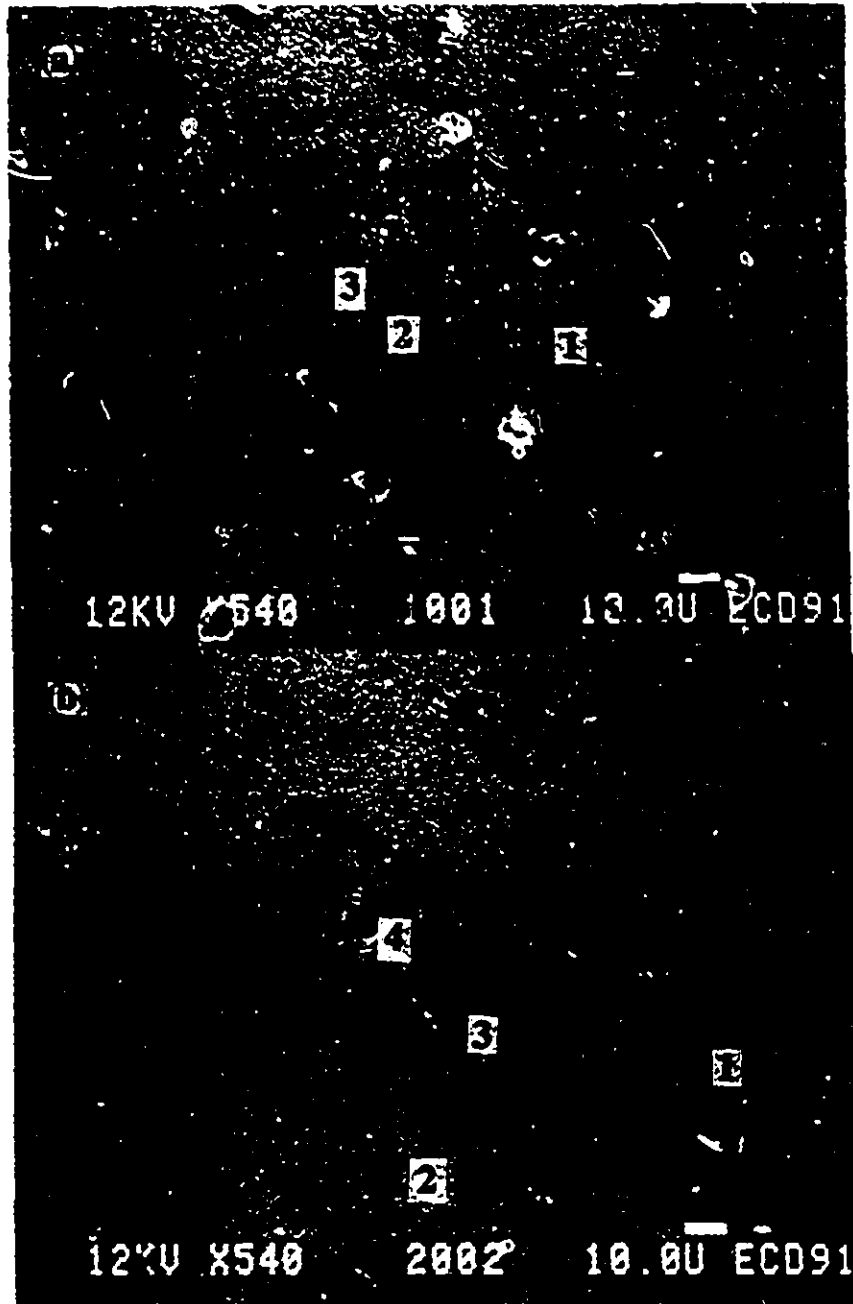


Fig. 29. SEM micrographs of S phase alloys.
(a) S phase, (b) S phase + 2% Be.

(identified as 2). The excess Al may be attributed to loss of the volatile Mg component during preparation of the alloy melt, and the oxide particles to some oxidation that invariably results during the preparation, melting, and stirring of the alloy melts.

The compositions of the phases identified in the micrographs, determined using WDS analysis for Be and O, and EDS for the remaining elements, are given in Table 1 and are estimated to be accurate to 2-3 at% of the absolute concentration for each of the elements (sensitivity limits of the analytical equipment). The composition of the S phase, determined as $\text{Al}_{51.3}\text{Cu}_{23.6}\text{Mg}_{25}$, is in good agreement with the stoichiometric formula for the line compound Al_2CuMg . The volume fractions of the phases given in Table 1 were obtained by image analysis, and estimated to be accurate to 20% of the values given.

The microstructure of the Be-containing S phase alloy is similar to that of the S phase, except for the presence of an additional impurity compound containing Be and Fe (identified as 4). The presence of Fe in the alloy can be traced to some Fe present as an impurity in the Al-5.23%Be master alloy used in the alloy's preparation. Based on the estimated volume fractions of the above phases, it appears that most of the Be (2% by weight) resides in the S phase and Al(α) phase, and the remainder is incorporated in one or more of the remaining phases, including the S phase, which cannot be detected due to the accuracy limits of the WDS and EDS analyses. A significant difference in the compositions of the phases between the two alloys is the decreased Mg and Cu content in the Al(α) phase for the Be-containing alloy. It is evident that Be has significantly decreased the solubility of both Cu and Mg in the Al(α) solid solution, $\text{Al}_{85.7}\text{Cu}_{4.7}\text{Mg}_{9.6}$ for S phase vs $\text{Al}_{94.8}\text{Cu}_{0.9}\text{Mg}_{4.2}$ for the Be-containing S phase alloy. This effect of Be in

reducing Mg solubility in Al(α) has also been reported by Fridlyander *et. al.* [137].

Table 1. Phases and the corresponding compositions in S phase alloy.

Sample	Phases (at.%)	Vol. Fraction (%) (estimated)
S phase alloy (Al ₂ CuMg)	1. Al _{10.5} Cu _{56.1} Mg _{6.1} O _{21.3}	< 5
	2. Al _{51.3} Cu _{23.6} Mg _{25.1}	75
	3. Al _{85.7} Cu _{4.7} Mg _{9.6}	20
S phase + 2 wt.%Be alloy	1. Al _{12.2} Cu _{63.0} Mg _{5.1} O _{19.7}	2
	2. Al _{51.2} Cu _{23.4} Mg _{25.4}	>85
	3. Al _{94.8} Cu _{0.9} Mg _{4.2}	10
	4. Al _{54.6} Mg _{33.2} Fe _{1.5} Be _{8.7} O _{2.1}	3

Powder samples of the alloys were analyzed by XRD, using Si as an internal calibration reference. The XRD patterns were analyzed using the "Appleman" program to search for the "best fitted" lattice constants for the known orthorhombic structure of S phase. The lattice constants, calculated from the diffraction patterns with an estimated accuracy of $\pm 0.001 \text{ \AA}$, are given in Table 2. There is a significant decrease ($\sim 0.25\%$) in the c parameter for the S phase alloy containing Be, indicating Be incorporation into the

S phase. Also, the ~15% increase in the microhardness for the S phase for the Be containing alloy (Table 2), is further evidence of significant Be incorporation into the S phase.

Table 2. S phase lattice constants and microhardness.

Samples	a_o (Å)	b_o (Å)	c_o (Å)	HV(0.050)
JCPDS*	4.000	9.250	7.150	
S phase	4.009	9.260	7.138	332±26
2 wt%Be	4.011(+0.05%)	9.269(+0.10%)	7.120(-0.25%)	383±17

* From the data file for powder X-ray diffraction pattern.

C. Be EFFECT on S' PHASE NUCLEATION

The EDS and WDS composition analysis of the S phase alloys indicate the incorporation of a significant amount of Be into the S phase, estimated at ~2at% or higher. This is supported by the XRD results showing ~0.25% decrease in the c lattice constant, which implies a substitutional replacement of either Al, Mg, or Cu atoms by the significantly smaller Be atom (atomic volume cm³/g-atom of Be is 4.9 vs 10.0 for Al,

14.0 for Mg, and 10.8 for Cu). The hardness increase for the S phase in the Be-containing alloy is also consistent with the substitutional replacement model, since the smaller Be atom would introduce a stress in the lattice.

1. Calculation of Nucleation Entropy

To calculate the nucleation entropy for the S phase, and the corresponding change due to Be incorporation, requires the formation entropy $\Delta S_{(Al_2CuMg)}$ for the compound, which is not available. Moreover, a calculation of the relative nucleation rates for the corresponding S' phases requires the interfacial energy $\gamma_{S'/Al(\alpha)}$, which is also not known. Nevertheless, a useful order-of-magnitude calculation of the relative nucleation rates can be obtained, since a formation entropy and interfacial energy can be estimated, and which (more importantly) can be assumed to be relatively unchanged by the incorporation of the small amount of Be into the S phase structure [80]. Most of the change (estimated at 90%) in nucleation entropy due to Be arises from the concentration of Be in the S' phase, and the decreased solubilities of Mg and Cu in Al(α).

The nucleation entropy for the S' phase is calculated for four cases:

- (a) the nucleation of Al_2CuMg in base alloy, using Mg and Cu solubilities from published ternary phase diagrams.
- (b) nucleation of $Al_{1.9}Be_{0.1}CuMg$ in the Be-containing base alloy, assuming a Be content of ~2.5at% replacing Al, and no Be effect on the solubilities of Mg and Cu in Al(α).
- (c) nucleation of Al_2CuMg in the Be-containing base alloy, using the Be-reduced solubilities of Mg and Cu in Al(α).

(d) nucleation of $Al_{1-x}Be_xCuMg$ in Be-containing base alloy, using the Be-reduced solubilities of Mg and Cu in $Al(\alpha)$.

The detailed reactions and calculations are shown for the first two cases only (c.f. Tables 3 and 4).

For the purpose of the calculations, the Be content in the supersaturated $Al(\alpha)$ solution, will be taken as the maximum Be solubility for the binary Al-Be phase diagram at 575 °C, i.e., 0.1at% (c.f. Fig. 2). The solubilities for Mg and Cu in the supersaturated $Al(\alpha)$ of the base alloy are estimated from the solvus line of the ternary diagram. The composition of the base alloy, Al-2.5Cu-1.2Mg (Al-1.08at%Cu-1.35at%Mg) or Al-6.2% Al_2CuMg , places the solvus line at approximately 460 °C, to give a supercooling (ΔT) of 270 K (cf. Fig.1(a), and saturated Cu and Mg solubilities of approximately 2.5 and 1.2% respectively (cf. Fig. 1(b)). In this case, the formation entropy for S phase is the principal unknown; however, as shown in other similar calculations, the formation entropy will not significantly change by the substitutional replacement of Al by 2.5at% Be, and as a result the formation entropy is not the important factor that mixing entropy is in determining the effect of Be incorporation [80]. For the purpose of this calculation, the formation entropy of 25 $JK^{-1}mol^{-1}$ will be used, which is in the range for other Al intermetallic compounds (e.g., 26.57 $JK^{-1}mol^{-1}$ for $TiAl_3$ at 463 K [138]).

Tables 3 and 4 give the appropriate reaction sequences required for removing the regular solution constraint on formation of the phases. The procedure is similar to that used in calculating the nucleation entropy for the $TiAl_3$ (and $TiAl_{2.4}Si_{0.6}$) in Al-Ti and Al-Ti-Si alloys [79]. The initial conditions for the base and Be-containing alloys are taken as

Al-1.08at%Cu-1.35at%Mg for both cases (a) and (b), with $\Delta T=270$ K. For case (b) the S' phase composition is $Al_{1.9}Be_{0.1}CuMg$, which corresponds to ~2.5at% Be incorporation. The concentrations in Tables 3 and 4 are all in atomic percent.

Table 3. Reaction sequence for calculating molar entropy of nucleation of Al_2CuMg at 463 K.

Reaction	ΔS Jmol ⁻¹ K ⁻¹
1a $4(Al-25Cu-25Mg)_{(s)}^{rs} \rightarrow 2Al_{(s)} + Cu_{(s)} + Mg_{(s)}$	-34.56
+	
2a $2Al_{(s)} + Cu_{(s)} + Mg_{(s)} \rightarrow Al_2CuMg$	25.00
+	
3a $\infty(Al-1.08Cu-1.35Mg)_{(s)}^{rs} \rightarrow 4(Al-25Cu-25Mg)_{(s)}^{rs} + \infty(Al-1.08Cu-1.35Mg)_{(s)}^{rs}$	-39.25
4a $\infty(Al-1.08Cu-1.35Mg)_{(s)}^{rs} \rightarrow Al_2CuMg + \infty(Al-1.08Cu-1.35Mg)_{(s)}^{rs}$	-48.81

Table 4. Reaction sequence for calculating molar entropy of nucleation of $Al_{1.9}Be_{0.1}CuMg$ at 463 K.

Reaction	ΔS Jmol ⁻¹ K ⁻¹
1b $4(Al-25Cu-25Mg-2.5Be)_{(s)}^{rs} \rightarrow 1.9Al_{(s)} + Cu_{(s)} + Mg_{(s)} + 0.1Be_{(s)}$	-37.86
+	
2b $1.9Al_{(s)} + Cu_{(s)} + Mg_{(s)} + 0.1Be_{(s)} \rightarrow Al_{1.9}Be_{0.1}CuMg$	25.00
+	
3b $\infty(Al-1.08Cu-1.35Mg-0.1Be)_{(s)}^{rs} \rightarrow 4(Al-25Cu-25Mg-2.5Be)_{(s)}^{rs} + \infty(Al-1.08Cu-1.35Mg-0.1Be)_{(s)}^{rs}$	-41.88
4b $\infty(Al-1.08Cu-1.35Mg-0.1Be)_{(s)}^{rs} \rightarrow Al_{1.9}Be_{0.1}CuMg + \infty(Al-1.08Cu-1.35Mg-0.1Be)_{(s)}^{rs}$	-54.74

Reaction 1a in Table 3 is for the (reverse) formation of 1 mole (4 g-atom) of the regular solid solution alloy Al-25Cu-25Mg alloy, for which the mixing entropy (-34.56 Jmol⁻¹K⁻¹) is calculated using equation

$$\Delta S_M^{reg} = -R [N_{Al} \ln N_{Al} + N_{Cu} \ln N_{Cu} + N_{Mg} \ln N_{Mg}] \quad (25)$$

Reaction 2a is the formation of 1 mole of Al₂CuMg at 463 K, for which the formation entropy of 25.00 Jmol⁻¹K⁻¹) is assumed. Reaction 3a is the nucleation reaction by which 1 mole of regular solid solution of Al-25Cu-25Mg is formed (precipitated) in an infinite (∞) amount of regular solid solution of Al-1.08Cu-1.35Mg, which is the composition of Al(α) for the base alloy, and assumed to be the composition at the solution treatment temperature for the alloy (575 °C). The entropy for reaction 3a (-39.25 Jmol⁻¹K⁻¹) is calculated using Eq. (16) to (20) for the ternary system. The reference of the regular solid solutions in 1a and 3a to the fcc structures for Al and Cu, and hcp structure for Mg removes transformation entropy from the calculation. Reaction 4a is obtained by adding reactions 1a to 3a which gives the nucleation reaction and corresponding nucleation entropy (-48.81 Jmol⁻¹K⁻¹) for the precipitation of one mole of real Al₂CuMg from a regular behaving supersaturated solid solution of Al-1.08Cu-1.35Mg at the aging treatment temperature of 463 K. The determination of the nucleation entropy of Al₂CuMg from the real solid alloy requires the appropriate thermodynamic information for the real solid alloy, which is not available. However, since the difference in molar entropies of mixing for regular and real solutions is small for dilute alloys (both converge and become zero at infinite dilution), the difference in the molar entropy for nucleation of Al₂CuMg in the real

vs. regular solution will likewise be small, and for the Cu and Mg concentrations in the present alloy ($N_{Cu}=0.011$, $N_{Mg}=0.014$) negligible.

The molar nucleation entropy for $Al_{1.9}Be_{0.1}CuMg$ is calculated as for Al_2CuMg , with the additional approximation that replacing 2.5at%Al with Be in the S phase lattice does not significantly change the formation entropy. The basis for this assumption is the structural similarity of Al_2CuMg and $Al_{1.9}Be_{0.1}CuMg$. The principal factors determining the entropy of a phase are structure and composition, which determine the bond energy. The structure is the principal factor determining bond energy, which has not changed, and the composition difference is small, and assumed negligible in comparison. It is noted that the approximately 12% increase (in magnitude) in the absolute molar nucleation entropy derives mostly from the Be contribution to the mixing entropy (c.f. reactions 4a and 4b), which is not significantly altered by errors introduced in the above approximation.

For the cases (c) and (d) the molar nucleation entropies for Al_2CuMg and $Al_{1.9}Be_{0.1}CuMg$ to precipitate in the Be-containing alloy are calculated based on the assumption that Be addition reduces Cu and Mg solubilities 20% in $Al(\alpha)$. This assumption can be made because Be addition has been found in several cases to cause a significant reduction in the solubilities of Mg and Cu in $Al(\alpha)$ as discussed earlier.

2. Nucleation Rate Comparison

A comparison of nucleation rates for the two intermetallic compounds can be obtained using Eq. (7), (12) and (15) with $f(\theta)=1$. Eq. (12) for ΔG^* incorporates the strain energy

associated with the phase change, and ΔG_v is replaced by $-\Delta S_v \Delta T$. The fraction volume changes ($\Delta V/V$) for Al_2CuMg formation is obtained from the gram-atomic volume for Al_2CuMg (9.957 cm^3) and Al (9.996 cm^3) as calculated from their respective lattice parameters [139]. For the $\text{Al}_{1.9}\text{Be}_{0.1}\text{CuMg}$, $\Delta V/V$ for Al_2CuMg is adjusted for the approximate volume decrease of $\sim 0.1\%$ due to Be incorporation (c.f. section B). The shear modulus of the Al matrix (μ_m) at 463 K is taken as $\sim 1/2$ of its room temperature value of $2.85 \times 10^4 \text{ Jcm}^{-3}$ [43], since at $T=463 \text{ K}$ relaxation processes will be operative [29] to decrease the elastic constants significantly. The S/Al(α) interfacial energy is not available, and for the purpose of the calculation $\gamma=1.0 \times 10^5 \text{ Jcm}^{-2}$ is used for both compounds. The above calculation for relative nucleation rates are summarized in Table 5.

Table 5. Comparison of relative nucleation rate

phase	V	$\Delta V/V$	W	ΔS_v	ΔG^*	$\frac{N(\text{Al}_{1.9}\text{Be}_{0.1}\text{CuMg})}{N(\text{Al}_2\text{CuMg})}$
	($\text{cm}^3/\text{g.at}$)	(10^{-3})	(J/cm^3)	($\text{JK}^{-1}\text{cm}^{-3}$)	(10^{23}J)	
(a) $\text{Al}_2\text{CuMg-Al}(\alpha)$	9.957	-3.90	0.11	1.23	15294.5	—
(b) $\text{Al}_{1.9}\text{Be}_{0.1}\text{CuMg-Al}(\alpha)$	9.947	-4.50	0.17	1.38	12140.7	1.39×10^2
(c) $\text{Al}_2\text{CuMg-Al}(\alpha)_{\text{Be}}$	9.957	-3.90	0.11	1.32	13192.3	5.2
(d) $\text{Al}_{1.9}\text{Be}_{0.1}\text{CuMg-Al}(\alpha)_{\text{Be}}$	9.947	-4.50	0.17	1.46	10786.3	1.16×10^3

Comparison of (a) and (b) in Table 5 indicates that the incorporation of 2.5at%Be into the Al_2CuMg phase can increase its nucleation rate by two orders of magnitude (assuming interfacial energies are not affected). A 20% decrease in Mg and Cu solubilities in $\text{Al}(\alpha)$ alone is also shown to increase the nucleation rate for Al_2CuMg more than five times (compare (a) and (c)). When the incorporation of 2.5at%Be into the Al_2CuMg phase is coupled with the decrease solubilities of Mg and Cu in $\text{Al}(\alpha)$, a more significant increase of nucleation rate is obtained (compare (a) and (d)). The above is useful only as a comparative calculation. However, it shows the role of nucleation entropy in stimulating precipitation of S phase, with the attendant refinement of the precipitate structure and increase in age hardening response of the Al-Cu-Mg alloy.

D. MECHANICAL PROPERTIES AND FRACTOGRAPHY

1. Tensile Properties and Impact Toughness

The yield and ultimate tensile strengths, elongation, and impact toughness (Charpy V notch) results for the alloys in the as-quenched and optimally aged (190 °C to peak hardness levels) conditions are given in Table 6. The mean values and standard deviation errors given in Table 6 are based on 6 samples, which are insufficient to allow any categorical determinations on the effect of Be on mechanical properties of the solution treated and quenched alloys. However, for the optimally precipitation hardened specimens, the Be-containing alloy shows a statistically significant increase in yield strength, tensile strength, elongation, and impact toughness. Generally, the Be-containing alloy specimens in the as quenched condition gave higher yield strength, which may be attributed to the

Table 6. Mechanical properties of the alloys in the solution treated and quenched (A.Q.), and precipitation hardened (P.H.) conditions.

alloy	heat treatment	0.002 YS (Mpa)	UTS (Mpa)	% Elong. (25 mm)	C _v (J)
base	A.Q.	123.1±14.6	247.0±11.0	30.7±2.0	38.7±0.7
base + 0.15%Be	A.Q.	131.2±12.6	244.2±12.6	29.1±0.6	37.6±0.5
base	P.H. (190°C)	210.8±4.8	281.3±13.0	25.2±0.8	24.8±1.8
base + 0.15%Be	P.H. (190°C)	220.2±7.9	306.2±11.6	27.6±0.8	27.2±3.4

solid solution strengthening effect of Be, and is consistent with the hardness results discussed earlier (cf Fig.6). However, the tensile strength, ductility and impact toughness of the solution treated and quenched Be-containing alloy are lower compared to the base alloy with the same treatment, and this may be attributable to the coarse Be particles (about 5 μm) evident in the microstructure (cf Fig. 4). The particle shape is critical in determining the fracture process in materials containing second phases. Large size particles (0.5-50 μm and above) do not generally contribute to strength, but play a critical role in determining the fracture toughness of the material. The flow stress and work-hardening rate for the alloys containing large particles are significantly higher than that of the single-phase matrix [76,140], and the presence of such particles in a highly strained region may cause the premature formation of voids, resulting in low strength and ductility. Fig. 30 is a fractograph of the Be-containing alloy showing the fractured Be particles and voids

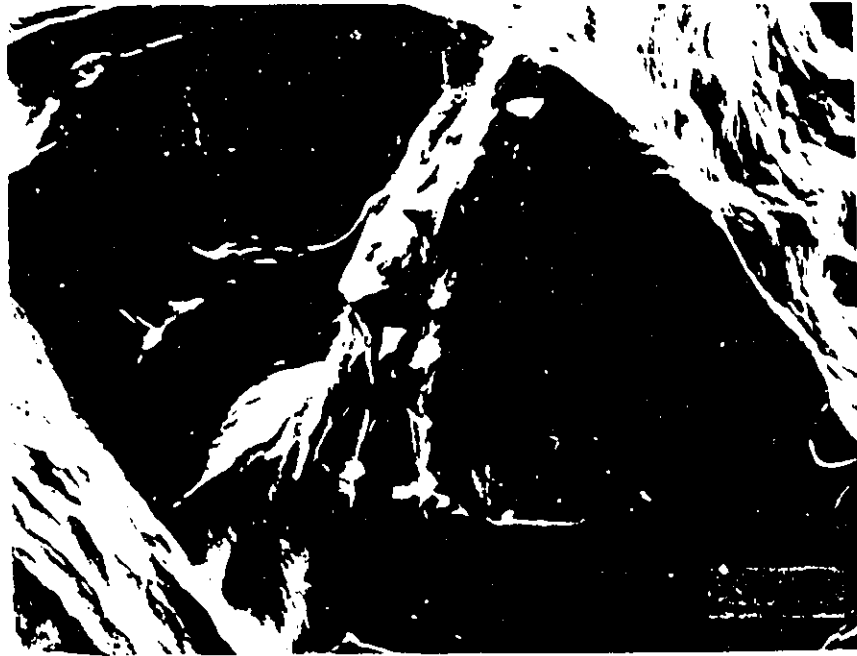


Fig. 30. SEM micrograph from fracture surface of a tensile specimen for the solution treated and quenched 0.15Be alloy.

that formed. The precipitation hardened Be-containing alloy (aged at 190 °C to peak hardness) shows an increase in yield and ultimate strengths of approximately 5% and 9% respectively, and an increase in ductility and impact toughness about 10% compared to the base alloy. This may be attributed to the refinement of the S' phase precipitate, and is in agreement with the results of Broek and Bowles [122], who showed that small S' precipitates are more effective in hindering dislocation motion in lowering the growth rate of fatigue-cracks.

The influence of precipitation on tensile strength, toughness and other mechanical properties depends principally on the strength, structure, spacing, size, morphology and distribution of the precipitate particles as well as on the degree of misfit or coherency with the matrix and on their relative orientation.

In the early stages of precipitation, the small coherent precipitates such as GP zones in Al alloys are of small interparticle spacings and can be readily sheared by dislocations during deformation. The shear or resisting force, which represents the strengthening effects, as summarized by Martin [76], may come from one or several of the following sources:

- Coherency hardening: coherency stress developed in the matrix by misfitting particles interacting with moving dislocations.
- Surface energy hardening: arises from the energy associated with the additional precipitate-matrix surface generated when a particle is sheared by the cutting dislocation.
- Order-hardening: due to the creation of an antiphase boundary when dislocations cut across precipitates which have an ordered lattice.

- Stacking-fault hardening: associated with the creation of a high energy surface because of the difference between the stacking-fault energy of the particle and that of the matrix.
- Modulus hardening: arises from differences between the elastic moduli of matrix and precipitates.

For strong precipitate particles, which are usually produced at later stages in the precipitation process, and are relatively large in size and have large interparticle spacings, the dislocations are able to bypass the precipitates by looping between them. In this situation the bypassing stress (τ) is given by the well known Orowan equation,

$$\tau = \frac{\mu b}{\lambda} \quad (26)$$

where μ is the shear modulus, b the Burgers vector, and λ the interparticle spacing.

It is obvious when the S' precipitate is refined and the density is increased, as in the case of Be-containing alloy, the particle spacing will become smaller and the shear stress, or strength will be increased.

The S' precipitates tend preferentially to form at grain or subgrain boundaries in the base alloy, which creates precipitation free zones (c.f. Fig. 23). The presence of PFZs diminished the alloy's mechanical properties. It was shown that Be addition inhibits formation of PFZs (c.f. Fig. 23), which may also contribute to the improvement in mechanical properties for the alloy.

2. Deformation Pattern and Fracture Behavior

The deformation mode for the tensile specimens aged to peak hardness at 190 °C were examined by TEM and the results are shown in Fig. 31. The micrographs show the formation of dislocation cells in the deformed structures. The SEM micrographs (Fig. 32) show the structures for both alloys characterized by the small dimples, indicating a ductile fracture mechanism. The SEM fractographs (Fig. 33) of the Charpy-V impact specimens also show a ductile fracture mode for both alloys.



Fig. 31. TEM micrographs from tensile specimens aged at 190°C to peak hardness. $\langle 100 \rangle_{\alpha}$ foils. (a) base alloy, (b) 0.15Be.

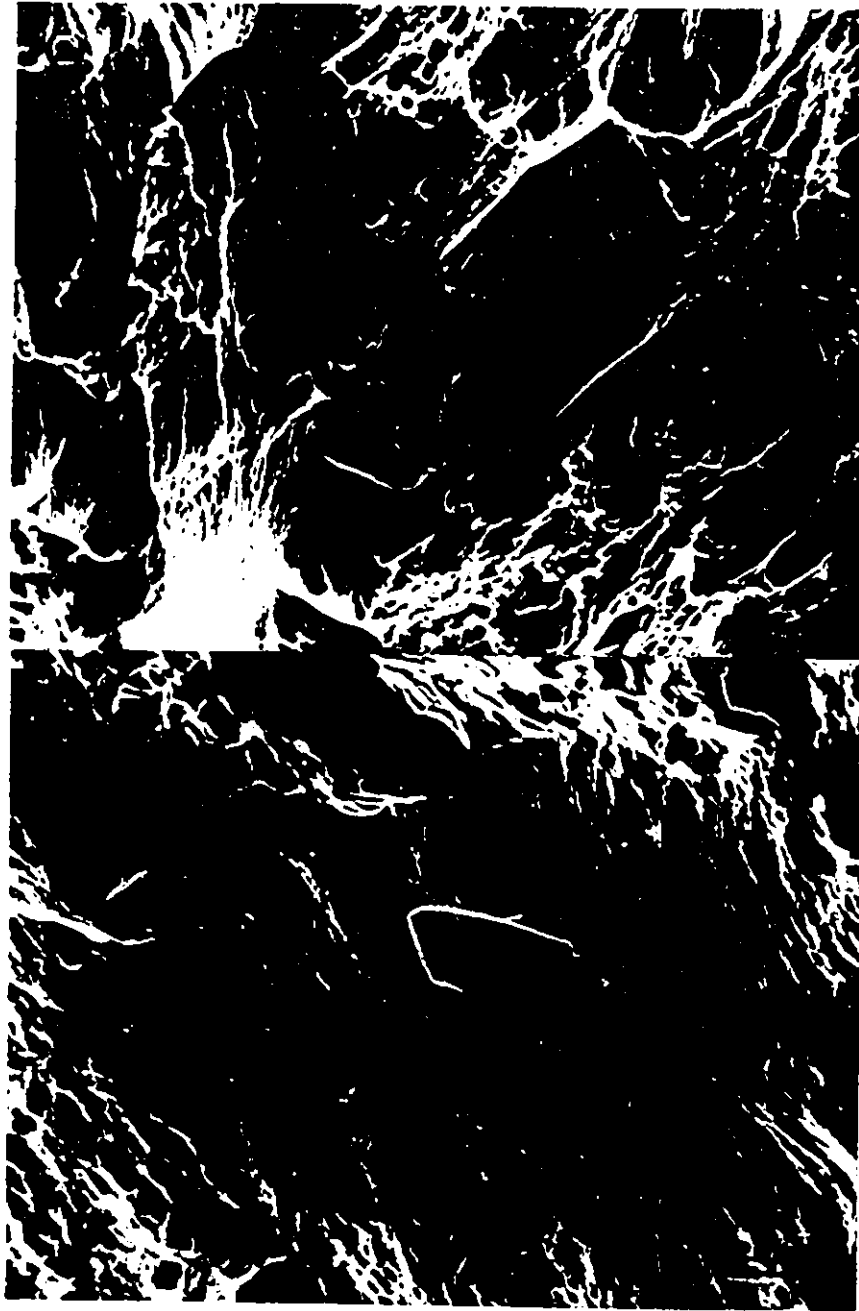


Fig. 32. SEM micrographs from fracture surface of tensile specimens aged at 190°C to peak hardness. (a) base alloy, (b) 0.15Be.



Fig. 33. SEM micrographs from fracture surface of Charpy-v test specimens aged at 190°C to peak hardness. (a) base alloy, (b) 0.15Be.

V. CONCLUSIONS

1. The addition of 0.15Be to Al-2.5Cu-1.2Mg alloy significantly increases the peak hardness levels obtained on age hardening, and is associated with refinement and an increase in the density of the S' precipitate.

2. The 0.15Be and 0.25Be alloys show no significant difference in precipitate density or age-hardening behavior, indicating that the optimum effect is obtained at Be saturation in the Al lattice.

3. The Be addition reduces the density of dislocation loops in the solution treated and quenched microstructure, which is attributed to the high Be-vacancy binding energy, and alters the single dislocation loop morphology to dislocation helices.

4. Natural aging (room temperature) up to two weeks shows no formation of S' precipitates in both base and Be-containing alloys.

5. The formation of S' precipitate is earlier for the Be-containing alloy when aged at 190 °C, and this is accompanied by the formation of a large number of dislocation loops by condensing the vacancies released by the Be atoms, indicating that Be is involved in the nucleation and precipitation of S' phase.

6. The precipitation of S' in both the base and Be-containing alloys obeys the Avrami equation.

7. The Be addition has no significant effect on the activation energy and growth parameter for the transformation. The basic lath- or rod-like morphology of S' precipitate

is not altered by Be addition. A mean activation energy of 113 kJ/mole indicates the precipitation of S' phase is volume-diffusion controlled.

8. The nuclei density-dependent k parameter is significantly higher for the alloy containing Be, which indicates a Be-enhanced nucleation rate, and is consistent with the higher density of precipitate particles in Be-containing alloy.

9. The preference for S' phase precipitation at grain or subgrain boundaries in the base alloy is inhibited in the Be-containing alloy.

10. The transition of S' to S phase at 350 °C aging temperature occurs after about 5 minutes' aging and is associated with an orientation change.

11. Up to 2.5at% Be can be incorporated into the S phase, resulting in a -0.25% decrease in the c lattice constant.

12. Be addition significantly decreases the solubility of both Mg and Cu in the Al(α) solid solution.

13. The incorporation of Be atoms into the S phase and the decrease in the solubilities of Cu and Mg in Al significantly increases the nucleation entropy and rate for the Be-containing alloy, which is consistent with the higher k parameter and observed higher S' precipitate density for the alloy containing Be.

14. The yield and tensile strengths, ductility, and impact toughness are increased significantly for the Be-containing alloy in the precipitation hardened condition compared to the base alloy. This is attributed to refinement of S' precipitate by the Be addition.

15. The basic ductile deformation and fracture mode of the alloy is not altered by the Be addition.

VI. SUGGESTIONS FOR FUTURE RESEARCH

1. The relationship of GPB zones to S' phase needs further study to unequivocally establish the occurrence of GPB→S' transition in the precipitation process. HVEM techniques are essential for the high resolutions required. Resistivity studies at lower temperature (RT to 150 °C) are required to obtain the kinetic data for the GPB→S' transition.

2. A more accurate determination of the Be solubility in S phase, and the solubilities of Cu and Mg in Al saturated with Be is essential for nucleation entropy calculations. Auger analysis for Be should be tried, and the solvus line of the Al (rich) corner of the quaternary calculated from available thermodynamic data and theoretical solution models.

3. A determination of the Al(α)/S interfacial energy, and the effect of Be is required for accurate calculations of the relative nucleation rates.

4. Several commercial alloys are based on S phase precipitation for age hardening and strengthening. The results of this study show considerable potential for improving the aging response and strength of these alloys by Be microalloying.

REFERENCES

1. W.S. Miller, M.P. Thomas, D.J. Lloyd and D. Creber: *Mat. Sci. & Tech.* **2**, 1210 (1986).
2. P.J. Gregson and H.M. Flower: *Acta Metall.* **33**, 527 (1985).
3. R. Grimes, A.T. Cornish, W.S. Miller and M.A. Reynolds: *Metals & Mat.* **1**, 357 (1985).
4. P.J. Gregson, H.M. Flower, C.N.J. Tite and A.K. Mukhopadhyay: *Mat. Sci. Tech.* **2**, 349 (1986).
5. P.J. Gregson, K. Dinsdle, S.J.Harris and B. Noble: *Mat. Sci. Tech.* **3**, 7 (1987).
6. H.M. Flower and P.J. Gregson: *Mat. Sci. Tech.* **3** 81 (1987).
7. R.N. Wilson: *J. Inst. Met.* **97**, 80 (1969).
8. R.N. Wilson, D.M. Moore and P.J.E. Forsyth: *J. Inst. Met.* **95**, 177 (1967).
9. N. Sen and D.R.F. West: *J. Inst. Met.* **97**, 87 (1969).
10. I.J. Polmear: *Trans Met. Soc. A.I.M.E.* **230**, 1331 (1964).
11. M.V. Hyatt: *Aluminum Alloys in the Aircraft Industry*, Stonehouse, Glos., Technicopy Ltd., p.31 (1978).
12. R.F. Ashton, D.S. Thompson and F.W. Gayle: in *Aluminum Alloys-their Physical and Mechanical Properties*, eds. E.A. Starke and T.H. Sanders, Warley, Eng. Mat. Advisory Service, vol. I, p.403 (1986).
13. J. Wadsworth and F.H. Froes: *JOM* p.12 (May 1989).
14. J.H. Auld, J.T. Vietz and I.J. Polmear: *Nature* **209**, 703 (1966).
15. I.J. Polmear: in *Proc. of the 10th Riso Int. Symp. Metall. Mat. Sci.: Mat. Architecture*, eds. J.B. Bilde-Sorensen *et al.*, Riso National Lab, Roskilde, Denmark, p.521 (1989).
16. J. Karov, W.V. Youdelis and R. Herring: *Mat. Sci. Tech.* **2**, 547 (1986).

17. J. Karov and W.V. Youdelis: *Mat. Sci. Tech.* **3**, 1 (1987).
18. T. Xiao and W.V. Youdelis: in *Proc. Inter. Symposium on Reduction and Casting of Aluminum*, ed. Christian Bidert, Pergamon Press, p.37 (1988).
19. T. Xiao and W.V. Youdelis: *Mat. Sci. & Tech.* **5**, 991 (1989).
20. R.E. Lewis, D.L. Yaney and L.E. Tanner: in *Aluminum-Lithium Alloys V, Proc. 5th Int. Al-Li Conf.*, eds. E.A. Starke, Jr. and T.H. Sanders, Jr., MCE, p.731 (1989).
21. W.C. Oliver, J. Wadsworth and T.G. Nieh: *Scripta. Met.* **21**, 1429 (1987).
22. A.E. Vidoz, D.D. Crooks, R.E. Lewis, I.G. Palmer and J. Wadsworth: *Rapidly Solidified Powder Aluminum Alloys, ASTM, STP 890*, eds. M.E. Fine and E.A. Starke, Jr., Philadelphia, PA, ASTM, p.237 (1986).
23. M. Volmer and A. Weber: *Z. Phys. Chem.* **119**, 277 (1925).
24. M. Volmer and H. Flood: *Z. Phys. Chem.* **170**, 273 (1934).
25. R. Becker and W. Döring: *Ann. Phys.* **24**, 719 (1935).
26. D. Turnbull and J.C. Fisher: *J. Chem. Phys.* **17**, 71 (1949).
27. I.S. Servi and D. Turnbull: *Acta. Metall.* **14**, 161 (1966).
28. A. Kelly and R.B. Nicholson: *Prog. Mater. Sci.* **10**, 151 (1963).
29. J.W. Christian: *The Theory of Transformations in Metals and Alloys*, Pergamon Press, Oxford (1965).
30. J.W. Christian: *The Theory of Transformations in Metals and Alloys*, 2nd Ed., Pergamon Press, Oxford (1975).
31. K.C. Russell: in *Phase Transformations*, ASM, Metals Park, OH, p.219 (1970).
32. R.B. Nicholson: in *Phase Transformations*, ASM, Metals Park, OH, p.269 (1970).
33. H.I. Aaronson, J.K. Lee and K.C. Russell: in *Precipitation Processes in Solids*, eds. K.C. Russell and H.I. Aaronson, Met. Soc. AIME, Warrendale, PA, p.31 (1978).
34. K.C. Russell: *Adv. Colloid and Interface Sci.* **13**, 205 (1980).
35. R.D. Doherty: in *Physical Metallurgy, Part II*, eds. R.W. Cahn and P. Haasen, North-

- Holland Physics Publishing, Amsterdam, p.933 (1983).
36. J.K. Lee, Y.Y. Earmme, H.I. Aaronsson and K.C. Russel: *Met. Trans.* 11A, 1837 (1980).
 37. J.K. Lee and W.C. Johnson: in *Solid-State Phase Transformations, the Pittsburg Conference*, ed. H.I. Aaronson, Met. Soc. AIME, Warrendale, PA, p.127 (1983).
 38. F.R.N. Nabarro: *Proc. Roy. Soc.* A175, 519 (1940).
 39. J. Burke: in *The Kinetics of Phase Transformation in Metals*, Pergamon Press, Oxford, p.132 (1965).
 40. N. Raghaven and M. Cohen: in *Treatise on Solid State Chemistry, Vol. 5*, ed. N.B. Hannay, Plenum Press, p.67 (1975).
 41. J.D. Eshelby: *Proc. Roy. Soc.* A241, 376 (1957).
 42. J.D. Eshelby: *Prog. in Solid Mechanics*, 2, 89 (1961).
 43. J.K. Lee, D.M. Barnett and H.I. Aaronsson: *Met. Trans.* 8A, 963 (1977).
 44. J.K. Lee, W.C. Johnson: *Scripta Met.*, 11, 477 (1977).
 45. R.B. Nicholson: in *Phase Transformations*, ASM, Metals Park, OH, p.269 (1970).
 46. H.B. Aaron and H.I. Aaronson: *Met. Trans.* 2, 23 (1971).
 47. J.W. Cahn: *Acta Metall.* 4, 441 (1956).
 48. J.W. Cahn: *Acta Metall.* 5, 168 (1957).
 49. E. Hornbogen and M. Roth: *Zeit. Metallkunde* 58, 842 (1967).
 50. W.C. Leslie: *Acta Metall.* 9, 1004 (1961).
 51. R. Gomez-Ramirez and G.M. Pound: *Met. Trans.* 4, 1563 (1973).
 52. C.C. Dollins: *Acta Metall.* 18, 1902 (1970).
 53. B.Ya. Lyubov and V.A. Solv-Yev: *Fiz. Metal. Metallography* 19, 333 (1965).
 54. F. C. Larche: in *Dislocations in solids, vol. 4*, ed. F.R.N. Nabarro, North-Holland Publishing company, Amsterdam, p.135 (1979).

55. G.W. Lorimer and R.B. Nicholson: in *The Mechanisms of Phase Transformations in Crystalline Solids*, The Metals Society, London, p.36 (1969).
56. M.H. Jacobs and D.W. Pashley: in *The Mechanisms of Phase Transformations in Crystalline Solids*, The Metals Society, London, p.43 (1969).
57. I.J. Polmear: *J. Australian Inst. Metals* 11, 246 (1966).
58. I.J. Polmear: *Mat. Sci. Forum* 13-14, 195 (1987).
59. A.H. Sully, H.K. Hardy and T.J. Heal: *J. Inst. Met.* 76, 269 (1949-50).
60. H.K. Hardy: *J. Inst. Met.* 80, 483 (1951-52).
61. H.K. Hardy: *J. Inst. Met.* 82, 236 (1953-54).
62. J.M. Silcock, T.J. Heal and H.K. Hardy: *J. Inst. Met.* 84, 23 (1955-56).
63. J.M. Silcock: *Phil. Mag.* 4, 1187 (1959).
64. K.M. Entwistle, J.H. Fell and Kang Ij Koo: *J. Inst. Met.* 91, 84 (1962-63).
65. E. Holmes and B. Noble: *J. Inst. Met.* 95, 106 (1967).
66. J.B.M. Nuyton: *Acta Metall.* 15, 1765 (1967).
67. B. Noble: *Met. Sci.* 2, 117 (1968).
68. S.K. Das *et. al.*: in *Septieme Congress International de Microscope Electronique, Grenoble*, p.533 (1970).
69. R. Sankaran and C. Laird: *Mat. Sci. Eng.* 14, 271 (1974).
70. H. Suzuki, M. Kanno and G. Itoh: *J. Jpn. Inst. Light Met.* 30, 3 (1980).
71. I.J. Polmear: *J. Inst. Metals* 97, 20 (1968).
72. A.T. Stewart and J.W. Martin: *J. Inst. Metals* 98, 62 (1970).
73. J.T. Vietz and I.J. Polmear: *J. Inst. Metals* 94, 410 (1966).
74. W.V. Youdelis and W. Fang: *Mat. Sci. Tech.* 7, 201 (1991).
75. W.V. Youdelis, W. Fang and T.D. Lowes: *Mat. Sci. Tech.* 6, 1227 (1990).

76. J.W. Martin: *Micromechanisms in Particle-Hardened Alloys*, eds. R.W. Cahn *et al.*, Cambridge Univ. Press (1980).
77. U. Köster: in *Recrystallization of Metallic Materials*, ed. F. Haessner, Riederer, Stuttgart, p.215 (1971).
78. W.V. Youdelis: *Met. Sci.* 9, 464 (1975).
79. W.V. Youdelis: *Met. Sci.* 13, 540 (1979).
80. W.V. Youdelis and C.S. Yang: *Metal Sci.* 16, 275 (1982).
81. S.P. Iyer and W.V. Youdelis: *Aluminum* 53, 252 (1977).
82. W.V. Youdelis and S.P. Iyer: *Aluminum* 2, 152 (1979).
83. W.V. Youdelis: *Met. Sci.* 12, 363 (1979).
84. W.V. Youdelis and O. Kwon: *Met. Sci.* 17, 379 (1983).
85. W.V. Youdelis and O. Kwon: *Met. Sci.* 17, 385 (1983).
86. G.W. Delamore and R.W. Smith: *Met. Trans.* 2, 1733 (1971).
87. J. Karov, W.V. Youdelis: *Mat. Sci. Tech.* 3, 394 (1987).
88. W.V. Youdelis and J. Karov: *Mat. Sci. Forum* 13-14, 483 (1987).
89. A. Hatab: *Master Thesis*, University of Windsor 1992.
90. M. Avrami: *J. Chem. Phys.* 71, 1103 (1939).
91. W.A. Johnson and R.F. Mehl: *Trans. Amer. Inst. Min. Engrs.* 135, 416 (1939).
92. C. Wert and C. Zener: *J. Appl. Phys.* 21, 5 (1950)
93. A.K. Jena, A.K. Gupta and M.C. Chaturvedi: *Acta metall.* 37, 885 (1989).
94. H.K. Hardy: *J. Inst. Metals* 83, 17 (1954-55).
95. J.M. Silcock: *J. Inst. Metals* 89, 203 (1960-61).
96. L.A. Willey: *Metals Handbook*, 8, 8th ed, ASM Metal Park, OH, p386, 1973.

97. C.G. Rhodes and G. Garmon: *Met. Trans.* 3, 1861 (1972).
98. J.L. Murray and D.J. Kahan: "*Bulletin of Alloy Phase Diagrams*", 4(1), 50 (1983).
99. H. Lambot: *Mem. Acad. Roy. Belg. Classe. Sci.* 26, 1609 (1950).
100. Yu.A. Bagaryatsky: *Zhur. Tech. Fiziki* 18, 827 (1948).
101. Yu.A. Bagaryatsky: *Doklady Akad. Nauk SSSR* 87, 559 (1952).
102. V. Gerold and H. Haberkorn: *Z. Metallk.* 50, 568 (1959).
103. A.A. Alekseyev, L.S. Ber, L.G. Klimovich and O.S. Korobov: *Fizika Metall. Metalloved.* 46, 548 (1978).
104. R.N. Wilson and P.G. Partridge: *Acta Met.* 13, 1321 (1965).
105. A.K. Gupta, P. Gaunt and M.C. Chaturvedi: *Phil. Mag.* 55, 325 (1987).
106. P.J. Gregson, C.J. Peel and B. Evans: in *Aluminum-Lithium Alloys III*, ed. C. Baker *et al.*, London, The Inst. of Metals, p516 (1986).
107. V. Radmilovic, G. Thomas, G.J. Shiflet and E.A. Starke, Jr.: *Scripta Metall.*, 23, 1141 (1989).
108. G.C. Weatherly: *Ph.D Thesis*, Univ. Cambridge (1966).
109. H. Perlitz and A. Westgren: *Ark. Kemi. Miner. Geol. B.* 16, 13 (1943).
110. G.C. Weatherly and R.B. Nicholson: *Phil. Mag.* 17, 801 (1968).
111. R. Horiuchi and Y. Minonishi: *J. Jap. Inst. Met.* 39, 936 (1970).
112. N. Sen and D.R.F. West: *J. Mat. Sci.* 3, 266 (1968).
113. K. Boyapati and I.J. Polmear: *Fatigue in Eng. Mat. & Struc.* 2, 23 (1979).
114. R.N. Wilson and P.J.E. Forsyth: *J. Inst. Met.* 94, 8 (1966).
115. S. Özbilen and H.M. Flower: *Acta Metall.* 31, 2993 (1989).
116. M.C. Chaturvedi, A.K. Gupta and A.K. Jena: *Mat. Sci. Eng.* A110, 187 (1989).

117. A.K. Gupta, M.C. Chaturvedi and A.K. Jena: *Mat. Sci. Tech.* **3**, 1012 (1987).
118. A.K. Gupta, M.C. Chaturvedi and A.K. Jena: *Mat. Sci. Tech.* **5**, 52 (1989).
119. M. Hansen and K.L. Dreyer: *Aluminum*, **22**, 134 (1940).
120. H.K. Hardy and T.J. Heal: in *The Mechanism of Phase Transformations in Metals and Alloys*, Monograph No. 18, p.1., Inst. Metals, London (1955).
121. D. Gualandi and M. Leoni: *Alluminio*, **26**, 203 (1957).
122. D. Broek and C.Q. Bowles: *J. Inst. Met.* **99**, 255 (1971).
123. A.A. Tavassoli: *Met. Sci.* **8**, 424 (1974).
124. X. Xia and J.W. Martin: *Mat. Sci. Eng.* **A128**, 113 (1990).
125. H.D. Peacock and J.W. Martin: in *Ref. 20*, p.1013 (1989).
126. M. Ahmad and T. Ericsson: in *Ref. 106*, p509 (1986).
127. H.M. Flower, P.J. Gregson, C.N.J. Tite and A. Mukhopadhyay: in *Proc. Int. Conf. on Aluminum Alloys, their Physical and Mechanical Properties*, eds. E.A. Starke and T.H. Sanders, Charlottesville, Va., Warley, Eng. Mat. Advis. Serv., vol.II, p743 (1986).
128. A.J. Shakesheff, D.S. Mcddarmaid and P.J. Gregson: *Mat. Sci. Tech.* **7**, 276 (1991).
129. J.B. Murphy: *Acta Metall.* **9**, 563 (1961).
130. E.S. Dwarakadasa, K.S. Raman and K.I. Vasu: *Scripta Met.* **2**, 639 (1968).
131. Y. Baba: *Sumitomo It Metal Tech. Rep.* **8(2)**, 1 (1967).
132. M. Ohta, F. Hashimoto and T. Tanimoto: *J. Phys. Soc. Japan* **22**, 352 (1967).
133. A. Van Den Beukel: *Phys. Stat. Sol.* **23**, 165 (1967).
134. E.S. Dwarakadasa: *Scripta Met.* **6**, 187 (1972).
135. S. Ceresara, A. Giarda and A. Sanchèz: *Phil. Mag.* **35(1)**, 97 (1977).
136. S. Özbilen and H.M. Flower: in *Aluminum-Lithium Alloys V, Proc. 5th Int. Al-Li Conf.*, eds. E.A. Starke, Jr. and T.H. Sanders, Jr., MCE, p651 (1989).

137. I.N. Fridiyander, K.P. Yatsenko, G.A. Nekrasova, V.S. Sandler, Z.G. Semenova and A.N. Gulin: *Met. Sci. Heat Treat.* 7, 599 (1970).
138. J.M. Stuve and M.J. Ferrante: U.S. Dept. of the Interior, Bureau of Mines Report R17834, 1974.
139. X-ray Powder Data File, ASTM, 1978.
140. D. Broek: *Elementary Engineering Fracture Mechanics*, 4th Ed., Martinus Nijhoff Publishers, Dordrecht, p48, 308 (1986).

PUBLICATIONS

1. W. Fang and W. V. Youdelis, "*Effect of Be on the Defect Structure and Morphology of S' Precipitate in Pseudo-binary Al(α)-S(Al_2CuMg) Alloy*", accepted for publication in the Symposium Proc. of 31st Annual CIM Conference of Metallurgists, August 1992, Edmonton, Alberta. (under Advances in Production and Fabrication of Light Metals).
2. W.V. Youdelis and W. Fang, "*The effect of Be on the Age-hardening of Al-2.5Cu-1.2Mg Alloy*", Proc. of Inter. Conference on Recent Advances in Science and Engineering of Light Metals, Japan Inst. of Light Metals, Tokyo, October, 1991, Ed. K. Hirano, H. Oikawa and K. Ikeda, p.917.
3. W. V. Youdelis and W. Fang, "*Calculated Al-Ti-Be Phase Diagram and Interpretation of Grain Refinement Results*", *Materials Science and Technology*, 7, 201 (1991).
4. W. Fang and W. V. Youdelis, "*Effect of Be on S phase Precipitation in Pseudo-binary Al(α)- Al_2CuMg Alloy*", Proc. Inter. Symposium on Production, Refining, Fabrication and Recycling of Light Metals, Ed. P. Tremblay and M. Bouchard, Pergamon Press, 1990. p.279.
5. W.V. Youdelis, W. Fang and T.D. Lowes, "*Precipitation and Age-Hardening Behavior of Al-0.2Ti-0.2Be Alloy*", *Materials Science and Technology*, 6, 1227 (1990).

VITA AUCTORIS

- 1959 Born in the People's Republic of China.
- 1982 Graduated with B.Sc, Department of Optical Materials,
Changchuen Institute of Optics and Fine Mechanics,
Changchuen, China.
- 1983 Engineer in China Academy of Space Technology,
Beijing, China.
- 1988 Graduated with M.A.Sc., Department of Engineering Materials,
University of Windsor, Windsor, Ontario, Canada.